University of Urbino Carlo Bo

Department of Biomolecular Sciences

Ph.D. Course in Biomolecular and Health Sciences
XXXVI cycle

The complexity of insulin-like growth factor 1 (IGF-1): development of innovative bio-molecular methods for detection and quantification of IGF-1 protein variants and study of their biological roles in physio-pathological conditions

Thesis written with the financial contribution of Regione Marche
(Progetto di Dottorato Innovativo a caratterizzazione industriale)

SSD: BIO/13

Coordinator:
Prof. Ferdinando Mannello
Supervisor:
Prof.ssa Elena Barbieri

Co-Supervisors:
Prof. Giosuè Annibalini
Prof. Giorgio Arnaldi

Ph.D. student:
Matteo Bocconcelli

ACADEMIC YEAR *2022/2023*

Abstract

The Insulin-like growth factor-1 (IGF-1) is a polypeptide growth factor with essential roles in physio-pathological conditions, including cellular growth and differentiation. Secretion of IGF-1 required proper post-translational modifications of IGF-1 prohormones (proIGF-1s), which include furin cleavage and N-glycosylation. This complex mechanism of IGF-1 production determines the presence of an IGF-1 pool composed of several IGF-1 protein variants: unglycosylated and glycosylated proIGF-1s, mature IGF-1, and E-peptides. Chapter I of the Thesis provides a description of the complex molecular mechanism regulating the production of the proIGF-1s and the currently available methods for detecting and quantifying these IGF-1 protein variants. Particular attention was paid to the recent evidence showing that proIGF-1s are stable intermediate of IGF-1 processing and have specific biological activities. Subsequently, we describe a system to produce a relatively high amount of the glycosylated proIGF-1Ea (glyc_proIGF-1Ea) based on HEK-293 cells stably expressing the human *IGF-1Ea* isoform. Recombinant components of the IGF-1 pool were characterized by High Resolution Mass Spectrometry (HRMS). Moreover, we used HRMS to detect the proIGF-1Ea and Ea-peptide in the cell culture supernatants of HEK-293 cells overexpressing the *IGF-1Ea* isoform. The different strategies adopted to increase the glyc_proIGf-1Ea yield and the protein stability were also described. The synthesis of new protein standards corresponding to different IGF-1 isoforms, combined with the use of HRMS technology, may provide a useful tool to characterize and quantify the different components of the IGF-1 poll in complex biological matrices. The II chapter describes the development of a fluorescent-based Western Blot (WB) for the simultaneous detection of the three different proIGF-1s and E-peptides. Specifically, we described the use of two different primary antibodies, which recognize different epitopes of proIGF-1 sequences, and two secondary antibodies conjugated to different fluorophores to develop a multiplex fluorescent WB able to discriminate between the different IGF-1 protein variants. Our results demonstrate the feasibility of simultaneously detecting different isoforms of the same protein using different fluorescence filter combinations. Furthermore, combining antibodies to two different epitopes of the same target protein increased the specificity and reliability of protein detection. In the III chapter, we analyzed the molecular mechanisms regulating the

production of proIGF-1Ea and the biological effect of IGF-1 on 3D Breast Cancer (BC) spheroids formation. We describe different cell-culture conditions that favor the MCF-7 and MDA-2B-231 spheroids formation and the effects of IGF-1 on spheroids growth, compactness, viability, and gene expression patterns of metabolic and epithelial to mesenchymal transition (EMT) markers. Our results highlight the value of 3D spheroid models to better understand the role of IGF-1 on multiple aspects of tumor progression, including cancer dormancy and EMT. The IV chapter describes the impact of N-glycosylation inhibition on IGF-1 production and IGF-1 receptor (IGF1R) signalling pathway activation in the context of diseases associated with aberrant N-glycosylation such as Congenital Disorder of Glycosylation (CDG). Using muscle cellular models and mice models we demonstrated that N-glycosylation inhibition reduces myoblast fusion and impairs the early stage of the myogenic program *in vitro* and decreased myogenic markers in mice muscles. Finally, muscle gly_proIGF-1Ea production and IGF1R signalling pathway activation were markedly inhibited after N-glycosylation inhibition. Our results offer new insights that increase understanding of possible impairments of the myogenic differentiation capacity in the pathological context of disorders of N-glycosylation.

CONTENT

ORIGINAL RESEARCH ARTICLES

This Thesis is based on the following original research articles, which will be referred to by their Roman numerals.

I. Matteo Bocconcelli**,** Giosuè Annibalini, Michele Menotta, Federica Biancucci, Roberta Saltarelli, Maria Elena Laguardia, Tomas Di Mambro, Mauro Magnani, Elena Barbieri. **Production of the IGF-1Ea glycosylated prohormone in HEK-293 cells and detection of the products by High Resolution Mass Spectrometry**. *In preparation.*

II. Matteo Bocconcelli, Roberta Saltarelli, Mauro De Santi, Elena Barbieri, Giosuè Annibalini. **Fluorescence-based multiplex western blot to simultaneously detect the insulin-like growth factor-1 (IGF-1) isoforms**. *In preparation.*

III. Matteo Bocconcelli, Giosuè Annibalini, Roberta Saltarelli, Rita Emili, Pierre Savagner Elena Barbieri. **Insulin-Like Growth Factor 1 promoted growth and tumor spheroid formation of breast cancer cells.** *In preparation.*

IV. Giosuè Annibalini, Laura Di Patria, Giacomo Valli, Matteo Bocconcelli, Roberta Saltarelli, Lorenzo Ferri, Laura Barberi, Amelia Morrone, Rita Barone, Renzo Guerrini, Antonio Musarò, Vilberto Stocchi, Elena Barbieri**. Impaired myoblast differentiation and muscle IGF-1 receptor signalling pathway activation after N-glycosylation inhibition.** *In preparation.*

Summary

CHAPTER I

Original Article

Production of the IGF-1Ea glycosylated prohormone in HEK-293 cells and detection of the products by High Resolution Mass Spectrometry

Matteo Bocconcelli[1], Giosuè Annibalini[1], Michele Menotta[1], Federica Biancucci[1], Roberta Saltarelli[1], Maria Elena Laguardia[2], Tomas Di Mambro[2], Mauro Magnani [1] Elena Barbieri[1]

[1]Department of Biomolecular Sciences, University of Urbino Carlo Bo, Urbino, Italy.
[2]Diatheva S.r.l., Via Sant'Anna 131135, Cartoceto, Italy

Abstract

Insulin-like growth factor-1 (IGF-1) is a key mediator of the anabolic and growth-promoting effects of growth hormone (GH). Quantitative measurement of IGF-1 is used for the diagnosis and management of patients with GH excess (acromegaly) and deficiency. IGF-1 can also be measured in alternative matrices, such as dried blood spots or urine samples to detect abuse in athletes. Immunoassays are generally used to quantify IGF-1 in clinical settings, although mass spectrometry methods have been recently developed to overcome immunoassay limits (e.g. different antibodies, standards, extraction methods and consistency between batches). Reliable IGF-1 quantification is also difficult due to the presence of different protein variants which are produced during the IGF-1 prohormone processing. In particular, IGF-1 is synthesized as a prohormone containing the mature IGF-1 region and E-domains in the C-terminal ends. Due to the alternative splicing of the *IGF-1* gene, three different IGF-1 prohormones (proIGF-1s) might be produced (i.e. proIGF-1Ea, proIGF-1Eb and proIGF-1Ec). These proIGF-1s contain the same mature sequences but different E-peptides. Proper maturation of proIGF-1s required complex steps of post-

translational modification which includes N-glycosylation of the Ea-peptide and cleavage of E-peptides by furin convertase. Recent evidence showed that proIGF-1s are stable intermediate of IGF-1 processing and have specific biological activities. The main aim of this study is to develop a HEK-293 cell-based system to produce the recombinant glycosylated proIGF-1Ea (glyc_proIGF-1Ea) useful for the characterization of IGF1 protein variants by High-Resolution Mass Spectrometry (HRMS). A bottom-up approach with trypsin digestion on the supernatant of the HEK-293 cells overexpressing the *IGF-1Ea* isoform allows the detection of several peptides corresponding to the mature IGF-1 sequence, while no peptide coverage was obtained for the Ea-peptide. Indeed, we showed a rapid degradation of glyc_proIGF-1Ea in culture supernatants which is partially reduced using a mutant isoform devoid of the furin cutting sites. The HRMS analyses of HEK-293 cells supernatants enriched with mutant glyc_proIGF-1Ea allow the identification of IGF-1 peptides corresponding to mature IGF-1, E-peptides and Ea-sequences with high confidence. The HRMS technique represents a promising method to detect the presence of proIGF-1s and E-peptides in biological matrices. The short sequence length of E-peptides, the presence of N-glycosylation sites, and the fast proIGF-1s turnover represent the major limiting factors in developing a HRMS-based method to detect and quantify the IGF-1 protein variants.

Introduction

Insulin-like growth factor (IGF-1) is a growth factor, produced in the liver in response to pituitary growth hormone (GH), with multiple roles in physio-pathological conditions including cellular growth and differentiation (Klement and Fink, 2016; Li et al., 2017). Interest in the analysis of IGF-1 levels has increased considerably and there is a growing demand to have access to a uniform and reliable method to quantify IGF-1 both in clinical and research settings. Like other protein hormones, IGF-1 has numerous protein variants due to genetic polymorphisms or mutations, post-transcriptional and post-translational modifications. This aspect places a strong limit on the reliability and reproducibility of the methods currently used for the measurement of IGF-1 which are mainly based on the use of antibodies (e.g. RIA or ELISA). The multiple isoforms derived from

IGF-1 and the differential expression of its transcripts in different physiological and pathologies conditions appear to be compatible with the distinct cellular responses observed to the different IGF-1 peptides and with the concept of a complex and possibly isoform-specific IGF-1 bioactivity. This concept is discussed in the present chapter, in the context of the broad range of modifications that this growth factor undergoes which might regulate its mechanism(s) of action. Thus, the development of a method for the detection and quantification of IGF-1 protein variants by mass spectrometry can be promising for clinical and scientific purposes. The human *IGF-1* gene is located on the long arm of chromosome 12 (12q23.2) and consists of six exons and five introns. It undergoes transcriptional and post-transcriptional modifications to produce multiple isoforms (Poreba and Durzynska, 2020). Due to alternative splicing of terminal exons 5 and 6 three different mRNA isoforms of the *IGF-1* gene are produced. The translation of these isoforms gives rise to three different IGF-1 prohormones (proIGF-1s): proIGF-1Ea, proIGF-1Eb and proIGF-1Ec. These prohormones have the same sequence of 70 amino acids that compose the IGF-1 mature protein, but they have different E-domains. The human Ea-domain has 35 amino acids, of which 16 are common in all E-domains. The remaining 19 amino acids are unique to this isoform. In addition, the Ea-domain also has a N-glycosylation site at the asparagine residue 92 (N92) fundamental for its correct processing and secretion (Annibalini et al., 2018). As a result, both unglycosylated proIGF-1Ea (unglyc_proIGF-1Ea of 11.7 kDa) and glycosylated proIGF-1Ea (glyc_proIGF-1EA of 17-22 kDa) were found in normal and IGF-1-overexpressing cells (Annibalini et al., 2018). The steps required for the correct proIGF-1Ea maturation are shown in Figure 1. On the other hand, the human Eb- and Ec-domains contain the common 16 amino acids and 61 and 24 additional isoform-specific amino acids, respectively. The predicted molecular weight of proIGF-1Eb is 16.5 kDa, while that of proIGF-1Ec is 12.5 kDa. The human Eb and Ec-domains lack potential N-linked glycosylation consensus sequences (Barton et al., 2006). Previously, proIGF-1s were considered "inactive precursors", but they are now recognized as stable intermediates of post-translational processing (Brisson and Barton, 2013).

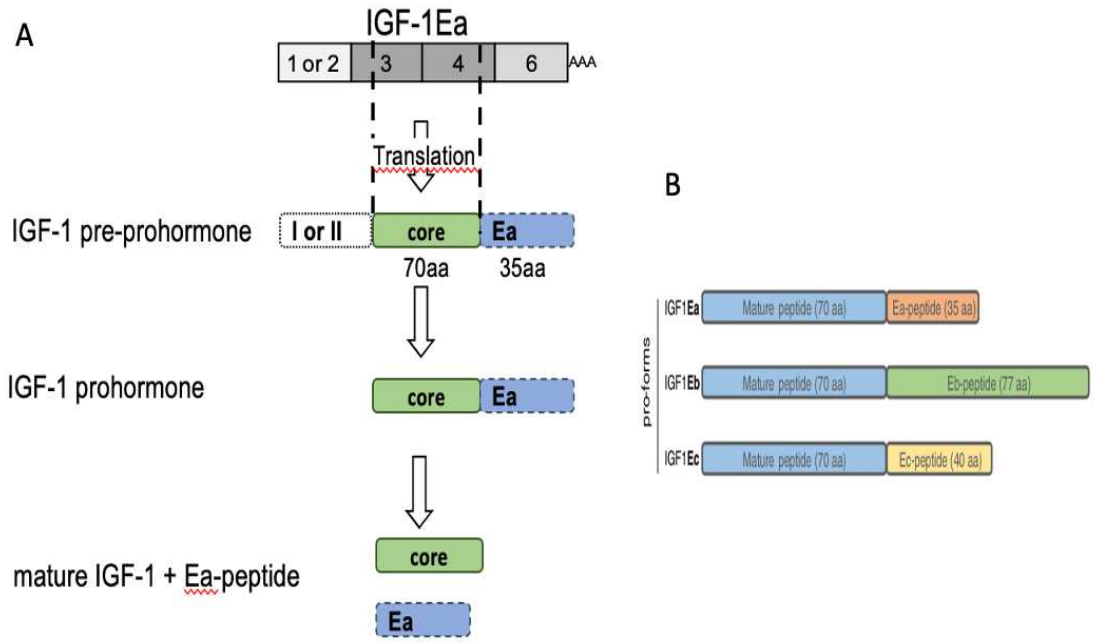

Figure 1. Processing of IGF-1Ea leading to the mature peptide. (A)The IGF-1 gene is translated into the IGF-1 pre-prohormone, containing a signal peptide in N-terminal, mature IGF-1 (core) and a C-terminal E-peptide extension. During translation, the N-terminal signal peptide is removed, and the resulting molecule is the IGF-1 prohormone. Conversion of proIGF-1 to mature peptide requires the endoproteolytic cleavage of the E-domain by proprotein convertases called Furin. (B) ProIGF-1Ea in the most expressed in human tissues and contains a potential N-glycosylation site in position N92 (De Santi et al., 2016).

As previously mentioned, recent studies have demonstrated that the IGF-1 proper maturation and secretion is mediated by the cleavage of furin proteases, which determine a pool of IGF-1, composed by glyc_proIGF-1Ea and mature IGF-1 (Annibalini et al., 2018). Moreover, Annibalini et al, demonstrated that intracellular IGF-1 is mainly expressed as proIGF-1Ea, not mature IGF-1 in HEK-293 (Annibalini et al., 2018). Furthermore, even at the extracellular level, the removal of the Ea peptide may be incomplete, in fact, the proIGF-1s are secreted and detected by cells overexpressing IGF-1 (De Santi et al., 2016) and can be also be relieved in normal and tumor cell lines culture supernatants (Miller et al., 2009; Pickard et al., 2017). Importantly, proIGF-1Ea also appears to have biological activity with

clinical relevance, independent of mature hormone (Miller et al., 2009; Wilson and White, 1998).The biological meanings of IGF-1 protein variants are currently unknown and the physiological and molecular mechanisms that regulate their expression in different tissues are still unclear. The presence of various transcripts is indicative of specific responses of cells to stimuli and they probably reflect the complexity of IGF-1 actions. In fact, although it is commonly believed that IGF-1 primarily exerts its biological effects through the mature peptide, various biological activities have been observed for different IGF-1 pro-forms and/or their E-peptides (De Santi et al., 2016). Recent evidence in humans has demonstrated that the IGF-1 prohormones are differentially transcribed depending on varying physio-pathological conditions such as exercise-induced muscle damage, endometriosis, and prostate cancer or cervical cancer (Philippou et al., 2014). In other studies, different IGF-1 isoform activities have been observed either when the peptides are exogenously administered or when they are over-expressed in different *in vitro* models (Armakolas et al., 2010; Philippou et al., 2014; Poudel et al., 2011). These studies demonstrated that IGF-1 prohormones are not simply precursors of mature IGF-1 (also called IGF-1 and core) and its presence in a variety of biological matrices (De Santi et al., 2016), suggest the importance of having a method of quantifying prohormone at both the intracellular and extracellular levels. In this chapter, we described a method based on mass spectrometry to measure the different components of IGF-1 in biological matrices (Remaggi et al., Ketha and Singh, 2015; Motorykin et al., 2021). Several immunoassay-based techniques have been developed to measure the mature IGF-1 level while, to date, there are no validated methods to detect and quantify the IGF-1 pro-hormones (Baskerville et al., 2017; Mongongu et al., 2021). Recently, the use of high-resolution mass spectrometry (HRMS), such as time-of-flight and orbitrap, for quantitative analysis of biological assays has increased significantly (Jung et al., 2021; Motorykin et al., 2021). In detail, a high-resolution mass analyzer provides a high degree of mass accuracy and is able to obtain individual isotopic peaks from a complex mixture of proteins, providing a greater quantitative specificity (Jung et al., 2021; Lim et al., 2021). Moreover, HRMS might provide important information on protein post-translational modifications such as N-glycosylation, acetylation, methylation, or phosphorylation. Interestingly, recent studies demonstrated the possibility of discriminating between circulating protein IGF-1 variants characterized by single amino acid changes by HRMS (Larkey et al., 2022; Motorykin et al., 2022).Here, we first described the production of fully

N-glycosylated proIGF-1Ea using HEK-293 which stably expressed the *IGF-1Ea* isoform. Subsequently, we described mass spectrometry profile of mature IGF-1, proIGF-1Ea and Ea-peptide using a HMR Spectrometry based on Orbitrap technology (Thermo Fisher).

Materials and Methods

Cell culture transfection assays

The HEK-293 cell lines were obtained from the American Type Culture Collection (ATCC, Rockville, MD, USA). Cells lines were cultured in DMEM media supplemented with 10% fetal bovine serum, 2 mM L-glutamine, 1x MEM Non-essential Amino Acid Solution, 0.1 mg/ml streptomycin and 0.1 U/L penicillin. Cells were maintained in a humidified incubator (5% CO_2) at 37 °C. All cell culture materials were purchased from Sigma-Aldrich (St. Louis, MO, USA). HEK-293 cells were cultured in DMEM without antibiotics at a density of 200000 cells per well in a 12-well plate. HEK-293 after 48 h of incubation, were transfected using TransIT®-X2 transfection reagent (Mirus Bio, Madison, WI, USA) according to the manufacturer's instructions. Briefly, the transfection complex was prepared by mixing 1 µg plasmid containing the his-tag *IGF-1Ea* sequence (Sino Biological), 100 µl of culture medium without FBS and antibiotics, and 1 µl x well of TransIT®-X2 Reagent. After a 30-minute incubation at room temperature, the mixture was added drop by drop to the cells. After 24 hours of incubation, cell lysates and supernatants were collected for western blot analyses. Chloromethylketone (CMK; 1 µM and 2.5 µM for 48h; Sigma-Aldrich) was used to inhibit furin enzyme and hence to enrich the culture media of IGF-1 prohormones. Deglycosylation of glyc_proIGF-1Ea was performed by incubation of glyc_proIGF-1Ea enriched media with 2500 U of PNGase F (New England Biolabs) for 3 hours at 37 °C, according to manufacturer's recommendations. Aliquot of proIGF-1Ea supernatant incubated with an equal volume of PNGase assay reaction buffer without the enzyme PNGase F was used as a control. Recombinant mature (core) IGF-1 was purchase from Sigma-Aldrich (cat. n. I3769) while synthetic Ea-peptide was generously gifted by Dr. Cavalleri (Istituto Nazionale dei Tumori, Milano).

Protein extraction and western blotting analysis

Cell bodies of transfected HEK-293 cells were lysed by adding 30-60 µl (depending on the cell quantity obtained) of lysis buffer containing: 20 mM HEPES (pH 7.9), 25% v/v glycerol, 0.42 M NaCl, 0.2 mM EDTA, 1.5 mM $MgCl_2$, 0.5% v/v Nonidet P 40, 1 mM DTT, 1mM NaF, 1 mM Na_3VO_4 and 1X complete protease inhibitor cocktail (Roche Diagnostics). The lysates were frozen and thawed twice and clarified by centrifugation at 12000 rpm for 10 min at 4°C. The protein concentration in each sample was determined using the Bradford colorimetric assay. Cell culture supernatants were concentrated with Amicon Ultra Centrifugal 3 KDa filter devices (Merck). Afterward, an equal amount of total protein was fractionated by SDS-PAGE on a 15 % of polyacrylamide gel and then transferred to PVDF or nitrocellulose membranes (Bio-Rad Laboratories Inc). Membranes were incubated overnight at 4°C with the primary antibodies directed toward IGF-1 Core (1:2000; cat. n. 500P11), purchased from Peprotech (Rocky Hill, New Jersey,USA), anti-E-peptide (Life Technology, cat. n. PA5-19382) and β-tubulin (1:2000; cat. n. 2146). Finally, the membranes were washed and incubated with appropriate HRP-conjugated secondary antibodies (Bio-Rad Laboratories Inc) at room temperature for 1 hour. After TBS-T washing, protein bands were visualized using Clarity Western ECL Substrate (Bio-Rad Laboratories Inc).

ELISA

Reagents available in the kit "DuoSet® ELISA DEVELOPMENT SYSTEM, Human IGF-I/IGF-1" (R&D system, catalog number DY291) were used for the development of the ELISA assay for the detection of IGF-1 pro-hormones. Specifically, either the primary anti-IGF-1 core antibody provided by the kit was used as a "capture antibody" for quantification of the total IGF-1 pool (mature IGF-1 + pro-hormones) or the anti-peptide E antibody (Life Technology, catalog number PA5-19382) was used for quantification of the pro-hormone of IGF-1. Coating was carried out overnight at room temperature on high-adhesion ELISA plates. The ELISA plate was washed three times with a buffer containing 0.05% Tween® 20 in PBS, pH 7.2-7 (for IGF-1 pool) or tris-saline buffer (TBS) (for pro-hormone of IGF-1). After blocking the plate with PBS + 1%BSA for 1 hour and three washes, the diluted sample was then added for

2 hours at room temperature. Supernatants of HEK-293 (IGF-1pool) cells were diluted in "reagent diluent" (5% Tween 20 in PBS, pH 7.2-7.4) for IGF-1 pool or in PBS +1% BSA for pro-hormone of IGF-1. After washing the plate, "Detection Antibody," i.e. anti-IGF-1 core antibody biotinylated for two hours, was added. A dilution of sterptavidin-HRP (1:40) was then prepared and, after washing the plate, added (100µL) to each well for 20 minutes. After three washes, the HRP enzyme substrate was added, i.e., a 1:1 dilution of Color Reagent A containing H_2O_2 and Color Reagent B containing Tetramethylbenzidine (R&D Systems, Catalog DY999) for 20 minutes and then 50µL of Stop solution containing 2N sulfuric acid (H_2SO_4). Plate readings were carried out at 450 nm using a correction wavelength of 570 nm on the ELISA plate reader (Model 680 Bio-Rad Laboratories). Analyses were performed using a 4-parameter log-logistic curve.

High-Resolution Mass Spectrometry sample preparation

Recombinant glyc_proIGF-1Ea and synthetic Ea-peptide were purified with Pierce C18 spin columns (Thermo Fisher) and dried with a Savant SpeedVac. Two to twenty pmol of intact recombinant proteins were directly loaded in the Orbitrap Exploris™ 240 Mass Spectrometer (Thermo Fisher Scientific) coupled with the Ultimate 3000 LC system. For protein digestion, the recombinant glyc_proIGF-1Ea (100 pmol) and HEK-293 supernatants (10 µg) were digested using the EasyPep Mini MS Sample Prep Kits (Thermo Fisher) and purified using the Pierce C18 spin columns (Thermo Fisher). All samples were diluted with 0.1% formic acid in water. Briefly, peptides were desalted online by Acclaim PepMap C18 Reversed Phase HPLC Column (Thermo Fisher Scientific), and then resolved with a Thermo RSLC Ultimate 3000 (Thermo Fisher Scientific) as previously described (Fraternale et al., 2023). The Proteome Discoverer Software (Thermo Fisher Scientific) was used for peptide identification.

Site direct mutagenesis

Site-directed mutagenesis was performed to mutate the three putative furin cleavage sites: amino acids K68 (Lysine), R71 (Arginine) and R77 (Arginine) on the sequence of the plasmid

human_IGF-1Ea C-His tag (Sino Biological). The composition of the PCR mutagenesis reactions performed on a SimpliAmp Thermal Cycler from Applied Biosystems was as follows: 12.5 µl of 5 × SuperFi PCR Master Mix (Thermo Fisher); 10 µM of each primer directed on the two second furin cut-site mutation sites (IGF-1-2FuK2F 5'-CCGGTCAGCTGTCTGTCCGTGCC-3' IGF-1-2FuK2R 5'-CAGAGGCAGCTGACCCGCAGGCTTG-3') and two different concentrations of plasmid respectively 10 ng/µl and 1 ng/µl of plasmid with DNA encoding for human *IGF-1Ea*_his. Subsequently, digestion with 20 U of of DpnI (Invitrogen) at 37° C for 1 h was performed to selectively digest the methylated progenitor plasmids, and the resulting PCR products were purified with GenElute PCR Clean-Up Kit (Sigma-Aldrich). Afterward, 2 µl of the purified PCR reactions were transformed by electroporation into electrocompetent E. coli cells with selection for ampicillin resistance. E. coli colonies were selected using the IGF-1F-BGHrev primer by real time PCR (Syber Select PCR Master Mix 30 cycles). Successful mutagenesis was confirmed by sequencing the plasmid DNA. Plasmids containing the pro_IGF-1EaKoFur sequence (R71 and R77) and the pro_IGF-1EaKoFur sequence (K68) were transfected using TransIT®-X2 transfection reagent (Mirus Bio, Madison, WI, USA) according to the manufacturer's instructions, and then cell bodies and supernatants were recovered and analyzed in Western blot.

Results

Production and quantification of His-tagged IGF-1Ea prohormone using HEK-293 cells

As first step to reproduce a protein that corresponds to the glycosylated proIGF1-Ea (glyc_proIGF-1Ea) HEK-293 cells overexpressing the *IGF-1Ea* isoform was generated by transient transfection with a commercial plasmid (Sino Biological) containing the full-length human *IGF1-Ea* isoform with a His-tag sequence, located in the carboxy-terminal sequence at the 3'-end of the gene (fig. 2A). This characteristic allows us to purify the glyc_proIGF-1Ea, porIGF-1Ea and free Ea-peptide. Western Blot analysis was performed to verify the product obtained in the HEK-293 supernatant (SN). Western blotting analysis using the anti-mature

IGF-1 antibody confirmed our previous finding (Annibalini et al., 2018) that cellular bodies of HEK-293 cells mainly expressed the proIGF-1Ea instead of the mature IGF-1. In particular, two distinct bands of about 13 kDa and 18 kDa, which correspond to the His-tagged unglycosylated and glycosylated proIGF-1Ea respectively, were detected in the cell lysate. On the contrary two main bands of 7.6 kDa (mature IGF-1) and 18-23 kDa (glyc_proIGF-1Ea) were detected in the cell culture SN. The molecular weight of these products suggested that HEK-293 cells secreted a pool of IGF-1 which includes both the mature IGF-1 of 7.6 kDa and glyc_proIGF-1Ea of 18-23 kDa (fig. 2B). Subsequently we used two different strategies to confirm the presence of the glyc_proIGF-1Ea in the culture SN. We treated the SN of HEK-293 cells with in the furin inhibitor chloromethylketone (CMK; 1 μM and 2.5 μM for 48h), an endopeptidase serine inhibitor. It acts as an alkylating agent and is known to interfere with the translation process. We confirmed the enrichment of the 18-23 kDa glyc_proIGF-1Ea band and the consequent decrease of the 7.6 kDa corresponding to the mature IGF-1 (fig. 2C). After treatment of cell culture SN with PNGase F, a peptide N-glycanase which releases N-linked glycans from glycoproteins, we observed a shift in the molecular weight of the 18-23 kDa bands to the unglycosylated proIGF-1Ea of 13 kDa (Fig. 2D). Subsequently, to obtain a more quantity of glyc_proIGF-1Ea, we generated HEK-293 cells that stably overexpress the His-tagged IGF-1Ea isoform using selection of hygromycin-resistance cells and single clone dilution. We obtained several clones that expressed relatively high concentrations of the glyc_proIGF-1Ea (fig. 2E) with a molecular band of 18-23KDa (in particular P7 and P8 clones)

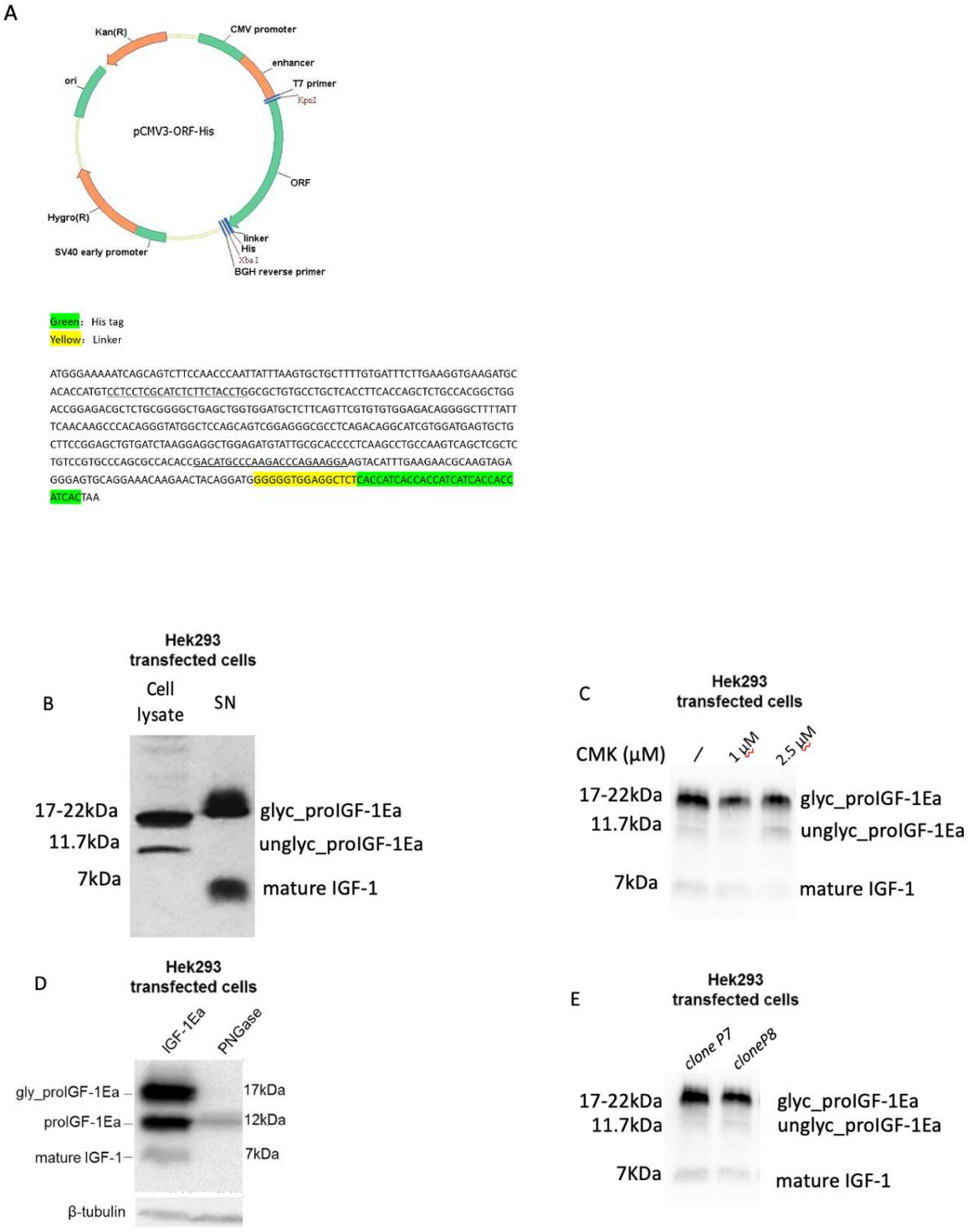

Figure 2. (A) Schematic representation of the commercial plasmid (Sino Biological) containing the *IGF-1Ea* sequence with the His-tag in the C-terminal. Immunoblotting of HEK-293, transfected with the full-length human *IGF1-Ea* isoform, by anti-mature IGF-1 antibody showed two distinct bands of about 13 kDa and 18 kDa, most likely representing the unglycosylated and glycosylated proIGF-1Ea

respectively, in the cell lysate. On the contrary two main bands of 7.6 kDa and 18-23 kDa were detected in the SN (B). The band of 7.6 KDa was not found in the SN of HEK-293 overexpressing the *IGF-1Ea_his* treated with different concentrations of CMK(C). The band at a molecular weight around 18 kDa disappeared when the SN of HEK293 overexpressing IGF-1Ea his vector was treated with PNGase (D). Immunoblotting of the HEK-293 SN stably overexpressed with the IGF-1Ea isoform showed an increased expression of the glyc_proIGF-1Ea compared to mature IGF-1 in clones named P7 and P8 (E).

Quantification of HEK-293 overexpressing IGF-1Ea_his by ELISA assay

After establishing the production by the HEK-293 of the gyc_proIGF-1Ea we used a home-made ELISA kit to quantify the proIGF-1Ea level in the HEK-293 SN. The ELISA approach used for the quantification of the glyc_proIGF-1Ea was the "sandwich" type and involved the use of anti-E-peptide antibody (RSVRAQRHTD) as the primary antibody followed by a secondary antibody capable of binding the "core" portion of IGF-1 (mature IGF-1). The lack of a standard for the pro-hormone of IGF-1 did not allow us to obtain an absolute quantitative data of the pro-hormone but only of the pool of IGF-1, which results to be about 1.4 ng/µL. By comparison with western blot detection system of IGF-1 pro-hormone using the antibody directed toward the common sequence of peptide E-peptide, we obtain an overall amount of the pro-hormone alone of about 0.7 ng/µL (Fig. 3C). As expected, in our HEK-293 SN transfected we have a pool of IGF-1, not only the expected mature IGF-1 but also the glycosylated one, and even if we transfected a lower quantity of the product, we always obtained a detectable production of glyc_proIGF-1EA (Fig. 3C). Analysis of the intracellular pool of IGF-1 by ELISA assay could be very useful for quantifying tissue IGF-1 (e.g., muscle) and discriminating the amounts of mature and pro-hormone IGF-1 present. This aspect is particularly important, given the recent results described earlier, showing that at the intracellular level IGF-1 is present mainly as a pro-hormone and not as a mature protein. In conclusion, this ELISA method for pro-hormone quantification of IGF-1 could be an important tool for discriminating the various components of the IGF-1 pool.

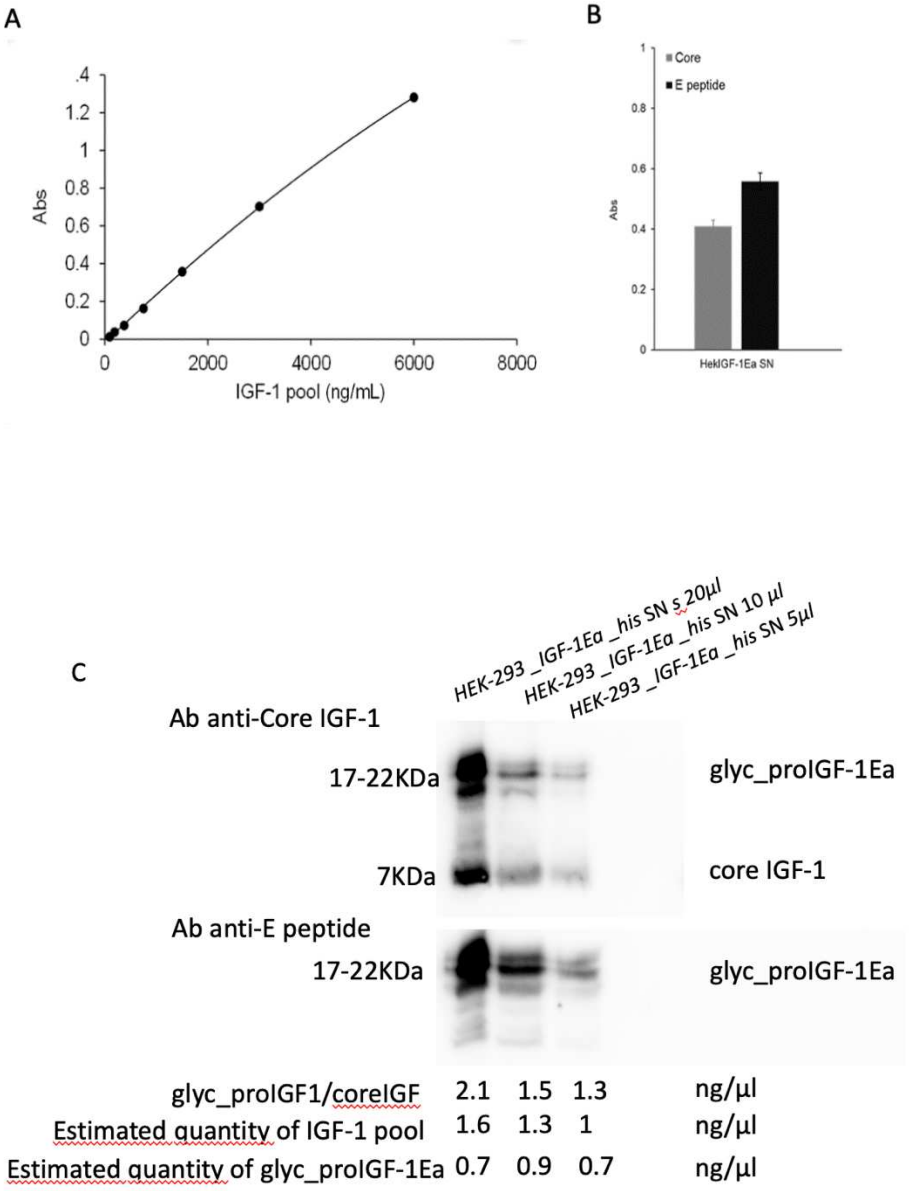

Figure 3. (A) Standard curve performed with the anti-core antibody of IGF-1. Quantification by ELISA of the pool of IGF-1 (1.4 ng/µL) by anti-core antibody and pro-hormone by anti-E-peptide antibody in the SN of HEK-293 overexpressing the *IGF-1Ea _his* plasmid (B). Immunoblotting analyses using an anti-IGF-1 mature antibody and anti-Ea peptide antibody on SN of HEK-293 overexpressing the *IGF-1Ea _his* plasmid showed an overall amount of the glyc_proIGF-1Ea alone of about 0.7 ng/µL (C).

Mass spectrum of synthetic EA-peptide

We obtained our first dataset using HMRS by analyzing the synthetic Ea-peptide (unglyc_Ea peptide) as shown in Fig. 4A. We loaded 1 pmole of the synthetic Ea peptide into the column without trypsin digestion. Fig. 4A displays the obtained peptides and their corresponding ion masses (MH^+), while Fig. 4C illustrates the fragmentation spectrum of the first peptide, which provided the highest sequence coverage of the Ea-peptide (sequence of Ea peptide: RSVRAQRHTDMPKTQKEVHLKNASRGSAGNKNYRM). As summarized in Figure 4A, the Ea peptide has been fully sequenced with high confidence, as indicated by the green color.

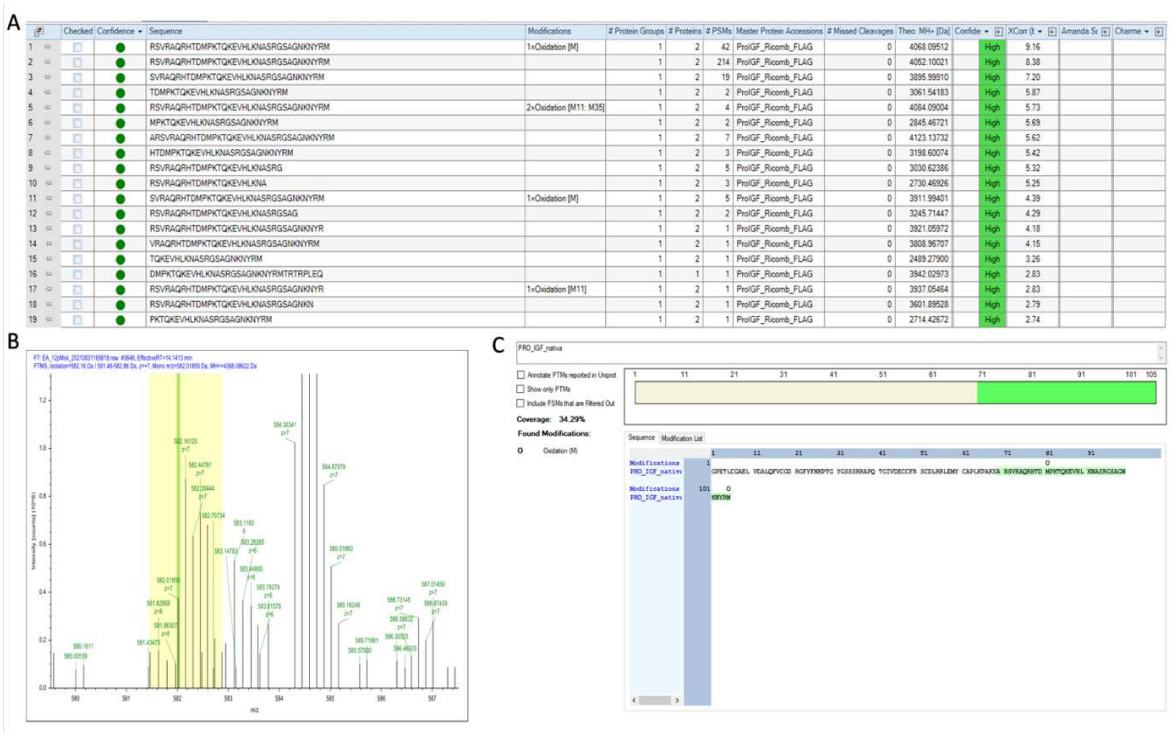

Figure 4. Sequencing of synthetic Ea peptide (unglyc_Ea peptide). Peptides obtained with high confidence are highlighted in green (A). (B) The fragmentation spectrum of the Ea peptide is shown in figure A, and amino acid sequence with a coverage of 100 % for the Ea-peptide, corresponding to 34.29% coverage of the proIGF-1Ea (C).

Mass Spectrum and of Recombinant proIGF-1Ea

Next, we analyzed the recombinant IGF1-Ea pro-hormone of commercial origin. The recombinant protein was obtained from the company Origene using HEK-293 cells transfected with the human *IGF-1Ea* isoform (NM_000618) The product description shows comassie blue staining of a protein of about 23000 Da, thus of a size compatible with the glyc_proIGF-1Ea, (it is important to note that this sequence contains about 3600 additional Da, due to the C-myc/DDK tag sequence) (Fig. 5).

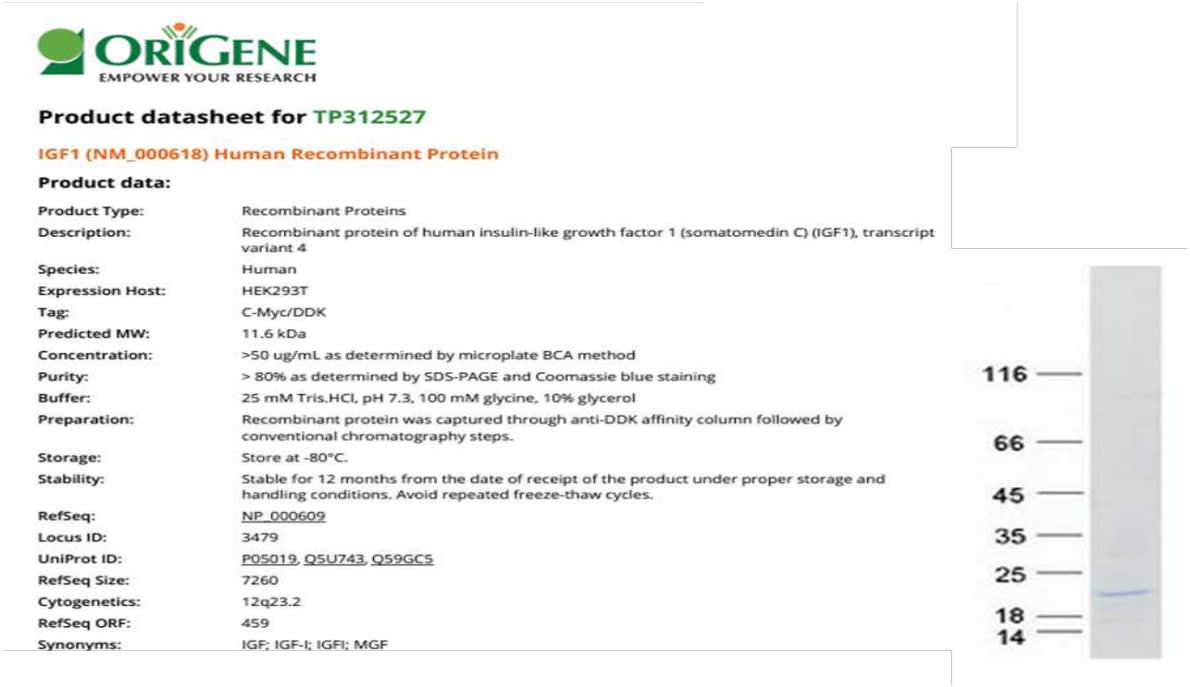

ORIGENE
EMPOWER YOUR RESEARCH

Product datasheet for TP312527

IGF1 (NM_000618) Human Recombinant Protein

Product data:

Product Type:	Recombinant Proteins
Description:	Recombinant protein of human insulin-like growth factor 1 (somatomedin C) (IGF1), transcript variant 4
Species:	Human
Expression Host:	HEK293T
Tag:	C-Myc/DDK
Predicted MW:	11.6 kDa
Concentration:	>50 ug/mL as determined by microplate BCA method
Purity:	> 80% as determined by SDS-PAGE and Coomassie blue staining
Buffer:	25 mM Tris.HCl, pH 7.3, 100 mM glycine, 10% glycerol
Preparation:	Recombinant protein was captured through anti-DDK affinity column followed by conventional chromatography steps.
Storage:	Store at -80°C.
Stability:	Stable for 12 months from the date of receipt of the product under proper storage and handling conditions. Avoid repeated freeze-thaw cycles.
RefSeq:	NP_000609
Locus ID:	3479
UniProt ID:	P05019, Q5U743, Q59GC5
RefSeq Size:	7260
Cytogenetics:	12q23.2
RefSeq ORF:	459
Synonyms:	IGF; IGF-I; IGFI; MGF

Figure 5. Recombinant protein Origene TP312527 used for HRMS analyses.

For the identification of the recombinant glyc_proIGF-1Ea by mass spectrometry the digestion with the furin enzyme was performed in order to promote proteolytic cleavage of the Ea-peptide. The report of this analysis is shown in Figure 6C, and it reveals almost complete coverage of the Ea-peptide with high confidence and only partial sequencing of the mature IGF-1. The failure to sequence the core portion of IGF-1 is likely due to increased "resistance" to fragmentation, given its "orderly" nature and the presence of three disulfide bridges that stabilize the tertiary structure of mature IGF-1. This result confirms that the recombinant protein corresponds to the glyc_proIGF-1Ea. However, the low degree of purity

found, probably related to the purification methods used, makes it difficult to use this protein as a standard for spectrometry analysis.

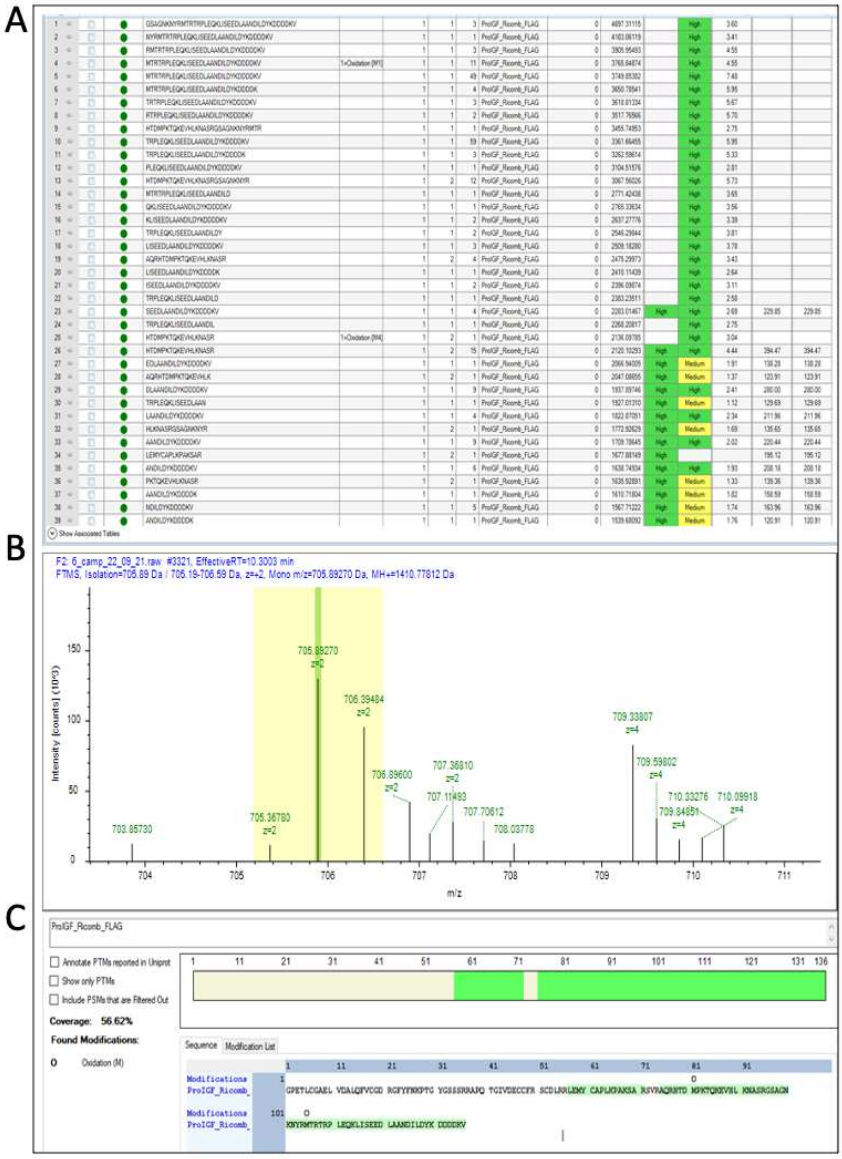

Figure 6. Sequencing of the recombinant protein Origene TP312527. (A) Sequence and relative abundance of the obtained peptides, (B) fragmentation spectrum of the first peptide shown in Figure A, (C) coverage of more than 56% of the proIGF-1Ea amino acid sequence.

Mass profile analysis of the supernatant of HEK-293 stably transfected with the human IGF-1Ea _his plasmid

The supernatant of HEK-293 cells transfected with the *IGF-1Ea_his* plasmid (about 30 mL) was concentrated with 3-kDa columns and then purified with C18 columns (Pierce C18 Spin Columns, Thermo Fisher), before being analyzed in HRMS column. Firstly, the sample was analyzed using a bottom-up approach involving trypsin digestion. Results obtained revealed good mass spectrum coverage of the IGF-1 core but not of the Ea-peptide (Fig. 7A). Similar results were obtained when the recombinant glyc_proIGF-1Ea was diluted in the HEK-293 cell culture media (Fig. 7C, D). Interestingly, using the software setting to non-trypsin digested (independently of digestion in trypsin) we obtained an increase in the mass spectrum coverage of the pro_IGF-1EA with high confidence on the Core peptide (75.24%). HRMS also recognized different peptides corresponding to the Ea-peptide but with a low medium confidence (Fig. 8A and 8B). These results suggest the presence of degradation phenomena of IGF-1 and Ea-peptide when SN are exposed to temperatures of 37°C for several hours. This hypothesis was strengthened by western blotting analysis of glyc_pro_IGF-1Ea in HEK-293 cell culture SN, treated and not with Furin (Fig. 8C and 8D). Complete degradation of the glyc_proIGF-1Ea in the SN exposed to 37°C 24 hours, was observed with or without furin. Notably, already significant degradation was visible after 4 hours exposure to 37°C for 4 hours, especially for the glyc_proIGF-1Ea (Fig. 8D). These data clearly showed a fast protein degradation, especially for glyc_proIGF-1Ea in the SN of HEK-293 cells exposed to 37°C. This probably caused non-specific glyc_proIGF-1Ea protein cutting, explaining the higher protein coverage obtained when the mass-spectrometry software was set to “non-trypsin digested”.

Figure 7. Peptides corresponding to proIGF-1Ea sequence in the SN of HEK-293 cells transfected with the *IGF1-Ea _his* plasmid (A and B) or in HEK.293 culture media added with recombinant glyc_proIGF-1Ea (C and D). SN was digested by trypsin. The result revealed a low coverage of about 33.33% (A) and 25.74% (C) with high confidence (B and C). All peptides correspond to the core IGF-1 sequence while none to the Ea-peptide.

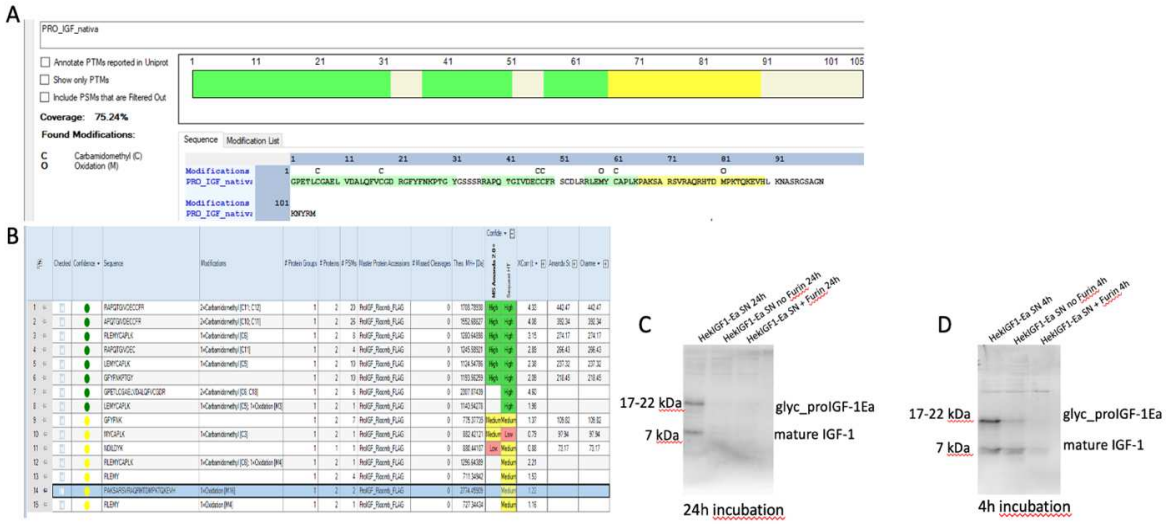

Figure 8. Peptides corresponding to IGF-1 sequence in the SN of HEK-293 cells transfected with the *IGF1-Ea _his* plasmid. SN was digested with trypsin but software was setting in the "non-trypsin digested". The amino acid coverage of pro-IGF-1Ea dramatically increased passing from about 33% (Fig. 7A) to 75.24% (A). With this approach, we also to identify peptides corresponding to the E-peptide but with low-medium confidence (B). Immunoblotting, by anti-mature IGF-1 antibody, showed two distinct bands of a molecular weight between 18-23 kDa and 7.6 kDa corresponding to glyc_proIGF-1Ea and mature IGF-1 respectively (C, D). 24 hours 37 °C incubation (with or without furin) determined a complete degradation of mature and glyc_proIGF-1Ea.The degradation of glyc_proIGF-1Ea was also observed after 4 hours 37 °C incubation (D).

Site-directed mutagenesis to improve production and of the glyc_proIGF-1EA level in the supernatants of HEK-293 supernatants

To try to overcome the limitation related to the glyc_proIGF-1Ea instability in the HEK293 SN, we decided to mutate the furin binding sites of the IGF-1Ea_his plasmid (Fig. 9A). We performed a site-directed mutagenesis approach on human_IGF-1Ea sequence at the level of the three amino acids: K (Lysine) 68, R (Arginine) 71 and R (Arginine) 77, respectively (fig 9B), representing the amino acid consensus sequence for the furin cutting sites.

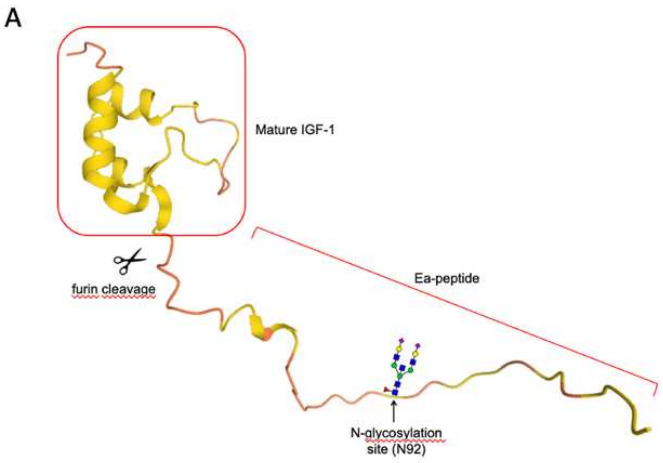

B

h-IGF-1 amminoacid sequence:

MGKISSLPTQLFKCCFCDFLKVKMHTMSSSHLFYLALCLLTFTSSATAGPETLCGAELV
DALQFVCGDRGFYFNKPTGYGSSSRRAPQTGIVDECCFRSCDLRRLEMYCAPLKPAKSA
RSVRAQRHTDMPKTQKEVHLKNASRGSAGNKNYRMGGGGSHHHHHHHHHH

Figure 9. Alphafold model of the human glyc_proIGF-1Ea (A); the human IGF-1Ea amino acid sequence: signal peptide (underlined), mature region (blue), Ea-peptide (red) and Furin cleavage sites K68, R71 and R77 (green) (B).

We obtained three different plasmids which contain the following mutations: K6: R71A and R77A mutations: K8: R71A; R77A and N92D mutations and P1: K68G mutation (Fig. 10 C,D,E). Interestingly, the mutation of furin cleavage sites did not modify the secretion of the proIGF-1Ea (HEK-K6 and HEK-P1) while the mutation of N92 sites, which represent the N-glycosylation sites, completely block the unglycosylated proIGF-1Ea secretion (HEK-K8), accordingly to previous results (Annibalini et al., 2018) (Fig. 10 A,B). For the following mass-spectrometry analyses we decided to use the P1 plasmid containing the K68G mutation since it shows a good enrichment of glyc_IGF-1Ea and the mutation occurs outside the Ea-peptide sequence (Fig. 10D).

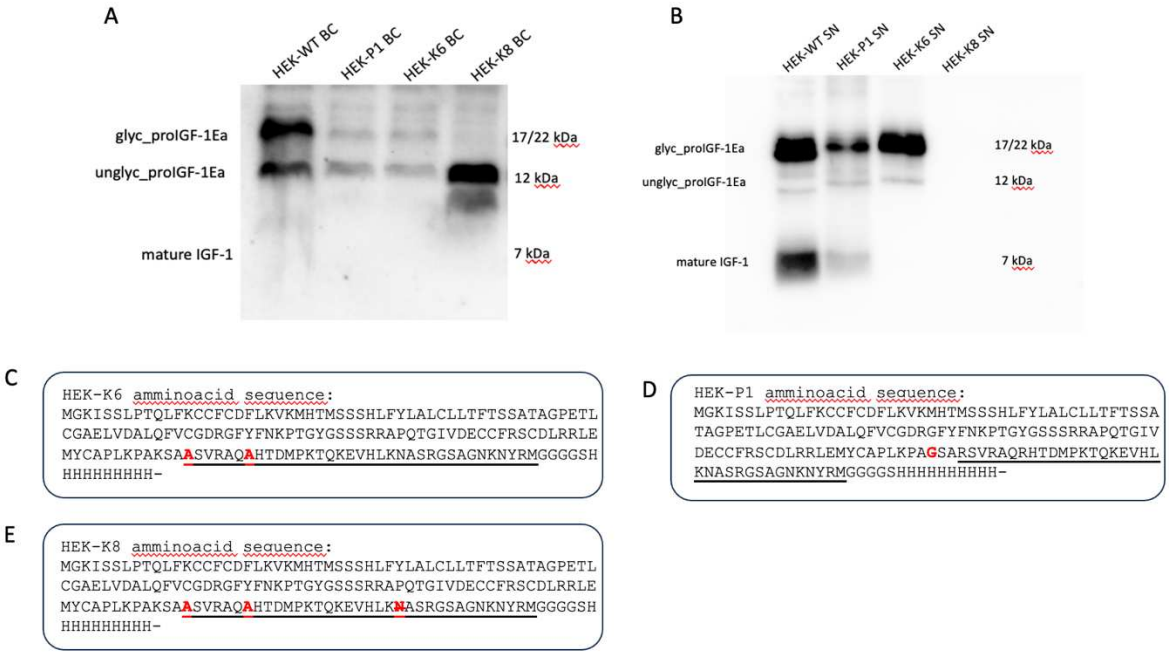

Figure 10. Effect of furin cutting sites mutation on the proIGF-1Ea production. HEK-293 were transiently transfected with four different plasmids: plasmid containing the wild type IGF-1Ea sequence (WT); (D) P1 (K68 to G68 mutation); (C) K6 (R71 to A71 and R77 to A77 mutations) and (E) K8 (R71 to A71; R77 to A77 and N92 to 92 mutations). After 48h cell bodies (A) and SN (B) were analyzed by western blot using an antibody directed against mature IGF-1 sequence. Cell bodies of HEK-293 cell transfected with WT, P1, and K6 plasmids showed two distinct bands of about 13 kDa and 18 kDa, corresponding to the unglycosylated and glycosylated IGF-1Ea prohormones, respectively (A). Only the unglycosylated IGF-1 pro-hormone was detected in K8 transfected cells, as expected. SN of HEK-293 cells transfected with P1 and K6 plasmids showed a marked enrichment of the IGF-1 pro-hormone respect to the mature IGF-1, while no band corresponding to IGF-1 was detected in K8-transfected cells (B).

The SN of HEK-293 cells transfected with the P1 (K68G mutation) plasmid was collected and analyzed by HRMS using a bottom-up approach as previously described (Fig. 11). Of particular interest were the APQTGIVDECCFRSCDLR, HTDMPK and EVHLK peptides which covered partial sequence of core, E-peptides and and Ea-petide. Moreover, although the HTDMPK peptide is only 6 amino acids long its corresponds to a unique IGF-1 peptides in the

mass-spectrometry database and hence useful for further analyses in targeted mass spectrometry analyses.

GPETLCGAELVDALQFVCGDRGFYFNKPTGYGSSSRRAPQTGIVDECCFRSCDLRRLEMYCAPLK**PA**G**G**SARSVR
AQR**HTDMPK**TQK**EVHLK**NASRGSAGNKNYRMGGGGSHHHHHHHHHH-

Figure 11. Peptides corresponding to IGF-1 sequence in the SN of HEK-293 cells transfected with the P1 (K68G mutation) plasmid. Peptides recognized by mass spectrometry with high confidence were highlighted.

Discussion

It is established that most peptide hormones and growth factors are initially synthesized as pro-hormones (Wilson and White, 1998) and endoproteolysis at specific sites convert them to the active forms. (Chrétien, 2013). In particular IGF-1, for its proper maturation and secretion, undergoes post-translational modifications such as N-glycosylation and the cleavage of E-peptides by furin convertase. These coordinated events determine the presence of an IGF-1 pool, composed by IGF-1 prohormones (proIGF-1s), glycosylated proIGF-1Ea (glyc_proIGF-1Ea), mature IGF-1 and E-peptides (Fig. 1). The presence of proIGF-1s and E-peptides in a variety of biological matrices and its potential independent biological activity (De Santi et al., 2016), makes their detection and characterization crucial and very interesting for different clinical and research applications. Thus, our primary aim was to characterize, purify, and obtain a protein corresponding to the IGF-1 pro-hormone, specifically the glyc_proIGF-1Ea. We decided to focus our attention on the IGF-1Ea isoforms since this variant represents the most expressed isoforms in different tissues, accounting for about 90% of *IGF-1* transcripts (Philippou et al., 2014). HEK-293 cells overexpressing the *IGF-1Ea* isoform were generated by transient transfection with a plasmid containing the full-length human *IGF1-Ea* isoform with a His-tag sequence at the 3'-end of the gene, which allows the purification of the proIGF-1Ea, glyc_proIGF-1Ea or Ea-peptide (Fig. 2A). Subsequently, we analyzed the IGF-1 protein produced in the HEK-293 cells cell bodies and

in the culture supernatants by western blotting (Fig. 2B). Our results confirm previous findings showing that intracellular IGF-1 is mainly expressed as proIGF-1, not mature IGF-1 (Annibalini et al., 2018). Then, to better characterize the IGF-1 protein pool produced in the HEK-293 cells we used two different strategies. First, we treated HEK-293 cells with the furin inhibitor chloromethylketone (CMK) and we confirmed an enrichment of the 18-22 kDa band (Fig. 2C) corresponding to the glyc_proIGF-1Ea. Subsequently, we treated the cell culture SN with PNGase F, a peptide N-glycanase which releases N-linked glycans from glycoproteins, and we observed a shift in the molecular weight of the 18-23 kDa band to the unglycosylated proIGF-1Ea of 13 kDa (glyc_proIGF-1Ea), as expected (Fig. 2D). In order to obtain more quantity of the glyc_proIGF-1Ea, we generated stably expressing *IGF-1Ea* HEK-293 cell line (Fig. 2E). Afterwards, the glyc_proIGF-1Ea was quantified using an ELISA assay developed to specifically recognize the proIGF-1s. Using this ELISA assay, we estimated a production of the IGF-1 pool (glyc_proIGF-1Ea + mature IGF-1) of about 1.4 ng/µL and of about 0.7 ng/ µL for the glyc_proIGF-1Ea (Fig. 3C). These data confirmed that the supernatants of HEK-293 stably expressing the IGF-1Ea isoform was enriched of both the mature IGF-1 and the glyc_proIGF-1Ea. Subsequently, we try to develop a method to identify and quantify the different components of the IGF-1 pool (i.e. mature IGF-1, proIGF-1Ea, and E-peptide) by high-resolution mass spectrometry (HRMS). Recent studied have highlighted that mass spectrometry represent the “gold standard” for detecting IGF-1 peptide, particularly in sports drug testing (Guha et al., 2013). Moreover, the differentiation of common IGF-1 variants characterized by single amino acid changes, was successfully performed by an HRMS approach (Guha et al., 2013). However, to the best of our knowledge, there are no studies addressing the use of HRMS to discriminate the component of the IGF-1 pool. Our HRMS analyses aim to characterize the mass spectrum of 1) a synthetic unglycosylated Ea-peptide, 2) a commercially available protein probably corresponding to the gly-proIGF-1Ea 3) a complex mixture obtained from the supernatants of HEK-293 cells overexpressing the His-tagged *IGF-1Ea* isoforms. The identification of peptide corresponding to the Ea-peptide was obtained both using synthetic Ea-peptide and commercially available recombinant glyc_proIGFEa, without trypsin digestion (Fig. 4). Subsequently, we analyzed the recombinant gly_proIGF1-Ea treated with furin to favor the cleavage between the core and Ea-peptide (Fig. 5). Interestingly, we identified with good confidence the Ea-peptide while we obtained a low coverage of the IGF-1 core sequence. This data is probably due to the fact

that the structured IGF-1 core region which contains three disulfide bonds, is more resistant toward the peptide fragmentation compared to the "intrinsically disordered" Ea-peptide (Annibalini et al., 2018; Babu et al.,2016) (Fig. 6). Subsequently, we set up the analysis of the IGF-1 pool in the supernatants of HEK-293 cells overexpressing the *IGF-1Ea* isoform. HRMS showed a good coverage of IGF-1 core region (Fig. 7A), while different peptides corresponding to the Ea-peptide were obtained only with a medium-low confidence (Fig. 7B). Unfortunately, similar results were obtained when the recombinant glyc_proIGF-1Ea was diluted in the HEK-293 derived culture media (Fig. 7C,D) suggesting that the glyc_proIGF-1Ea and particularly the Ea-peptide undergo degradation. Accordingly, when the same data of HRMS was analyzed by software set to “non-trypsin digested”, the coverage of the Ea-peptide strongly increased, suggesting that the Ea-digestion was largely independent of the trypsin digestion (Fig. 8A,B). These data were confirmed by immunoblotting analyses which confirm a fast degradation of glyc_proIGF-1Ea in the HEK-293 cell culture supernatants (Fig. 8C,D). To try to reduce the glyc_proIGF-1Ea degradation, we mutated the putative furin cutting sites of the proIGF-1Ea by site-directed mutagenesis. In particular, we carried out three different plasmids with the following mutations: K6: R71A and R77A mutations (Fig. 10C); K8: R71A; R77A and N92 to D92 mutations (fig. 10D) and P1: K68G mutation (Fig. 10E). Immunoblotting analyses revealed that in the cell lysates of HEK-293 cell transfected with WT, P1, and K6 plasmids two distinct bands of about 13kDa and 18kDa were present, corresponding to the unglycosylated and glyproIGF-1Ea, respectively (Fig. 10A). In the cell culture supernatants, an enrichment of the glyc_proIGF-1Ea with respect to the mature IGF-1 was revealed, demonstrating a successful mutation of furin cleave sites (Fig. 10B). Interestingly, the mutation of furin cleave sites did not affect the secretion level of IGF-1, while the mutant lacking the N-glycosylation site (K8) showed the absence of secreted glyc_proIGF-1Ea, corroborating our previous finding that correct N-glycosylation is obligatory for proper IGF-1 protein secretion (Fig. 10B) (Annibalini et al., 2018). The HEK-293 supernatants obtained from cells transfected with furin-mutated plasmids were enriched of the glyc_proIGF-1Ea and showed, at least in part, a reduction of the degradation phenomena. Using these HEK-293 supernatants, mass spectrometry analyses identified three distinct peptides corresponding to the glyc_proIGF-1Ea in the HEK-293 supernatants. One of these peptides (HTDMPK) is unique for the common region of the E-peptides and might be useful to detect the presence of this IGF-1 domain by mass spectrometry. The

synthesis of protein standards corresponding to different IGF-1 isoforms represents a step forward for the development of new methods to detect and quantify IGF-1 protein variants in biological matrices like human serum. Regarding this, nowadays mass is becoming one of the most widely used tools in the IGF-1 detection, and it is even more interesting to note that Motorkyn et al, in a cohort of more than 240,000 patients, have identified in the C-terminal core segment, at the level of furin cutting sites, some clinically relevant protein variants with a possible impact in the production of the mature peptide rather than the prohormone. Our data indicate that the short sequence length of the Ea-peptide, the presence of N-glycosylation and its rapid degradation represents the major limiting factor to develop a HRMS-based method to detect and quantify the proIGF-1s and E-peptides. Using a bottom-up approach, we were able to identify several IGF-1 peptides corresponding to proIGF-1 and/or E-peptides in a cell culture supernatant. The development of a top-down approach for proIGF-1 and E-peptide detection (without tryptic digestion), and for the Ea-peptide N-glycan characterization will be fundamental, in order to propose a IGF-1 isoform standard. The implementation of this project will allow the development of a new method to monitor, detect and quantify IGF-1 protein variants, useful for, research, clinical and diagnostic purposes.

References

Albrethsen, J., Frederiksen, H., Johannsen, T.H., Andersson, A.-M., Juul, A., 2018. Clinical proteomics: Insights from IGF-I. Clinica Chimica Acta 477, 18–23. https://doi.org/10.1016/j.cca.2017.11.034

Annibalini, G., Contarelli, S., De Santi, M., Saltarelli, R., Di Patria, L., Guescini, M., Villarini, A., Brandi, G., Stocchi, V., Barbieri, E., 2018. The intrinsically disordered E-domains regulate the IGF-1 prohormones stability, subcellular localisation and secretion. Sci Rep 8, 8919. https://doi.org/10.1038/s41598-018-27233-3

Armakolas, A., Philippou, A., Panteleakou, Z., Nezos, A., Sourla, A., Petraki, C., Koutsilieris, M., 2010. Preferential expression of IGF-1Ec (MGF) transcript in cancerous tissues of human prostate: Evidence for a novel and autonomous growth factor activity of MGF E peptide in human prostate cancer cells. Prostate 70, 1233–1242. https://doi.org/10.1002/pros.21158

Babu, M.M., 2016. The contribution of intrinsically disordered regions to protein function, cellular complexity, and human disease. Biochem Soc Trans 44, 1185–1200. https://doi.org/10.1042/BST20160172

Barton, E.R., 2006. The ABCs of IGF-I isoforms: impact on muscle hypertrophy and implications for repair. Applied Physiology, Nutrition, and Metabolism 31, 791–797. https://doi.org/10.1139/h06-054

Baskerville, C.L., Bamford, N.J., Harris, P.A., Bailey, S.R., 2017. Comparison and validation of ELISA assays for plasma insulin-like growth factor-1 in the horse. Open Vet J 7, 75. https://doi.org/10.4314/ovj.v7i1.12

Brisson, B.K., Barton, E.R., 2013. New Modulators for IGF-I Activity within IGF-I Processing Products. Front Endocrinol (Lausanne) 4. https://doi.org/10.3389/fendo.2013.00042

Chrétien, M., 2013. How the Prohormone Theory Solved Two Important Controversies in Hormonal and Neural Peptide Biosynthesis. Front Endocrinol (Lausanne) 4. https://doi.org/10.3389/fendo.2013.00148

De Santi, M., Annibalini, G., Barbieri, E., Villarini, A., Vallorani, L., Contarelli, S., Berrino, F., Stocchi, V., Brandi, G., 2016. Human IGF1 pro-forms induce breast cancer cell

proliferation via the IGF1 receptor. Cellular Oncology 39, 149–159. https://doi.org/10.1007/s13402-015-0263-3

Fraternale, A., De Angelis, M., De Santis, R., Amatore, D., Masini, S., Monittola, F., Menotta, M., Biancucci, F., Bartoccini, F., Retini, M., Fiori, V., Fioravanti, R., Magurano, F., Chiarantini, L., Lista, F., Piersanti, G., Palamara, A.T., Nencioni, L., Magnani, M., Crinelli, R., 2023. Targeting <scp>SARS-CoV</scp> -2 by synthetic dual-acting thiol compounds that inhibit Spike/ <scp>ACE2</scp> interaction and viral protein production. The FASEB Journal 37. https://doi.org/10.1096/fj.202201157RR

Guha, N., Cowan, D.A., Sönksen, P.H., Holt, R.I.G., 2013. Insulin-like growth factor-I (IGF-I) misuse in athletes and potential methods for detection. Anal Bioanal Chem 405, 9669–9683. https://doi.org/10.1007/s00216-013-7229-y

Jung, Y.J., Seo, H.S., Kim, J.H., Song, K.Y., Park, C.H., Lee, H.H., 2021. Advanced Diagnostic Technology of Volatile Organic Compounds Real Time analysis Analysis From Exhaled Breath of Gastric Cancer Patients Using Proton-Transfer-Reaction Time-of-Flight Mass Spectrometry. Front Oncol 11. https://doi.org/10.3389/fonc.2021.560591

Ketha, H., Singh, R.J., 2015. Clinical assays for quantitation of insulin-like-growth-factor-1 (IGF1). Methods 81, 93–98. https://doi.org/10.1016/j.ymeth.2015.04.029

Klement, R.J., Fink, M.K., 2016. Dietary and pharmacological modification of the insulin/IGF-1 system: exploiting the full repertoire against cancer. Oncogenesis 5, e193–e193. https://doi.org/10.1038/oncsis.2016.2

Larkey, N.E., Fatica, E.M., Singh, R.J., 2022. Differentiation of Common IGF-1 Variants Using HRMS COM Determination with Follow-Up MS/MS Verification. pp. 227–237. https://doi.org/10.1007/978-1-0716-2565-1_21

Li, H., Batth, I.S., Qu, X., Xu, L., Song, N., Wang, R., Liu, Y., 2017. IGF-IR signaling in epithelial to mesenchymal transition and targeting IGF-IR therapy: overview and new insights. Mol Cancer 16, 6. https://doi.org/10.1186/s12943-016-0576-5

Lim, H., Lee, S.Y., Park, Y., Jin, H., Seo, D., Jang, Y.H., Moon, D.W., 2021. Mass spectrometry imaging of untreated wet cell membranes in solution using single-layer graphene. Nat Methods 18, 316–320. https://doi.org/10.1038/s41592-020-01055-6

Miller, B.S., Khosravi, M.J., Patterson, M.C., Conover, C.A., 2009. IGF system in children with congenital disorders of glycosylation. Clin Endocrinol (Oxf) 70, 892–897. https://doi.org/10.1111/j.1365-2265.2009.03531.x

Mongongu, C., Coudoré, F., Domergue, V., Ericsson, M., Buisson, C., Marchand, A., 2021. Detection of LongR ^{3} -IGF-I, Des(1-3)-IGF-I, and R ^{3} -IGF-I using immunopurification and high resolution mass spectrometry for antidoping purposes. Drug Test Anal 13, 1256–1269. https://doi.org/10.1002/dta.3016

Motorykin, I., Li, A., Wu, Z., 2022. Monitoring and Identifying Insulin-Like Growth Factor 1 Variants by Liquid Chromatography–High-Resolution Mass Spectrometry in a Clinical Laboratory. pp. 239–251. https://doi.org/10.1007/978-1-0716-2565-1_22

Motorykin, I., Li, H., Clarke, N.J., McPhaul, M.J., Wu, Z., 2021. Isotopic Peak Index, Relative Retention Time, and Tandem MS for Automated High Throughput IGF-1 Variants Identification in a Clinical Laboratory. Anal Chem 93, 11836–11842. https://doi.org/10.1021/acs.analchem.1c02566

Motorykin I, Mu J, Miller BS, Li A, Clarke NJ, McPhaul MJ, Wu Z. Detection rate of IGF-1 variants and their implication to protein binding: study of over 240,000 patients. Clin Chem Lab Med. 2023 Oct 10. doi: 10.1515/cclm-2023-0709. Epub ahead of print. PMID: 37811857.

Philippou, A., Maridaki, M., Pneumaticos, S., Koutsilieris, M., 2014. The Complexity of the IGF1 Gene Splicing, Posttranslational Modification and Bioactivity. Molecular Medicine 20, 202–214. https://doi.org/10.2119/molmed.2014.00011

Pickard, A., Durzynska, J., McCance, D.J., Barton, E.R., 2017. The IGF axis in HPV associated cancers. Mutation Research/Reviews in Mutation Research 772, 67–77. https://doi.org/10.1016/j.mrrev.2017.01.002

Poreba, E., Durzynska, J., 2020. Nuclear localization and actions of the insulin-like growth factor 1 (IGF-1) system components: Transcriptional regulation and DNA damage response. Mutation Research/Reviews in Mutation Research 784, 108307. https://doi.org/10.1016/j.mrrev.2020.108307

Poudel, B., Bilbao, D., Sarathchandra, P., Germack, R., Rosenthal, N., Santini, M.P., 2011. Increased cardiogenesis in P19-GFP teratocarcinoma cells expressing the propeptide IGF-1Ea. Biochem Biophys Res Commun 416, 293–299. https://doi.org/10.1016/j.bbrc.2011.11.028

Remaggi, G., Saleri, R., Andrani, M., Satolli, F., Rodighiero, E., Elviri, L., 2022. Development and single laboratory validation of a targeted liquid chromatography-triple quadrupole mass spectrometry-based method for the determination of insulin like growth factor-1

in different types of milk samples. Food Chem X 13, 100271. https://doi.org/10.1016/j.fochx.2022.100271

Wilson, H.E., White, A., 1998. Prohormones: their Clinical Relevance. Trends in Endocrinology & Metabolism 9, 396–402. https://doi.org/10.1016/S1043-2760(98)00098-8

CHAPTER II

Original Article

Fluorescence-based multiplex western blot to simultaneously detect the insulin-like growth factor-1 (IGF-1) isoforms

Matteo Bocconcelli, Roberta Saltarelli, Mauro De Santi, Elena Barbieri, Giosuè Annibalini.

University of Urbino Carlo Bo, Department of Biomolecular Sciences, Urbino, Italy.

Abstract

Insulin-like growth factor-1 (IGF-1) is a secreted growth factor, critical for the growth and development of many tissues. Its overexpression is also implicated in the beginning and progression of different malignancies. The *IGF-1* gene contains 6 exons and due to alternative splicing at the 3'-end of the *IGF-1* gene three different isoforms might be produced: the *IGF-1Ea*, *Eb* and *Ec* splice variants. The translation of these isoforms determines the production of three different precursor peptides named IGF-1Ea, Eb and Ec prohormones (proIGF-1s). These proIGF-1s contain the same IGF-1 mature sequence, responsible for the IGF-1 receptor (IGF1R) binding and activation, but different carboxy-terminal extension called Ea, Eb, Ec peptides or domains, implicated in different post-transcriptional process. In this paper, we present a fluorescent-based multiplex western blot able to discriminate and quantify simultaneously the mature IGF-1, proIGF-1s and E-peptides in the same sample. HEK-293 cells were transiently transfected with plasmids containing the

IGF-1Ea, IGF-1Eb, IGF-1Ec isoform or an empty vector. Two different antibodies, which recognize the mature sequence or a common region of the E-peptide domains, were used to recognize mature, proIGF-1s and E-peptides which were discriminated with secondary antibodies conjugated to different fluorophores. Our results demonstrate the feasibility of simultaneously detecting different isoforms of the same protein using different fluorescence filter combinations. Furthermore, combining antibodies to two different epitopes of the same target protein increased the specificity and hence greater reliability in protein detection.

Introduction

Western blotting (WB) is the most spread and informative technique in the field of biology research and is widely used to determine the presence, size and relative abundance of specific proteins in complex mixtures. WB is performed with five main steps: (1) the separation of proteins based on their size by gel electrophoresis; (2) the transfer of proteins to a nitrocellulose or polyvinylidene difluoride (PVDF) membrane; (3) labeling using a primary antibody specific to the protein of interest; 4) incubation with a secondary antibody directed against the primary antibody; and 5) visualization. Visualization methodology has evolved with time to improve safety and sensitivity and is typically attained through a secondary antibody conjugated to an enzyme or a fluorescent molecule (Sajjad et al., 2018). The chemiluminescence approach is based on an enzymatic reaction between hydrogen peroxide and luminol. The reaction is catalyzed by antibody-conjugated horseradish peroxidase (HRP) and results in light emission. Traditional chemiluminescence detection emits light at a relatively low intensity and for a short period of time. Enhanced chemiluminescence detection was developed to amplify the signal and has become the dominant technique for revealing proteins in WB (Huang and Amero, 1997). This technique enables the detection of picograms of protein usually visualized with X-ray film or a digital charge-coupled device (CCD) imager. Although it offers excellent sensitivity, this technique is a one-colour method that detects a single protein target and does not facilitate normalization or comparative analysis. In recent years, the use of fluorescent probes in WB

stands out for their convenience, safety, sensitivity, and straightforward quantification (Gingrich et al., 2000; Kondo et al., 2018; Patton, 2000). The main advantage of using fluorescently-labeled antibody probes rather than chemiluminescence is the ability to multiplex analysis such as the visualization of different target proteins with similar molecular weight (e.g. phosphorylated and non-phosphorylated isoforms of a protein). Furthermore, another advantage is the increased linearity and accuracy of quantification since no enzymatic amplification is involved and blots can be catalogued for extended periods of time when stored properly. The main drawbacks of fluorescent WB are: low sensitivity compared to chemiluminescence, and strong high background fluorescence of membranes. In this regard, the introduction of antibodies directly labelled with near-infrared (IR) dyes, the use of low fluorescence membrane and news fluorescence-optimized blockers have significantly improved fluorescent WB sensitivity (Patonay and Antoine, 1991; Silva and McMahon, 2014). In this paper, we present a fluorescent-based WB able to reveal different protein isoforms (proteoforms) of human insulin-like growth factor-1 (IGF-1). IGF-1 is a growth factor, critical for the growth and development of many tissues and is also implicated in the beginning and progression of different malignancies (Hakuno and Takahashi, 2018). Alternative splicing of the *IGF*-1 gene produces three different mRNA isoforms in humans: *IGF-1Ea*, *IGF-1Eb* and *IGF-1Ec* (Annibalini et al., 2016; Philippou et al., 2014b). The translation of these mRNA variants gives rise to three different IGF-1 prohormones (proIGF-1s): proIGF1Ea, proIGF1Eb and proIGF1Ec in humans (De Santi et al., 2016b). These prohormones contain the same central region, named mature IGF-1 peptide or core region, and three C-terminal domains called Ea- Eb- and Ec-peptides or domanis. The human Ea-domain is composed of 35 amino acids; the first 16 amino acids of Ea-domain are common in all E-domains, while 19 aa are unique to this isoform. The human Ea-domain contains a N-glycosylation site on the asparagine residue at position 92 (N92) (Annibalini et al., 2018). Accordingly, both unglycosylated proIGF-1Ea (~12 kDa) and glycosylated proIGF-1Ea (~17–22 kDa) were found in normal and IGF-1-overexpressing cells (Annibalini et al., 2018; Di Patria et al., 2022). The human Eb- and Ec-domains contain the 16 common amino acids and 61 and 24 additional isoform-specific amino acids respectively, with a predicted molecular weight of 16.5 kDa for proIGF-1Eb and 12.5 kDa for proIGF-1Ec. The human Eb- and Ec-domains lack potential N-linked glycosylation consensus sequences (Annibalini et al., 2018). Several steps are required for the formation and secretion of the mature IGF1 peptide. Initially, the IGF-1 mRNA

isoforms are translated as pre-prohormones containing a signal peptide, the core region, and the Ea, Eb or Ec peptides. After cleavage of the signal peptide, the proIGF-1s containing the core region and the Ea, Eb or Ec peptides, undergo other post-translational modifications before secretion. These processes included: a) cleavage of the E-peptides by the intracellular protease furin convertase to release mature IGF-1 and E-peptides, b) N-glycosylation of the Ea peptide and c) differential subcellular localization of proIGF-1s (Annibalini et al., 2018; Philippou et al., 2014b). Because of the complex post-transcriptional and post-translational regulation of IGF-1 production, different pools of IGF-1 proteins might exist intra- and extra-cellularly. This IGF-1 protein heterogeneity makes it difficult to discriminate the different IGF-1 proteoforms. Here, we used two different antibodies, one specific for the IGF-1 core region and one for the common region of E-peptides, to simultaneously differentiate the different IGF-1 proteoforms by fluorescence WB.

Materials and Methods

Cell transfection and protein extraction

HEK-293 cells were cultured in DMEM without antibiotics at a density of 1.5 x10^5 cells per well in a 12-well plate. When the cell confluence reached approximately 60% confluence were transiently transfected using the TransIT®-X2 System (Mirus Bio, LLC, TEMA ricerca) following the manufacturer's instructions. Briefly, the TransIT-X2:DNA complexes were distribute to cells in complete growth medium. One µg of plasmid constructs containing the *IGF-1Ea*, *IGF-1Ea* or *IGF-1Ec* were used. Plasmid details have been previously published (Annibalini et al., 2018; De Santi et al., 2016). After 24 h of incubation, the cells were harvested, centrifuged at 200 g for 5 min and washed once with PBS. Then, cell bodies were collected and resuspended in lysis buffer containing: 20 mM HEPES (pH 7.9), 25% v/v glycerol, 0.42 M NaCL, 0.2 mM EDTA, 1.5 mM MgCl2, 0.5% v/v Nonidet P 40, 1mM DTT, 1mM Naf, 1mM Na_3VO_4, and 1X complete protease inhibitor cocktail (Roche Diagnostics). The lysates were frozen and thawed twice and clarified by centrifugation at 12.000 g for 10 min at 4 °C. The supernatant was collected and the protein concentration was determined by

Bradford assay. Recombinant mature (core) IGF-1 was purchase from Sigma-Aldrich (cat. n. I3769) while synthetic Ea-peptide was generously gifted by Dr. Cavalleri (Istituto Nazionale dei Tumori, Milano).

Electrophoresis and Western Blotting Analysis

The protein samples (20 or 30 µg) were prepared in dithiothreitol-containing Laemmli sample buffer to a total volume of 20 µl. Polyacrylamide gels (15%) of 1.0-mm thickness were handcast and samples were electrophoresed in tris-glycine running buffer (25 mM tris base, 192 mM glycine, and 0.1% SDS) at 150 V until the dye front reached the end of the gel. Proteins from the polyacrylamide gel were transferred to a nitrocellulose membrane (0.20 µm pore size, BioRad) in a Mini Trans-Blot Electrophoretic Transfer Cell (Bio-Rad) under classical conditions with 25 mM tris, 192 mM glycine, 0.02% SDS, and 20% methanol at 100 V for 1 hour. After transfer, the membrane was blocked with filtered 5% BSA in Tris-Buffered Saline (TBS) on a shaking platform for 1 hour at room temperature. After blocking, membranes were incubated overnight at 4°C with blocking solution plus 0.05% Tween 20 containing or a single or a mix of following primary antibodies: the rabbit polyclonal anti-Human IGF1 antibody which recognizes the core epitope (1:2000; n. 500P11 PeproTech) and the goat polyclonal IGF1 antibody against E-peptide domain (proIGF-1s) (1:2000; no. PA5-19382 Invitrogen). Membranes were removed from primary antibody solution and washed with TBS plus 0.05% Tween 20 (TBS-T) for 15 min for 3 time. For fluorescence detection after washing, membranes were incubated in the dark for 1 hour at room temperature with TBS-T containing the mix of the following secondary antibodies: Donkey anti-Rabbit IgG Alexa Fluor Plus 680 (Invitrogen Catalog # A32802, 1:20.000 dilution) and Donkey anti-Goat IgG Alexa Fluor Plus 800 (Invitrogen Catalog # A32930, 1:40.000 dilution). Finally, membranes were removed from secondary antibody solution and washed with TBS-T on the dark in a staking platform for 15 min for 3 time. To remove residual Tween 20, which is highly autofluorescent, the membranes were washed for 5 min in TBS. Low Fluorescence PVDF Membrane (Bio-Rad, cat. N. 1620264) and EveryBlot Blocking Buffer (Bio-Rad, cat. N. 12010020) were also used to compare blot background. For chemiluminescence detection, the immunoreactive bands were revealed by the single appropriate horseradish peroxidase

(HRP)-conjugated secondary antibodies (Bio-Rad). Peroxidase activity was detected with the enhanced chemiluminescence detection method (ECL Bio-Rad). Fluorescencent and chemiluminescent images were obtained on the ChemiDoc MP Imaging System (Bio-Rad) and analyzed by the Image Lab Touch Software version 6.0.1 (Bio-Rad).

Results

Firstly, we used a primary antibody specific to the core IGF-1 region and one specific to the common region of the E-peptides to analyze the IGF-1 pool using a traditional chemiluminescence detection system. Two different western blot gels were loaded with: 1) 20 µg of the cell lysate of Hek293 transiently transfected with a vector containing the human *IGF-1Ea* sequence, 2) 50 ng of the recombinant mature IGF-1 and 3) 50 ng of the synthetic Ea-peptide. The first blot was hybridized with the anti-core IGF-1 antibody (Fig. 1A upper panel) and the second one with the anti-E-peptide antibody (Fig. 1A, lower panel).

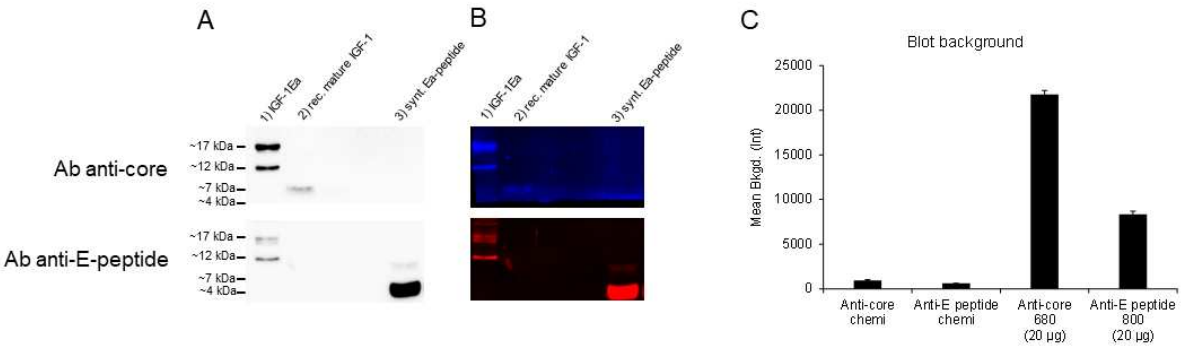

Figure 1. Comparison between WB band patterns obtained by chemiluminescence (A) or fluorescent (B) methods. (C) The background intensity of chemiluminescence and fluorescent blot membranes. 1) IGF-1Ea: 20 µg of the cell lysate of Hek293 transiently transfected with a vector containing the human *IGF-1Ea* sequence, 2) ric. mature IGF-1: 50 ng of the recombinant mature IGF-1 and 3) synt. Ea-peptide: 50 ng of the synthetic Ea-peptide. Ab anti-core: antibody directed against the core IGF-1 region; Ab anti-E-peptide: antibody directed against the common region of E-peptides.

Two distinct bands of ~17 kDa and ~12 kDa were detected in the Hek293 cell lysate by the antibody specific to the core IGF-1 (Fig. 1A upper panel) and the E-peptide (Fig. 1A, lower panel). These bands correspond to the glycosylated and unglycosylated proIGF-1Ea (Annibalini et al., 2018). The recombinant mature IGF-1 (band of ~7 kDa) and Ea-peptide (band of ~3 kDa) proteins were recognized only by the anti-core IGF-1 antibody and anti-E-peptide antibody, respectively. Subsequently, we used a similar experimental setting to analyse the IGF-1 proteoforms by a fluorescent WB approach. In particular, a first blot was hybridized with the anti-core IGF-1 antibody which was detected by a secondary anti-rabbit fluorescent antibody (Alexa Fluor Plus 680) (Fig. 1B, upper panel) and the second one with the anti-E-peptide antibody which was detected by a secondary anti-goat fluorescent antibody (Alexa Fluor Plus 800) (Fig. 1B, lower panel). A marked increase of blot background was found with fluorescent WB compared to chemiluminescence (Fig. 1C). We tried to optimize the signal-to-background ratio using low-fluorescent membrane and specific blocking buffer, although none of these strategies were effective (not shown). Despite this limit, WB banding was similar between the chemiluminescence and fluorescent methods. Subsequently, we tried to optimize the simultaneous detection of different IGF-1 proteoforms by the hybridization of WB membrane with a mixture of the anti-IGF-1 core and anti-E-peptide antibodies followed by the detection with different fluorescent secondary antibodies. To reduce the background signal, we decided to increase the amount of Hek293 cell lysate from 20 µg to 30 µg. The western blot gel was loaded with: 1) 30 µg of the cell lysate of Hek293 transiently transfected with an empty vector; 2) 30 µg of the cell lysate of Hek293 transiently transfected with a vector containing the human *IGF-1Ea* sequence; 3) 50 ng of the recombinant mature IGF-1; 4) 50 ng of the synthetic Ea-peptide; a mixture of 30 µg of the cell lysate of Hek293 transiently transfected with a vector containing the human *IGF-1Ea* sequence and 5) 50 ng of the recombinant mature IGF-1 or 6) 50 ng of the synthetic Ea-peptide or 7) 50 ng of the recombinant mature IGF-1 and synthetic Ea-peptide (Fig. 2A).

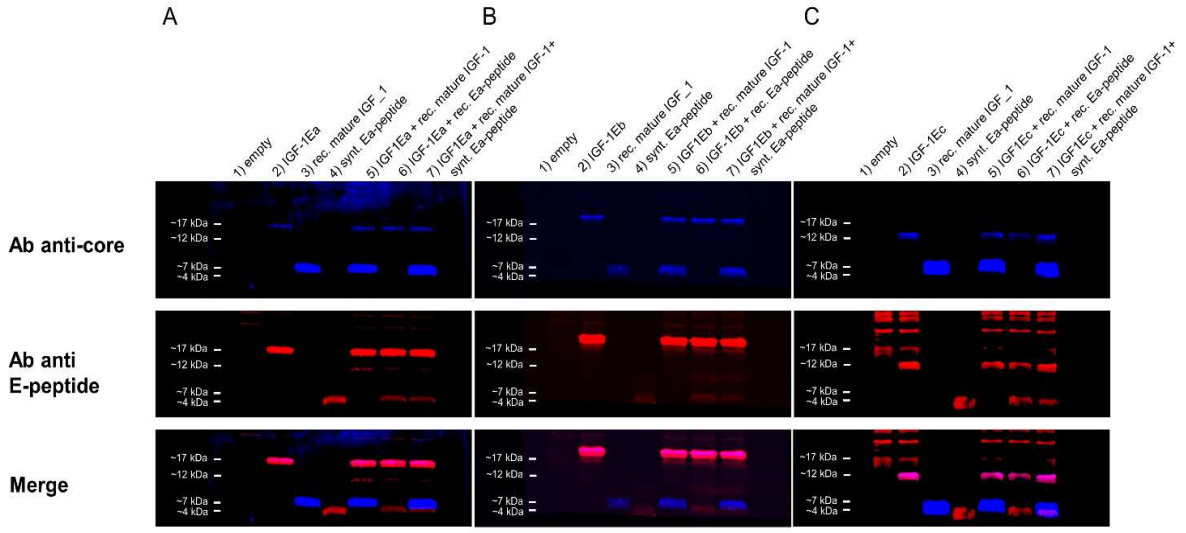

Figure 2. Simultaneously detection of IGF-1 proteoforms by fluorescent WB. Hek293 cells were transiently transfected with a vector containing the human (A) *IGF-1Ea,* (B) *IGF-1Eb* or *(C) IGF-1Ec* sequence. 1) empty: 30 µg of the cell lysate of Hek293 transiently transfected with an empty vector; 2) IGF-1Ea, IGF-1Eb, IGF-1Ec: 30 µg of the cell lysate of Hek293 transiently transfected with a vector containing the human *IGF-1Ea, IGF-1Eb or IGF-1Ec* sequence, 3) ric. mature IGF-1: 50 ng of the recombinant mature IGF-1 and 4) synt. Ea-peptide: 50 ng of the synthetic Ea-peptide. 5) sample 2) plus 50 ng of the recombinant mature IGF-1; 6) sample 2) plus 50 ng of the synthetic Ea-peptide; 7) sample 2) plus 50 ng of the recombinant mature IGF-1 and 50 ng of the synthetic Ea-peptide. Ab anti-core: antibody directed against the core IGF-1 region; Ab anti-E-peptide: antibody directed against the common region of E-peptides.

As shown in Fig. 2A (upper panel), the anti-IGF-1 core antibody recognizes the glycosylated proIGF-1Ea (band of ~17kDa) and the recombinant mature IGF-1 (band of ~7k Da). The anti-E-peptide antibody recognizes the glycosylated proIGF-1Ea (band of ~17k Da), the faint band corresponding to unglycosylated proIGF-1Ea (band of ~12 kDa) and the recombinant synthetic Ea-peptide (band of ~3k Da) (Fig. 2A, middle panel). Notably, merged images of the anti-IGF-1 core and the anti-E-peptide antibodies allow to show simultaneously the different IGF-1 proteoforms, easily distinguishing between mature IGF-1 (blue bands), E-peptides (red bands) and IGF-1Ea prohormones (fuchsia bands) (Fig. 2A, lower panel). We next evaluate

the western blot banding pattern observed in HEK-293 cells transfected with a vector containing the human *IGF-1Eb* (Fig. 2B) or *IGF-1Ec* (Fig. 2C) sequences. As shown in the merged panel of Fig. 2B (lower panel), the expression pattern showed a fuchsia band of slightly higher mass of ~17kDa representing the IGF-1Eb prohormone, and the expected blue and red bands corresponding to mature IGF-1 and Ea-peptide, respectively. Similar results were obtained in IGF-1Ec transfected cells (Fig. 2C), although several non-specific bands were observed using the anti-E-peptide antibody against the empty-vector transfected cells. This unexpected result might be due to the low expression level of IGF-1 proteoforms in the *IGF-1Ec*-transfect cells compared to other plasmids. The increased amount of cell lysate proteins loaded in the western blotting ameliorates the background membrane signal, however it still remained higher compared chemiluminescent blot (Fig 3).

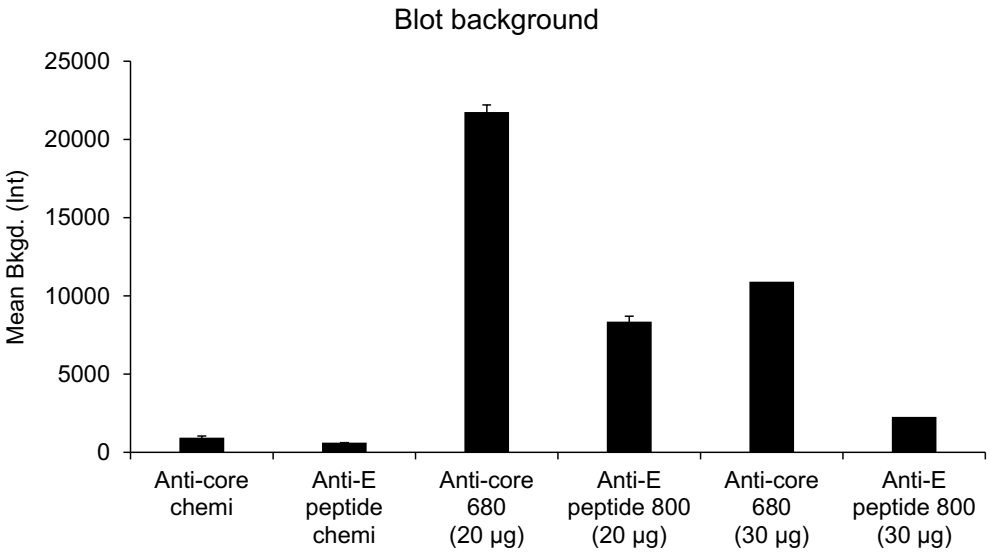

Figure 3. The background intensity of chemiluminescence and fluorescent blot membranes loaded with different amount of protein lysate.

Discussion

Here, we describe a strategy to simultaneously detect the IGF-1 proteoforms by fluorescent WB. Using a mixture of two primary antibodies which recognize different epitopes of the IGF-1 proteoforms and two different fluorescent secondary antibodies, we were able to recognize and discriminate the different components of the complex IGF-1 pool in the same blot. Multiplexed detection by fluorescent WB might offers many experimental benefits. Firstly, fluorescent WB avoids the stripping and re-probing or to compare separate blots. These procedures might introduce errors: stripping can cause inconsistent protein loss that compromises quantification; inadequate stripping of antibodies gives rise to spurious or confusing bands; and inconsistencies in loading and transfer cause substantial blot-to-blot variation. Secondly, the ability to unambiguously detect two targets in the same sample lane makes the analysis more accurate, particularly when two different proteoforms have similar molecular weight (e.g. mature IGF-1 and E-peptides). The increases of experimental throughput and the wide dynamic range, making it unnecessary to use long exposure times or ultra-high sensitivity ECLs, represent other interesting features of fluorescent WB. Finally, using a mixture of primary antibodies that bind to different epitopes of the same protein some proteoforms were simultaneously detected by the two primary antibodies (e.g. proIGF-1s). Using merged images these bands were simply and clearly identified (e.g. fuchsia bands corresponding to glycosylated IGF-1Ea, IGF-1Eb and IGF-1Ec prohormones, Fig. 2A-C). The simultaneous detection of the same protein with two different antibodies, typically used in sandwich ELISA, provides an important advantage in terms of increasing the specificity of target protein detection. This was dramatically shown by the several non-specific bands recognize only by the E-peptide antibody in the negative control sample (HEK-293 cells transfected with an empty vector, Fig. 2C). None of these bands are also recognize by the anti-IGF-1 core antibody (i.e. are fuchsia), clearly representing non-specific proteins. The main limit of fluorescent WB remains the membrane autofluorescence which was only partially reduced using low-fluorescent membrane and near-infrared (IR) dye-conjugated secondary antibodies. The higher blot background compared to chemiluminescent makes difficult to detect and especially quantify low abundant proteins with fluorescent WB.

References

Annibalini, G., Bielli, P., De Santi, M., Agostini, D., Guescini, M., Sisti, D., Contarelli, S., Brandi, G., Villarini, A., Stocchi, V., Sette, C., Barbieri, E., 2016. MIR retroposon exonization promotes evolutionary variability and generates species-specific expression of IGF-1 splice variants. Biochimica et Biophysica Acta (BBA) - Gene Regulatory Mechanisms 1859, 757–768. https://doi.org/10.1016/j.bbagrm.2016.03.014

Annibalini, G., Contarelli, S., De Santi, M., Saltarelli, R., Di Patria, L., Guescini, M., Villarini, A., Brandi, G., Stocchi, V., Barbieri, E., 2018. The intrinsically disordered E-domains regulate the IGF-1 prohormones stability, subcellular localisation and secretion. Sci Rep 8, 8919. https://doi.org/10.1038/s41598-018-27233-3

De Santi, M., Annibalini, G., Barbieri, E., Villarini, A., Vallorani, L., Contarelli, S., Berrino, F., Stocchi, V., Brandi, G., 2016. Human IGF1 pro-forms induce breast cancer cell proliferation via the IGF1 receptor. Cellular Oncology 39, 149–159. https://doi.org/10.1007/s13402-015-0263-3

Di Patria, L., Annibalini, G., Morrone, A., Ferri, L., Saltarelli, R., Galluzzi, L., Diotallevi, A., Bocconcelli, M., Donati, M.A., Barone, R., Guerrini, R., Jaeken, J., Stocchi, V., Barbieri, E., 2022. Defective IGF-1 prohormone N-glycosylation and reduced IGF-1 receptor signaling activation in congenital disorders of glycosylation. Cellular and Molecular Life Sciences 79, 150. https://doi.org/10.1007/s00018-022-04180-x

Gingrich, J.C., Davis, D.R., Nguyen, Q., 2000. Multiplex Detection and Quantitation of Proteins on Western Blots Using Fluorescent Probes. Biotechniques 29, 636–642. https://doi.org/10.2144/00293pf02

Hakuno, F., Takahashi, S.-I., 2018. 40 YEARS OF IGF1: IGF1 receptor signaling pathways. J Mol Endocrinol 61, T69–T86. https://doi.org/10.1530/JME-17-0311

Huang, D., Amero, S.A., 1997. Measurement of Antigen by Enhanced Chemiluminescent Western Blot. Biotechniques 22, 454–458. https://doi.org/10.2144/97223bm18

Kondo, Y., Higa, S., Iwasaki, T., Matsumoto, T., Maehara, K., Harada, A., Baba, Y., Fujita, M., Ohkawa, Y., 2018. Sensitive detection of fluorescence in western blotting by merging images. PLoS One 13, e0191532. https://doi.org/10.1371/journal.pone.0191532

Patonay, G., Antoine, M.D., 1991. Near-Infrared Fluorogenic Labels: New Approach to an Old Problem. Anal Chem 63, 321A-327A. https://doi.org/10.1021/ac00006a716

Patton, W.F., 2000. A thousand points of light: The application of fluorescence detection technologies to two-dimensional gel electrophoresis and proteomics. Electrophoresis 21, 1123–1144. https://doi.org/10.1002/(SICI)1522-2683(20000401)21:6<1123::AID-ELPS1123>3.0.CO;2-E

Philippou, A., Maridaki, M., Pneumaticos, S., Koutsilieris, M., 2014. The Complexity of the IGF1 Gene Splicing, Posttranslational Modification and Bioactivity. Molecular Medicine 20, 202–214. https://doi.org/10.2119/molmed.2014.00011

Sajjad, S., Do, M.T., Shin, H., Yoon, T., Kang, S., 2018. Rapid and efficient western blot assay by rotational cyclic draining and replenishing procedure. Electrophoresis 39, 2974–2978. https://doi.org/10.1002/elps.201800195

Silva, J.M., McMahon, M., 2014. The Fastest Western in Town: A Contemporary Twist on the Classic Western Blot Analysis. Journal of Visualized Experiments. https://doi.org/10.3791/51149

CHAPTER III

Original Article

Insulin-Like Growth Factor-1 promoted growth and tumor spheroid formation of breast cancer cells

Matteo Bocconcelli[1], Giosuè Annibalini[1], Roberta Saltarelli[1], Rita Emili[2], Pierre Savagner [3], Elena Barbieri[1]

[1]Department of Biomolecular Sciences, University of Urbino Carlo Bo, Italy

[2]U.O.C. Oncologia, AST Pesaro Urbino, Ospedale Santa Maria della Misericordia, Urbino, Italy.

[3] IINSERM UMR 1186, Integrative Tumor Immunology and Immunotherapy, Gustave Roussy, Faculty of Medicine, University Paris-Saclay, 94805 Villejuif, France

Abstract

Background: insulin-like growth factor-1 (IGF-1) regulates different aspects of tumor progression in two-dimensional breast cancer (BC) models including proliferation, survival, cell-matrix interactions and migration, while available evidence in BC spheroid models is scarce. **Aim**: to investigate the effect of IGF-1 treatment on MCF-7 and MDA-MB-231 spheroid formation, viability and mRNA expression of metabolic and epithelial-mesenchymal transition (EMT) genes. **Methods**: BC cells were cultured in a U-shaped low attachment 96-Well microplates Nunclon™ Sphera™ with different glucose concentrations (from 0 to 4,5 g/L) and Fetal Bovin Serum (FBS) (from 0,1 to 10%) and treated with recombinant IGF-1 (200 ng/mL). Spheroids morphological parameters (area, round and solidity), viability (Calcein-

AM/Propidium Iodide staining and RealTime-Glo™ MT Cell Viability Assay) and relative quantification of gene expression were performed over 5 days of spheroid formation. **Results**: glucose and FBS depletion inhibited spheroids formation both in MCF-7 and MDA-MB-231 cells, as expected. IGF-1 treatment partially maintained viability and promoted spheroids formation in BC cells starved of glucose and FBS. Unexpectedly, spheroid growth in high glucose (4.5 g/L) and high FBS (>5%) concentrations were less compact with a corona of loose cells compared to spheroids grown under physiological glucose concentrations (0,8 g/L) and low FBS (0.1%). IGF-1 treatment did not modify spheroid morphological parameters and viability under high glucose and FBS culture conditions. On the contrary, IGF-1 stimulated the formation of more compact and viable MCF-7 spheroids in normal glucose and low FBS culture conditions. Molecular data showed an increase of glucose metabolism-related genes (*GAPDH*, *LDHA* and *PKM*), epithelial to mesenchymal transition (EMT) transition (increased *CDH1* and *VIM* mRNAs and decreased *SNAI1* expression) and decreased *KRAS4A/KRAS4B* mRNA ratio in IGF-1-treated MCF-7 spheroids compared to control. **Conclusions**: BC spheroids can be used as an *in vitro* model to better understand the role of IGF-1 system on multiple aspects of tumor progression, including cancer dormancy and EMT transition.

Introduction

IGF-1 cellular actions are mediated by the key signaling component of the IGF-1 system, which includes IGF-1 (ligand), the IGF-1 receptor (IGF-1R), and IGF-1 binding proteins (IGFBPs) (Philippou et al., 2014c). This system plays a crucial role in normal organ development, such as the nervous system, where IGF-1 signaling regulates neuronal proliferation, apoptosis, and cell survival (Barton, 2006; Dyer et al., 2016). Nonetheless, the IGF-1 system is also involved in several pathophysiological processes as well as in the development of different types of solid tumors, including breast cancer (BC) (Christopoulos et al., 2015; Weroha and Haluska, 2012). BC is the most common invasive cancer type among women (Katsura et al., 2022). The chances of survival are influenced by many prognostic factors, including hormonal factors (Pollak, 2012). Concerning that, various studies have been conducted to evaluate possible associations between circulating IGF-1 levels and the risk of developing BC and recurrence (Farabaugh et al., 2015). A study conducted to analyze the risk of breast cancer in the UK biobank female cohort have shown that there is an association between higher circulating IGF-1 levels and the development of breast cancer (Ianza et al., 2021; Murphy et al., 2020). An higher IGF-1 expression is correlated with the luminal A tumor subtype and both higher IGF-1 level and IGF-1R gene expression are associated with increased cell proliferation and with a poor prognosis (Aaltonen et al., 2014; Alkhayyal et al., 2020). Another study found over-expression of IGF-1R in 90% of BC cases, with higher levels in malignant cells than normal tissue and is associated with poor prognosis in patients with early BC (Nielsen et al., 2004; Taunk et al., 2010). Furthermore, there are other data supporting detrimental effects of IGF-1 in other cancer types such as prostate (Armakolas et al., 2010), cervical (KOCZOROWSKA et al., 2011) and colorectal tumor (Kasprzak, 2012). IGF-1 increased cell proliferation and reduced apoptosis in two-dimensional (2D) cancer cell models, even at physiologically relevant concentrations (Casa, 2008). Recently, the use of three-dimensional (3D) cell culture models, such as spheroids and organoids, have gained interest due to the possibility to mimic the tumor microenvironment and the biological processes related to tumor progression, recurrence, and dormancy (Casson et al., 2018; Doffe et al., 2022; Fontana et al., 2020). In this study, we analyze the effect of high physiological concentration of IGF-1 on MCF-7 (Luminal A) and MDA-MB-231

(Triple Negative) spheroid formation (Bytautaite and Petrikaite, 2020). BC spheroids formation and the role of IGF-1 was also evaluated in the presence of microenvironment stress conditions that naturally occur in solid tumor (Zaarour et al, 2023), using serum and glucose starvation.

Materials and Methods

MCF-7 and MDA-MB-231 spheroid preparation

MCF-7 and MDA-MB-231 cells were obtained from the American Type Culture Collection (ATCC, Rockville, MD, USA). Cells were growth in DMEM media supplemented with 10% fetal bovine serum, 2 mM L-glutamine, 1x MEM Non-essential Amino Acid Solution, 0.1 mg/ml streptomycin and 0.1 U/L penicillin. Cell viability were determined by the LUNA-II™ Automated Cell Counter (Logos Biosystems, Twin Helix) with trypan blue staining BC spheroids were formed in U-shaped low attachment 96-well microplates (Nunclon™ Sphera™, ThermoFisher) at a density of about 6.000 cells per well with 200 ul of DMEM medium without phenol red. Different glucose (from 0 to 4,5 g/L) and Fetal Bovin Serum (FBS) (from 0,1 to 10%) concentrations were used to form spheroids. After cell seeding, the 96 well plate was centrifuged at speed of 300 x g for 3 min. and maintained in a humidified incubator (5% CO_2) at 37 °C and allowed to grow for 5 days. Spheroids morphological parameters (area, round and solidity) viability and gene expression analysis were performed over 5 days of formation.

Preparation of HEK-293 cell medium enriched of IGF-1

HEK-293 overexpressing the *IGF-1Ea* isoform or an empty vector were seeded in a 12-well plate at density of about 150.000 cells per well in a DMEM medium without phenol red with 2,4 g/l of glucose concentration and low FBS concentration (0,1% FBS). After 24h HEK-293 cells were washed with sterile PBS and shifted in the DMEM medium without glucose and

FBS for 48 h. The IGF-1 level in the culture media were quantified using an ELISA assay (R & D System, cat. n. DY291).

Breast Cancer spheroids vitality assays

BC spheroids vitality was assessed by staining the cells directly in the 96-well plate with 2 ul of Propidium Iodide (0.1M) (PI) and 1 ul of Calcein AM (1 mM) diluted 1/30. The plate was incubated at 37 °C and 5% CO_2 for 120 min with PI and for 30 min with the Calcein AM and then analyzed using the TOUP CAM TM E31SPM05000KPA digital camera connected to a Leica microscope DMLB and the Toup View software. BC spheroids vitality was assessed also using RealTime Glo™ MT Cell Viability Assay (Promega), according to manufacture's instruction. Briefly, three BC spheroids were collected, and 0.6 µl of MT Cell Viability Substrate and 0,6 µl of NanoLuc® Enzyme were added in a 50 µl of DMEM medium. BC spheroids were incubated in a cell culture incubator at 37°C and 5% CO_2 for 1 hour. Luminescence was quantified by the Fluoroskan FL luminometer plate-reader (Thermo Fisher Scientific).

RNA extraction, cDNA synthesis and quantitative real-time polymerase chain reaction

BC spheroids were recovered from the U-shaped low attachment 96-Well microplates using cut tips. BC spheroids were lysed adding 100 ul of QIAzol Lysis Reagent (Qiagen, cat. n. 79306) and stored at -80 degrees. The total RNA was extracted using the RNeasy Mini Kit (Qiagen, cat. n. 74106). The amount and quality of RNA were assessed with the SpectraMax QuickDrop Micro-Volume UV-Vis Spectrophotometer (Molecular Devices, San Jose, CA, USA). The complementary DNA was synthesized from 500 ng of total RNA using the PrimeScript RT Master Mix (Takara Bio Europe). Genes of interest were quantified in an Applied Biosystems StepOnePlus™ Real-Time PCR System using PowerUp SYBR Green Master Mix (Thermo Fisher Scientific, Monza, Italy). All amplification reactions were performed in duplicate. The amplification conditions were: 50°C for 2 min followed by 40 cycles of two-steps at 95°C for 15 s and 60°C for 60 s. At the end of each run, a melting curve

analysis from 65 °C to 95 °C was performed to exclude the presence of non-specific products or primer dimers. The data were normalized using 36B4 gene. The relative expression levels were calculated using the $2^{-\Delta\Delta Ct}$ method (Pfaffl, 2001).

Statistical analysis

Data are represented as mean ± SD of at least three independent experiments. Statistical analyses were performed using independent samples t-test, repeated measures ANOVA or two-way ANOVA as appropriate, followed by Bonferroni's multiple comparison post hoc tests. A p-value < 0.05 was considered statistically significant.

Results

IGF-1 promotes growth, tumor spheroid formation and viability of breast cancer spheroids

Firstly, we analysed the effects of different glucose (from 0 to 4,5 g/L) and FBS (from 0,1 to 10%) concentrations on MCF-7 and MDA-MB-231 spheroids formation. Using high glucose (4.5 g/L) and FBS (5-10%) DMEM media the MDA-MB-231 cells formed a fairly compact spheroid after 2-3 days (T2-T3) post-seeding (Fig. 1A). Live/dead assay on MDA-MB-231 spheroids show the different distribution of live (external) and dead (internal) cells in the spheroid structure, as expected (Keller et al., 2021). The behavior of MCF-7 cells completely differed compared to MDA-MB-231 cells (Fig. 1B). In particular, when MCF-7 were grown in high glucose and FBS DMEM media failed to form a compact spheroid and only cell aggregates were observed. Collagen, hyaluronic acid or Poly-L-Lysine matrix did not ameliorate the MCF-1 spheroids formation in high glucose and FBS DMEM media (not shown). Subsequently, we tried to obtain more compact MCF-7 spheroids using DMEM media with low glucose and/or FBS concentration. Interestingly, more compact MCF-7

spheroid formation was observed with physiological glucose concentrations (0,8 g/L) and low FBS (0.1%) (Fig. 1C).

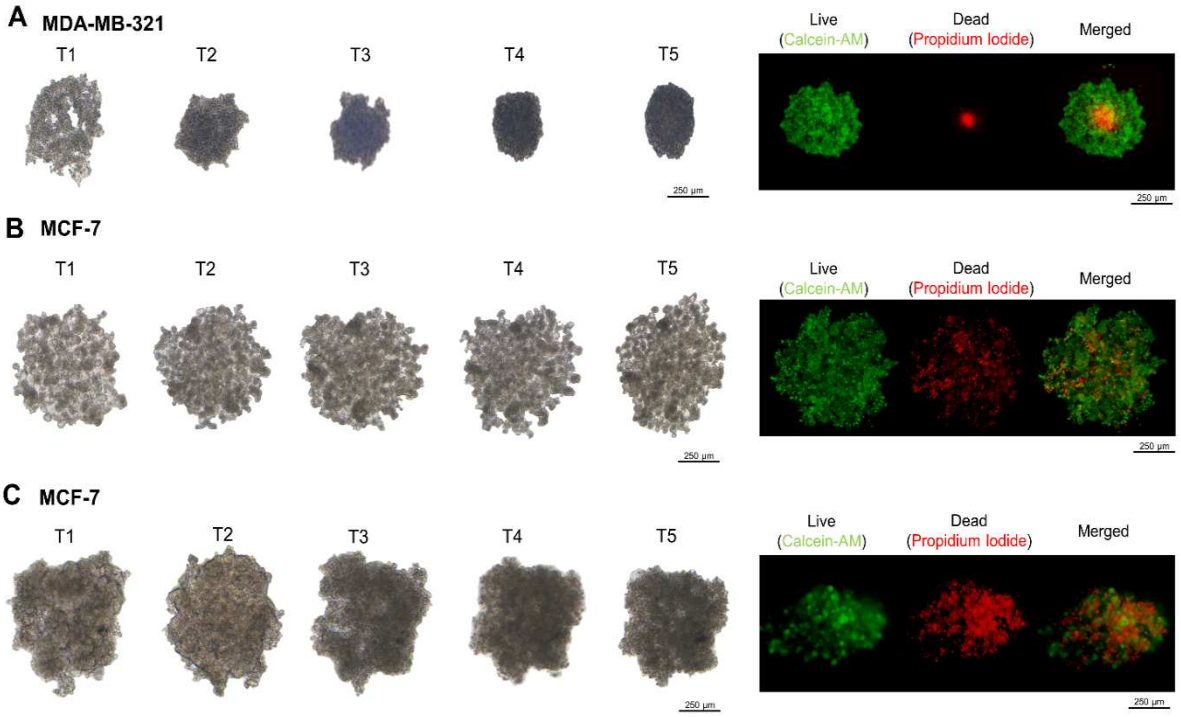

Figure 1. Effect of different glucose and FBS concentrations on MDA-MB-231 and MCF-7 spheroid formation.(A)MDA-MB-231 spheroids cultured in high glucose (4.5 g/L) and FBS (5 %) DMEM medium.(B) MCF-7 spheroids cultured in high glucose (4.5 g/L) and FBS (5 %) DMEM medium and in physiological glucose concentrations (0,8 g/L) and low FBS (0.1%)(C).The right panel shows the Calcein-AM (green, live cells) and Propidium Iodide (red, dead cells) staining.

Subsequently, we analyzed the effect of 200 ng/mL IGF-1 treatment on MDA-MB-231 and MCF-7 spheroids formation. IGF-1 treatment increased MDA-MB-231 spheroid area and cell viability compared to the untreated cells (Fig. 2A).

Figure 2. Effect of IGF-1 treatment (200 ng/mL) on MDA-2B-231 spheroid formation. MDA-2B-231 were cultured in high glucose (4.5 g/L) and FBS (5 %) DMEM medium. The right panel shows the Calcein-AM (green, live cells) and Propidium Iodide (red, dead cells) staining.

In MCF-7 cells grown in low-normal glucose medium (0.8 g/L glucose and 0.1 % FBS), IGF-1 treatment (200 ng/mL) promoted spheroid formation, circularity and compactness (Fig. 3). Moreover, MCF-7 spheroids treated with IGF-1 showed a well-defined outer perimeter and were more viable compared to untreated cells, with a necrotic core composed of dead cells and a perimeter of live proliferating cells (Fig. 4).

Figure 3. Effect of IGF-1 treatment (200 ng/mL) on MCF-7 spheroid formation. MCF-7 were cultured in low glucose (0.8 g/L) and FBS (0.1 %) DMEM medium. The right panel shows the MCF-7 spheroids area. # Significantly different compared to CTR p=0.05; * significantly different compared to T1 p=0.05.

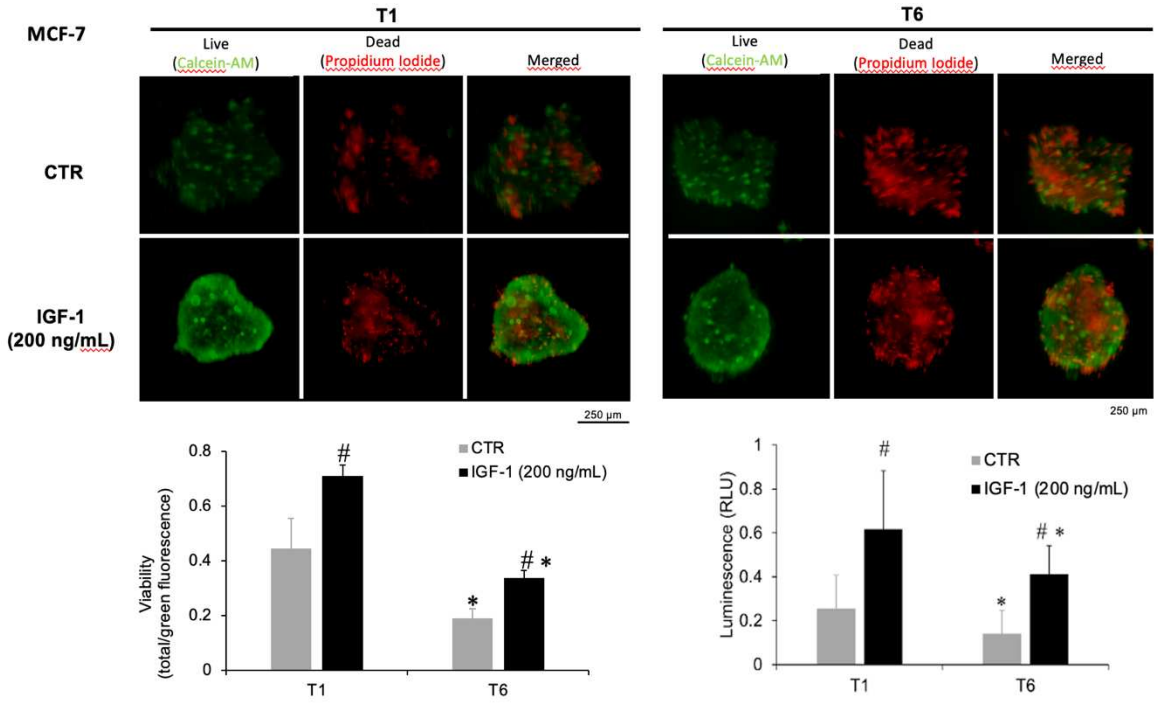

Figure 4. Effect of IGF-1 treatment (200 ng/mL) on MCF-7 spheroid viability measured by Live/Dead fluorescent assay and RealTime-GloTM MT Cell Viability Assay (bottom-right graph). Calcein-AM (green, live cells) and Propidium Iodide (red, dead cells) staining. # Significantly different compared to CTR p=0.05; * significantly different compared to T1 p=0.05.

Similar results were observed in MCF-7 cultured with the medium obtained from HEK-293 overexpressing the IGF-1Ea isoform (Fig. 5C). Interestingly, neither medium obtained from HEK-293 overexpressing the empty vector (Fig. 5A) nor that obtained from HEK-293 overexpressing the IGF-1Ea isoform but cultured in 0 g/L glucose (Fig. 5B) increased the MCF-7 spheroid formation. Accordingly, we found that the IGF-1 levels in the culture supernatant were undetectable in HEK-293 overexpressing the empty vector and very low in HEK-293 overexpressing the IGF-1Ea isoform cultured in 0 g/L glucose (7.7 ± 1.2 ng/mL) compared to those cultured in 2.4 g/L glucose (101.7 ± 28.7).

Figure 5. Effect of HEK-293 conditioned medium on MCF-7 spheroid formation. Cell culture supernatant obtained from HEK-293 cells transfected with (A) an empty vector or a vector containing the IGF-1Ea isoform in (B) medium without glucose (0 g/L) or (C) with 2.4 g/L of glucose.

IGF-1 increases gene expression of metabolic and EMT markers

Subsequently, we analyzed a panel of genes related to metabolism (*GAPDH, GLUT1, HK1, HK2, LDHA, PKM and VDAC*), EMT (*CDH1*, *VIM*, *SNAI1* and *Erα*) and KRAS isoforms during the early phases (day 1) of MCF-7 spheroid formation (Fig. 6). Molecular data showed an increase of *GAPDH, LDHA and PKM* mRNA expression in IGF-1-treated spheroids compared to CTR (Fig. 6A). Concerning EMT markers, we observed an increase of *CDH1* and *VIM* mRNA level while SNA1 expression decreased in IGF-1-treated MCF-7 spheroids compared to CTR (Fig. 6B). Finally, IGF-1 treatment decreased the KRAS4A/KRAS4Bratio (Fig. 6C). Similar results were obtained after treatment of MCF-7 spheroids with medium of HEK-293 cells overexpressing the IGF1Ea isoform (not shown). These results are in line with recent studies highlighting an important role of IGF-1 on cellular metabolism and EMT models (Işeri et al., 2011; Zhao et al., 2017), indicating a possible role of the IGF-1 system on multiple aspects of tumor progression.

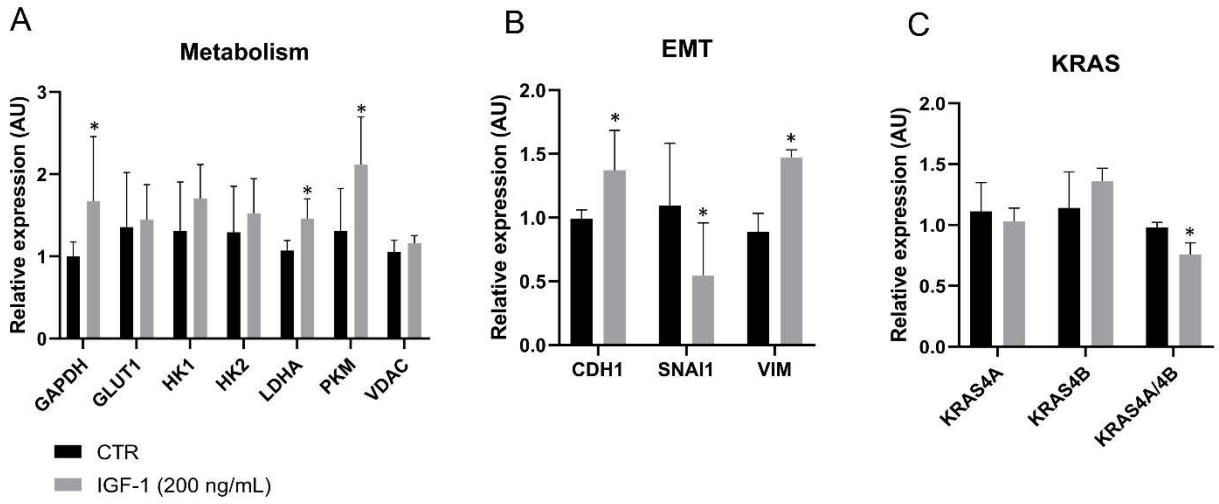

Figure 6. Effect of IGF-1 treatment (200 ng/mL) on (A) metabolism genes, (B) EMT-related genes and (C) KRAS isoforms mRNAs. * Significantly different compared to CTR p=0.05.

Discussion

In this study, we investigated the role of IGF-1 on BC spheroid formation. viability and mRNA expression of metabolic and epithelial-mesenchymal transition (EMT) genes. Several studies have demonstrated a key role of IGF-1 in BC development, recurrence and disease severity, especially in luminal A subtype (Farabaugh et al., 2015; Ianza et al., 2021). Molecular mechanisms explaining the pro-tumorigenic functions of IGF-1 have been mainly studied in 2D cell models while the effects of IGF-1 on more complex and organized models, such as spheroids are relatively scarce. Here, we analyzed the effect of IGF-1 on spheroid formation using both MDA-MB-231 and MCF-7 cells. According to scientific literature, MCF-7 cells (luminal A model) are more responsive and sensitive model toward the action of IGF-1 due to the greater abundance of IGF-1R on their cell surface compared to MDA-MB-231 cells (triple-negative BC model) (O'Flanagan et al., 2016; Panagiotis et al., 2017; Zhang et al., 2021). Here, we demonstrated that MCF-7 and MDA-MB-231 spheroid formation varies with cell culture conditions. In particular, MDA-MB-231 were capable of forming a fairly compact spheroid under high glucose (4.5 g/L) and FBS (5%) medium and without IGF-1 treatment (Fig. 1A). IGF-1 treatment partially increases MDA-MB-231 spheroid area and cells viability

(Fig. 2). Interestingly, MCF-7 behave differently compared to MDA-MB-231. In fact, MCF-7 failed to form compact spheroids in high glucose and serum cell culture medium (Fig. 1B). On the contrary, low-normal glucose medium partially promoted MCF-7 spheroids formation and compactness (Fig. 1C). More interestingly, IGF-1 treatment (200 ng/mL) stimulated the formation of compact MCF-7 spheroids in a low-normal glucose medium, with a well-defined boarder area (Fig. 3). IGF-1 treatment increased the MCF-7 spheroids viability assessed by fluorescent Live/Dead assay and luminescent RealTime-GloTM assay (Fig. 4). Interestingly, similar results were obtained seeded MCF-7 spheroids with medium of HEK-293 cells overexpressing the *IGF1Ea* isoform (Fig. 5C). On the contrary, neither cell culture medium obtained form HEK-293 cells overexpressing an empty vector or the *IGF1Ea* isoforms but grown in DMEM medium without glucose increased the MCF-7 spheroid formation. This result was in accordance with our previous studies showing that glucose is necessary for correct IGF-1Ea N-glycosylation and IGF-1 secretion. Subsequently, we evaluated the effect of IGF-1 on the modulation of metabolic-related genes (GAPDH*, GLUT1, HK1, HK2, LDHA, PKM* and *VDAC*), EMT process (*CDH1*, *SNAI1, VIM*) and the mRNA isoforms of the oncogene *KRAS*. It's well established the role of IGF-1 in increasing cell proliferation, protein synthesis and growth, cell-matrix interactions and inhibiting apoptosis and metabolism, especially glucose uptake (Weroha and Haluska, 2012). Particularly, *Kasprzak et* al reported an interaction between the IGF-1 system and the activation of glucose transporters (e.g., GLUT1) and key glycolytic enzymes (e.g., LDHA, LDH5, HK II, and PFKFB3) in colorectal cancer (Kasprzak, 2021). In addition, several studies have emphasized its role in increasing the EMT, a biological process that enables a polarized epithelial cell, which usually interacts with the basement membrane through its basal surface, to undergo several biochemical changes (Işeri et al., 2011; Lv et al., 2021; Perks et al., 2015). This transformation allows the cell to acquire a mesenchymal cell phenotype, which includes increased migratory capacity, invasiveness, resistance to apoptosis, and elevated production of ECM components. (Kalluri and Neilson, 2003). Concerning that, it is widely described that during the transition to an epithelial state to a mesenchymal state of cancer cell, gene expression of *Cadherin-1* (*CDH1)* Vimentin (*VIM*) and *Snail Family Transcriptional Repressor 1* (*SNAI1*) (Loh et al., 2019; Perks et al., 2015; Walsh and Damjanovski, 2011) are modulated. Accordingly, to these studies, we found that IGF-1 treatment increased *CDH1* and *VIM* mRNA expression and decreased *SNAI1* levels and *KRAS4A/KRAS4B* mRNA ratio in MCF-7 spheroids. In conclusion, here we

demonstrated that IGF-1 treatment increased the spheroid formation and viability, also modulating gene expression of metabolism and EMT markers. Future analyses about the glycolytic pathway's enzymatic activity will help us confirm and strengthen molecular data obtained from qPCR. In addition, Next Generation Sequencing (NGS) on BC spheroids can help to elucidate the molecular mechanisms through which IGF-1 affects spheroids structure, metabolism and oncogenic EMT process. These results highlight how the development of 3D tumor model for BC will allow us to increase our knowledge of the role of IGF-1 on multiple aspects of tumor progression, suggesting an involvement of IGF-1 on the structure, metabolism and oncogenic EMT function of BC tumor spheroids. Moreover, scanning electron microscope (SEM) and transmission electron microscope (TEM) analyses will be planned to further investigate BC spheroids morphological aspects and to improve the visualization on cellular organization and structural composition of spheroids. To conclude this 3D BC model will be used e, to elucidate and study a possible pharmacological action regarding the effect of the N-glycosylation inhibition (e.g. tunicamycin, 2-deoxy-d-glucose, glucose starvation, imminosugar, ALG3 mutants) on IGF-1 production and IGF-1R activation.

References

Aaltonen, K.E., Rosendahl, A.H., Olsson, H., Malmström, P., Hartman, L., Fernö, M., 2014. Association between insulin-like growth factor-1 receptor (IGF1R) negativity and poor prognosis in a cohort of women with primary breast cancer. BMC Cancer 14, 794. https://doi.org/10.1186/1471-2407-14-794

Alkhayyal, N., Talaat, I., Vinodnadat, A., Maghazachi, A., Abusnana, S., Syrjanen, K., Bendardaf, R., 2020. Correlation of Insulin-like Growth Factor 1 Receptor Expression With Different Molecular Subtypes of Breast Cancer in the UAE. Anticancer Res 40, 1555–1561. https://doi.org/10.21873/anticanres.14102

Armakolas, A., Philippou, A., Panteleakou, Z., Nezos, A., Sourla, A., Petraki, C., Koutsilieris, M., 2010. Preferential expression of IGF-1Ec (MGF) transcript in cancerous tissues of human prostate: Evidence for a novel and autonomous growth factor activity of MGF E peptide in human prostate cancer cells. Prostate 70, 1233–1242. https://doi.org/10.1002/pros.21158

Barton, E.R., 2006. The ABCs of IGF-I isoforms: impact on muscle hypertrophy and implications for repair. Applied Physiology, Nutrition, and Metabolism 31, 791–797. https://doi.org/10.1139/h06-054

Bytautaite, M., Petrikaite, V., 2020. Comparative Study of Lipophilic Statin Activity in 2D and 3D in vitro Models of Human Breast Cancer Cell Lines MDA-MB-231 and MCF-7. Onco Targets Ther Volume 13, 13201–13209. https://doi.org/10.2147/OTT.S283033

Casa, A.J., 2008. The type I insulin-like growth factor receptor pathway: a key player in cancer therapeutic resistance. Frontiers in Bioscience Volume, 3273. https://doi.org/10.2741/2925

Casson, J., Davies, O.G., Smith, C.-A., Dalby, M.J., Berry, C.C., 2018. Mesenchymal stem cell-derived extracellular vesicles may promote breast cancer cell dormancy. J Tissue Eng 9, 204173141881009. https://doi.org/10.1177/2041731418810093

Christopoulos, P.F., Msaouel, P., Koutsilieris, M., 2015. The role of the insulin-like growth factor-1 system in breast cancer. Mol Cancer 14, 43. https://doi.org/10.1186/s12943-015-0291-7

Doffe, F., Bonini, F., Lakis, E., Terry, S., Chouaib, S., Savagner, P., 2022. Designing Organoid Models to Monitor Cancer Progression, Plasticity and Resistance: The Right Set Up for the Right Question. Cancers (Basel) 14, 3559. https://doi.org/10.3390/cancers14153559

Dyer, A.H., Vahdatpour, C., Sanfeliu, A., Tropea, D., 2016. The role of Insulin-Like Growth Factor 1 (IGF-1) in brain development, maturation and neuroplasticity. Neuroscience 325, 89–99. https://doi.org/10.1016/j.neuroscience.2016.03.056

Farabaugh, S.M., Boone, D.N., Lee, A. V., 2015. Role of IGF1R in Breast Cancer Subtypes, Stemness, and Lineage Differentiation. Front Endocrinol (Lausanne) 6. https://doi.org/10.3389/fendo.2015.00059

Fontana, F., Raimondi, M., Marzagalli, M., Sommariva, M., Gagliano, N., Limonta, P., 2020. Three-Dimensional Cell Cultures as an In Vitro Tool for Prostate Cancer Modeling and Drug Discovery. Int J Mol Sci 21, 6806. https://doi.org/10.3390/ijms21186806

Ianza, A., Sirico, M., Bernocchi, O., Generali, D., 2021. Role of the IGF-1 Axis in Overcoming Resistance in Breast Cancer. Front Cell Dev Biol 9. https://doi.org/10.3389/fcell.2021.641449

Işeri, Ö.D., Kars, M.D., Arpaci, F., Atalay, C., Pak, I., Gündüz, U., 2011. Drug resistant MCF-7 cells exhibit epithelial-mesenchymal transition gene expression pattern. Biomedicine & Pharmacotherapy 65, 40–45. https://doi.org/10.1016/j.biopha.2010.10.004

Kalluri, R., Neilson, E.G., 2003. Epithelial-mesenchymal transition and its implications for fibrosis. Journal of Clinical Investigation 112, 1776–1784. https://doi.org/10.1172/JCI20530

Kasprzak, A., 2021. Insulin-Like Growth Factor 1 (IGF-1) Signaling in Glucose Metabolism in Colorectal Cancer. Int J Mol Sci 22, 6434. https://doi.org/10.3390/ijms22126434

Kasprzak, A., 2012. Differential expression of IGF-1 mRNA isoforms in colorectal carcinoma and normal colon tissue. Int J Oncol. https://doi.org/10.3892/ijo.2012.1706

Katsura, C., Ogunmwonyi, I., Kankam, H.K., Saha, S., 2022. Breast cancer: presentation, investigation and management. Br J Hosp Med 83, 1–7. https://doi.org/10.12968/hmed.2021.0459

Keller, F., Bruch, R., Clauder, F., Hafner, M., Rudolf, R., 2021. Extracellular Matrix Components Regulate Bone Sialoprotein Expression in MDA-MB-231 Breast Cancer Cells. Cells 10, 1304. https://doi.org/10.3390/cells10061304

KOCZOROWSKA, M.M., KWASNIEWSKA, A., GOZDZICKA-JOZEFIAK, A., 2011. IGF1 mRNA isoform expression in the cervix of HPV-positive women with pre-cancerous and cancer lesions. Exp Ther Med 2, 149–156. https://doi.org/10.3892/etm.2010.174

Loh, C.-Y., Chai, J., Tang, T., Wong, W., Sethi, G., Shanmugam, M., Chong, P., Looi, C., 2019. The E-Cadherin and N-Cadherin Switch in Epithelial-to-Mesenchymal Transition: Signaling, Therapeutic Implications, and Challenges. Cells 8, 1118. https://doi.org/10.3390/cells8101118

Lv, J., Liu, C., Chen, F.-K., Feng, Z.-P., Jia, L., Liu, P.-J., Yang, Z.-X., Hou, F., Deng, Z.-Y., 2021. M2-like tumour-associated macrophage-secreted IGF promotes thyroid cancer stemness and metastasis by activating the PI3K/AKT/mTOR pathway. Mol Med Rep 24, 611. https://doi.org/10.3892/mmr.2021.12249

Murphy, N., Knuppel, A., Papadimitriou, N., Martin, R.M., Tsilidis, K.K., Smith-Byrne, K., Fensom, G., Perez-Cornago, A., Travis, R.C., Key, T.J., Gunter, M.J., 2020. Insulin-like growth factor-1, insulin-like growth factor-binding protein-3, and breast cancer risk: observational and Mendelian randomization analyses with ∼430 000 women. Annals of Oncology 31, 641–649. https://doi.org/10.1016/j.annonc.2020.01.066

Nielsen, T.O., Andrews, H.N., Cheang, M., Kucab, J.E., Hsu, F.D., Ragaz, J., Gilks, C.B., Makretsov, N., Bajdik, C.D., Brookes, C., Neckers, L.M., Evdokimova, V., Huntsman, D.G., Dunn, S.E., 2004. Expression of the Insulin-Like Growth Factor I Receptor and Urokinase Plasminogen Activator in Breast Cancer Is Associated with Poor Survival. Cancer Res 64, 286–291. https://doi.org/10.1158/0008-5472.CAN-03-1242

Perks, C., Zielinska, H., Holly, J., Bahl, A., 2015. Epithelial-to-mesenchymal transition in breast cancer: a role for insulin-like growth factor I and insulin-like growth factor–binding protein 3? Breast Cancer: Targets and Therapy 9. https://doi.org/10.2147/BCTT.S43932

Pfaffl, M.W., 2001. A new mathematical model for relative quantification in real-time RT-PCR. Nucleic Acids Res 29, 45e–445. https://doi.org/10.1093/nar/29.9.e45

Philippou, A., Maridaki, M., Pneumaticos, S., Koutsilieris, M., 2014. The Complexity of the IGF1 Gene Splicing, Posttranslational Modification and Bioactivity. Molecular Medicine 20, 202–214. https://doi.org/10.2119/molmed.2014.00011

Pollak, M., 2012. The insulin and insulin-like growth factor receptor family in neoplasia: an update. Nat Rev Cancer 12, 159–169. https://doi.org/10.1038/nrc3215

Taunk, N.K., Goyal, S., Moran, M.S., Yang, Q., Parikh, R., Haffty, B.G., 2010. Prognostic significance of IGF-1R expression in patients treated with breast-conserving surgery and radiation therapy. Radiotherapy and Oncology 96, 204–208. https://doi.org/10.1016/j.radonc.2010.03.009

The COOH-terminus of the IGF-1Ec Isoform Enhances the Proliferation and Migration of Human MCF-7 Breast Cancer Cells, 2017. . Anticancer Res 37. https://doi.org/10.21873/anticanres.11643

Walsh, L.A., Damjanovski, S., 2011. IGF-1 increases invasive potential of MCF 7 breast cancer cells and induces activation of latent TGF-β1 resulting in epithelial to mesenchymal transition. Cell Communication and Signaling 9, 10. https://doi.org/10.1186/1478-811X-9-10

Weroha, S.J., Haluska, P., 2012. The Insulin-Like Growth Factor System in Cancer. Endocrinol Metab Clin North Am 41, 335–350. https://doi.org/10.1016/j.ecl.2012.04.014

Zaarour RF, Ribeiro M, Azzarone B, Kapoor S, Chouaib S. Tumor microenvironment-induced tumor cell plasticity: relationship with hypoxic stress and impact on tumor resistance. Front Oncol. 2023 Oct 11;13:1222575. doi: 10.3389/fonc.2023.1222575. PMID: 37886168; PMCID: PMC10598765.

Zhao, C., Wang, Q., Wang, B., Sun, Q., He, Z., Hong, J., Kuehn, F., Liu, E., Zhang, Z., 2017. IGF-1 induces the epithelial-mesenchymal transition via Stat5 in hepatocellular carcinoma. Oncotarget 8, 111922–111930. https://doi.org/10.18632/oncotarget.22952

CHAPTER IV

Original Article

Impaired myoblast differentiation and muscle IGF-1 receptor signalling pathway activation after N-glycosylation inhibition

Giosuè Annibalini[1], Laura Di Patria[1], Giacomo Valli[2], Matteo Bocconcelli[1], Roberta Saltarelli[1], Lorenzo Ferri[3], Laura Barberi[4], Amelia Morrone[3,5], Rita Barone[6,7], Renzo Guerrini[3,5], Antonio Musarò[4], Vilberto Stocchi[8], Elena Barbieri[1]

[1]University of Urbino Carlo Bo, Department of Biomolecular Sciences, Urbino, Italy;
[2]University of Brescia, Department of Clinical and Experimental Sciences, Brescia, Italy
[3]Meyer Children's Hospital IRCSS, Molecular and Cell Biology Laboratory of Neurometabolic Diseases, Neuroscience Department, Florence, Italy;
[4]University of Rome La Sapienza, DAHFMO-Unit of Histology and Medical Embryology, Rome, Italy;
[5]University of Florence, Department of NEUROFARBA, Florence, Italy;
[6]University of Catania, Child Neurology and Psychiatry Unit, Department of Clinical and Experimental Medicine, Catania, Italy;
[7]Oasi Research Institute-IRCCS, Reseach Unit of Rare Diseases and Neurodevelopmental Disorders, Troina, IT;
[8] University San Raffaele, Department of Human Sciences for the Promotion of Quality of Life, Roma, IT.

Keywords

Myoblast differentiation, N-glycosylation, IGF1R signalling pathway, muscle atrophy, PMM2, Congenital Disorders of Glycosylation

Summary statement

Reduced myogenic differentiation, IGF-1 production and IGFR signalling pathway activation could be key factors in the pathophysiology of muscle-related manifestations commonly found in congenital disorders of N-glycosylation.

Abstract

The role of N-glycosylation in the myogenic process remains poorly characterized. We evaluated the impact of N-glycosylation inhibition by Tunicamycin (TUN) or by phosphomannomutase 2 (*PMM2*) gene knockdown on C2C12 myoblast differentiation. Moreover, the effect of chronic treatment with TUN on tibialis anterior (TA) of WT and MLC/mIgf-1 transgenic mice, which overexpress muscle *Igf-1Ea* mRNA isoform, was investigated. TUN-treated and *PMM2* knockdown C2C12 showed reduced lectin binding and increased ER-stress-related gene expression compared to control. Myogenic markers and myotube formation were reduced both in TUN-treated and *PMM2* knockdown C2C12. Body and TA weight of WT and MLC/mIgf-1 mice were not modified by TUN treatment, while the lectin binding profile slightly decreased in the TA muscle of WT mice. Notably, TUN treatment increased atrophy markers, particularly in the TA muscle of WT mice. Finally, the IGF-1 production and IGF1R signalling pathways activation was reduced due to N-glycosylation inhibition. Chronic TUN-challenge models can help to elucidate the molecular mechanisms through which diseases associated with aberrant N-glycosylation, such as Congenital Disorders of Glycosylation (CDG), affect muscle and other tissue functions.

Introduction

Myogenesis is a complex and highly regulated process that requires myoblast proliferation, alignment of cells, and subsequent fusion into multinucleated myotubes [1]. Many steps of myogenesis can be recapitulated *in vitro* through myogenic cell lines such as mouse C2C12 and rat L6E9, which in the absence of mitogenic stimuli form multinucleated myotubes [1]. The myogenic program is tightly coupled to a complex network of signal transduction pathways regulating the expression of myogenic regulatory factors (MRFs), a group of basic helix-loop-helix transcription factors that include: MyoD, Myf5, myogenin and Mrf4 [1,2]. Besides the canonical MRF, other molecular actors such as insulin-like growth factor-1 (IGF-1) are directly involved in the myogenesis process [3]. The primary effects of IGF-1 are mediated by binding to the IGF-1 receptor (IGF1R), a ligand-activated receptor tyrosine kinase. IGF1R signal transduction occurs through the PI3K/AKT/mTOR and RAF/MEK/ERK pathways which promotes muscle protein synthesis and inhibits muscle protein degradation [4]. Growing evidence highlights the role of protein glycosylation in myoblast fusion and differentiation [5–9]. Gundry R.L. et al. identified 128 glycosylated proteins in the C2C12 myoblast cell surface, including Insulin Receptor (IR) and IGF1R [10]. More recently, Blazev R. et al. demonstrated a dynamic change in proteomic, N-glycomic and N-glycoproteomic during rat L6 myotube formation [9]. Interestingly, the abundances of lectins and enzymes involved in glycan biosynthesis and remodeling were modulated after the differentiation of myoblasts toward myotubes, suggesting that temporal and site-specific glycosylation is important for skeletal muscle cell development, differentiation, and function [9]. During myoblast differentiation, increased binding of lectins with different carbohydrate specificities [11,12] and regulation of N-glycan content of glycoproteins [9], including several integrins and growth factor receptors, has been shown. The role of proper protein muscle glycosylation in human diseases is dramatically illustrated by the group of dystroglycanopathies, genetic disorders caused by the defective O-mannosylation of α-Dystroglycan protein [13]. However, in contrast to the extensively studied O-mannosyl glycan defect, the role of muscle protein N-glycosylation remains poorly characterized. Early evidence suggested that pharmacological inhibition of N-glycosylation by Tunicamycin (TUN), an antibiotic that interferes with the transfer of N-acetylglucosamine-1-phosphate

from uridine 5-diphosphate-N-acetylglucosamine to dolichol monophosphate in the first steps of protein N-glycosylation, blocked fusion of embryonic quail muscle cells [14]. More recently, Xia et al. demonstrated that TUN treatment of C57BL/6 J mice increased ER stress markers in the liver, decreased liver *IGF-1* mRNA expression and IGF-1 serum level and reduced body growth and body weight gain [15]. However, the impact of TUN treatment on muscle tissues was not analysed in this study. Moreover, a wide spectrum of neuromuscular syndromes ranging from muscle dystrophies to congenital myopathies/myastenic syndromes have been associated with Congenital Disorders of Glycosylation (CDG) caused by genetic N-glycosylation defects [16]. According to a recently updated classification system, CDG are inborn errors of metabolism following a Mendelian pattern of inheritance characterized by "substantial hypoglycosylation in one or more cell types" [17]. Over 160 CDG have been reported in protein and lipid glycosylation accounting for more than 200 phenotypes [17]. PMM2-CDG is caused by pathogenetic variants in the *PMM2* gene encoding the enzyme phosphomannomutase 2 (PMM2) that converts mannose-6-phosphate to mannose-1-phosphate, the obligatory precursor for GDP-mannose production and hence N-linked glycosylation [18]. The global suppression of N-glycosylation occurring in PMM2-CDG leads to a variety of symptoms affecting multiple systems. In patients with PMM2-CDG prominent cerebellar ataxia due to progressive cerebellar atrophy in association with other neuromuscular symptoms such as peripheral neuropathy causes functional disability with most patients unable to walk independently [19,20]. Notwithstanding this evidence, the rate and severity of myopathy in PMM2-CDG are still unexplored. In the present study, using mouse C2C12 we evaluate the impact of N-glycosylation inhibition by TUN or PMM2 knockdown by CRISPR/Cas9 on myoblast differentiation. Moreover, 6-week-old wild-type (WT) and MLC/mIgf-1 transgenic FVB mice, overexpressing the *insulin-like growth factor-1Ea* (*Igf-1Ea*) isoform under the control of the myosin light chain (MLC) promoter [21], were chronically challenged with a sub-phenotypic dose of TUN to mimic mild CDG-like condition. Tibialis anterior (TA) and extensor digitorum longus (EDL) muscles were collected to evaluate the impact of N-glycosylation inhibition on lectin binding, ER-stress-related gene expression and IGF-1 signalling pathway activation. We demonstrated that TUN-treatment as well as PMM2 downregulation inhibit C2C12 myoblast fusion and impair the early stage of the myogenic program. TUN treatment decreased myogenic markers in TA and EDL muscles of WT and MLC/mIgf-1 mice while atrogene expression increased only in WT mice. Finally,

muscle IGF-1Ea prohormone production and IGF1R signalling pathway activation were markedly inhibited after TUN treatment. Our results offer new insights which increase understanding of possible impairments of the myogenic differentiation capacity in the pathological context of disorders of N-glycosylation.

Materials and Methods

Cell cultures

C2C12 mouse myoblasts (Sigma-Aldrich, Italy), CRISPR-CTR and CRISPR-PMM2 C2C12, and rat L6E9 myoblasts [38] were cultured in Dulbecco's Modified Eagle Medium (DMEM) supplemented with 10% heat-inactivated fetal bovine serum (FBS), 2 mM glutamine, penicillin (100 U/mL) and streptomycin (100 µg/mL), and maintained in a 5% CO_2 atmosphere at 37 °C. To induce C2C12 myogenic differentiation, C2C12 myoblasts at 80–90% confluence were transferred to a differentiation medium (DM) containing 2% horse serum, as previously described [39]. To activate myogenic differentiation of rat L6E9, myoblasts were switched to a DM containing DMEM plus 1% bovine serum albumin [38]. The C2C12 was maintained in the DM for 6 days, while L6E9 for 4 days. For TUN (cat. no. T7765; Sigma-Aldrich) treatment, C2C12 and L6E9 myoblasts were incubated with 0.01 µg/ml of TUN for 24 h and then for 6 days (C2C12) or 4 days (L6E9) in the DM. Cells were harvested on day 1 (C2C12 and L6E9) and days 4 (L6E9) and 6 (C2C12) after the induction of the differentiation. All cell lines were routinely screened for the absence of mycoplasm contamination by PCR using the Mycoplasm Detection kit (abm, cat. num G238, SIAL srl, Italy). All mutant cell lines are available from the authors upon request.

WT and MLC/mIgf1 transgenic mice

Jackson Laboratories' FVB female mice were utilized as embryo donors for the generation of MLC/mIgf1 transgenic animals, as previously described [21]. Animals were kept in ventilated cages (4-5 per cage) in a room with constant temperature (22°C) and humidity (45%–55%), and with 12:12 hr light/dark cycle. Each cage was equipped with wood shavings, bedding and a cardboard tube for enrichment and spontaneous physical activities. The mice had access to a constant supply of food (Teklad Global 18% Protein Rodent Diet (Envigo, Huntingdon, UK) and water. Every four months, sentinel mice were examined for any potential infection listed in the FELASA recommendations. Female WT and MLC/mIgf1 transgenic animals of 6 weeks of age were used for all the experiments. Animals were randomly allocated to sham or TUN groups. All experiments were conducted within the animal welfare regulations and guidelines.

C2C12 and L6E9 fusion index scoring

At the time of interest, C2C12 and L6E9 cell cultures were washed with phosphate-buffered saline (PBS) (8 g/L NaCl, 1.15 g/L Na_2HPO_4, 0.2 g/L KH_2PO_4, 0.2 g/L KCl), fixed for 15 min at room temperature with 4% formaldehyde/PBS and permeabilized in 0.5% Triton X-100/PBS for 4 min. A mouse monoclonal antibody against Myosin heavy chain (MF20 at the 1:2 dilution; obtained from DSHB) was incubated at 37 °C for 1 h followed by incubation at 37 °C for a 30-min with 1:100 fluorescein-conjugated goat anti-mouse IgG (Biolegend, San Diego, CA, USA). Cells were stained with DAPI (2-(4-amidinophenyl)-1H-indole-6-carboxamidine) for nuclear visualization and mounted in Mowiol 4-88 (Sigma-Aldrich) slides. Images were acquired using the TOUPCAM^{TM} E31SPM05000KPA digital camera connected to a Leica microscope DMLB and the ToupView software. Fusion index was determined by counting the number of nuclei in differentiated myotubes using ImageJ software and expressed as a percentage of the total number of nuclei.

CRISPR-CTR and CRISPR-PMM2 cellular senescence quantification

Cellular senescence was evaluated via detection of the SA-βgal activity in CRISPR-CTR and CRISPR-PMM2 cells. Wild type cells were also treated with 600 µM hydrogen peroxide (H_2O_2) for 2 hours and served as positive control [40]. Myoblasts at 80–90% confluence were washed twice with PBS, fixed for 5 minutes at room temperature with 4% paraformaldehyde and washed again three times in PBS. Cells were then incubated overnight at 37 °C without CO_2 with freshly prepared staining solution at pH 6 according to Chen et al. [40]. After the incubation, 6 random images per well (10X objective) were collected using a digital camera (ColorView, Soft Imaging Systems) adapted to an inverted microscope (Olympus CKX41). The senescent cells responding to the SA-βgal activity (identified by a blue ring usually around the nucleus) were manually counted with the ImageJ software and the ratio of senescent cells was calculated.

RNA extraction, cDNA synthesis, and qRT-PCR

Total RNA was extracted and purified using the Omega Bio-Tek E.Z.N.A.™ Total RNA kit (VWR International) according to the manufacturer's instructions. The amount of RNA was assessed with SpectraMax® QuickDrop™ Micro-Volume Spectrophotometer (Molecular Devices, CaRli biotec) and the complementary DNA was synthesised from 500 ng of total RNA using Takara PrimeScript™RT Master Mix (Takara Bio Inc., Diatech Lab Line Srl). Subsequently, quantitative RT-PCR (qRT-PCR) was performed with 2 µl of cDNA and 300 nM of each primer in an Applied Biosystems StepOnePlus™ Real-Time PCR System using PowerUp SYBR Green Master Mix (Applied Biosystems). The qRT-PCR conditions were: 50°C for 2 min, 95°C for 2 min followed by 40 cycles of two steps at 95°C for 15 s and 60°C for 60 s. The relative mRNA expression of target genes was normalized to *GAPDH* internal control. The genes of interest and the sequence of the specific primer used in qRT-PCR quantification are listed in supplementary data Table S1.

Immunoblotting and Lectin Blotting

Cells were lysed adding 40-60 µl of lysis buffer containing: 20 mM HEPES (pH 7.9), 25% v/v glycerol, 0.42 M NaCl, 0.2 mM EDTA, 1.5 mM $MgCl_2$, 0.5% v/v Nonidet P-40, 1 mM DTT, 1 mM NaF, 1 mM Na_3VO_4, and 1X complete protease inhibitor cocktail (Roche Diagnostics). The lysates were frozen and thawed twice and clarified by centrifugation at 12000 rpm for 10 minutes at 4 °C. Protein concentration in each sample was determined using the Bradford colorimetric assay (Bio-Rad Laboratories) and the DU-640 UV Spectrophotometer (Beckman Coulter). The protein samples (20-30 µg total proteins) were electrophoresed through 10% SDS-PAGE, and then transferred to nitrocellulose or PVDF membranes (Bio-Rad Laboratories) for immunoblotting. Primary antibodies against phospho-IGF1R β (1:2000; cat. n. 3024 Cell Signaling Technology), total IGF1R β (1:2000; cat. n. 3027 Cell Signaling Technology), phospho-Akt (Ser473) (1:2000; cat. n. 9271 Cell Signaling Technology), total Akt (1:2000; cat. n. 9272 Cell Signaling Technology), phospho-p44/42 (ERK1/2) (1:2000; cat. n. 9101 Cell Signaling Technology), total p44/42 (ERK1/2) (1:2000; cat. n. 9102 Cell Signaling Technology), PCNA (1:5000, cat. n. MAB 424R Millipore), MF20 (1:500, DSHB), mouse/rat biotinylated IGF-1 antibody (1:300, cat. n. BAF791 R&D Systems) were incubated overnight at 4°C. For lectin blotting, membranes were probed with biotinylated Concanavalin A (Con A, 1:1000), Phaseolus vulgaris leucoagglutinin (PHA-L, 1:200) and Aleuria Aurantia (AAL, 1:400) lectins (Vector laboratories, D.B.A. Italia) at room temperature while shaking for 1 h. After washes, the membranes were incubated with the appropriate horseradish peroxidase (HRP)-conjugated secondary antibody (against primary antibodies) or streptavidin-HRP (for IGF-1 and biotinylated lectins) at room temperature for 1 hour and were then washed three times. Deglycosylation of TA and EDL muscle proteins was performed by incubation tissue lysates with 2.5 U of PNGase F (Sigma-Aldrich; cat. num. P7367) for 2 hours at 37 °C, according to the manufacturer's recommendations. An aliquot of tissue lysates incubated with an equal volume of PNGase assay reaction buffer without the enzyme PNGase F was used as a control. Blots were developed using Clarity Western ECL Substrate (Bio-Rad Laboratories) and were quantified using the ChemiDoc MP (Bio-Rad Laboratories) equipped with Image Lab software.

PMM2 knockdown by CRISPR/Cas9

For CRISPR/Cas9 silencing, 5.0×10^4 C2C12 cells/well were seeded in 12-well plates and transfected with 1 µg of the PMM2 Double Nickase plasmid (cat. no. sc-424790-NIC; Santa Cruz Biotechnology, D.B.A. Italia) or the corresponding Double Nickase Control plasmid (cat. no. sc-437281; Santa Cruz Biotechnology, D.B.A. Italia) using the TransIT-X2® Transfection Reagent (Mirus Bio, TEMA ricerca) for 48 h. Following the manufacturer's protocol, the selection was performed with puromycin (cat. no. P9620; Sigma-Aldrich), and clones were selected and analyzed using qRT-PCR and PMM2 enzymatic activity assay.

PMM enzymatic activity assay

CRISPR-CTR and CRISPR-PMM2 C2C12 cells were washed twice in PBS, scraped, pelleted by centrifugation and resuspended in lysis buffer (20 mM Hepes, 25 mM KCl, 1 mM dithiothreitol and 1x protease inhibitor mixture) and then briefly sonicated and incubated at 4°C for 15 min. Afterwards, the cell lysates were centrifuged at 15000 rpm for 10 min at 4°C to remove cellular debris. Protein concentration of each freshly prepared cell lysate was determined with Bradford Reagent (Sigma-Aldrich). PMM enzymatic activity was assayed as reported by Van Schaftingen (1995) [41] with slight modification. Briefly, PMM activity was measured at 32°C in Hepes 20 mM pH 7.5 containing $MgCl_2$ 5 mM, $NADP^+$ 0.25 mM, in the presence of 0.3 mM Mannose-1-P as the substrate, 1µM Glc-1,6-P_2 as the activator, 2.8 U/ml glucose 6-phosphate dehydrogenase, 3.7 U/ml phosphoglucose isomerase and 3.9 µg/ml phosphomannose isomerase. The reaction started by adding 50 µg/mL of cell lysates. The activity was followed spectrophotometrically for 60 min at 340 nm, recording the reduction of $NADP^+$ to NADPH. One Unit is the amount of enzyme that catalyzes the conversion of 1 µmol of substrate per min under this condition.

Statistical analysis

Sample size was determined based on practicability and prior experience with the C2C12 [39], L6E9 [38]and MLC/Igf1 [21]models. Data are represented as mean ± s.d. of at least three independent experiments. The biological replicate numbers are indicated as the n numbers in the Figure legends. Variables of interest were checked for normal distribution using the Shapiro–Wilks test and parametric statistical analysis was employed to determine significant differences. Results for mRNA expression were not normally distributed and therefore log-transformed and reanalysed. Statistical analyses were performed using Student's t-test or two-way ANOVA as appropriate, followed by Bonferroni's multiple comparison post hoc tests. A p-value < 0.05 was considered statistically significant.

Results

TUN treatment and C2C12 myoblast differentiation

C2C12 myoblasts remained viable for up to 72 h when incubated in the lowest TUN concentration (0.01 µg/ml). The cells appeared healthy by phase-contrast microscopy and retained the capacity to exclude trypan blue (cytotoxicity CTR= 1.7% ± 1.8%; TUN 0.01 µg/ml for 72h= 1.8% ± 0.5; p= 0.92). At the highest concentration (0.05 µg/ml) cytotoxic effects became apparent, and the myoblasts appeared highly vacuolated and started to detach from the dish surfaces (cytotoxicity CTR= 1.7% ± 1.8%; TUN 0.05 µg/ml for 72h= 50.5% ± 3.3%; p < 0.0001). Thus, a concentration of 0.01 µg/ml was used to evaluate the effect of chronic low-dose TUN treatment on C2C12. TUN was added to proliferating C2C12 myoblasts 24 hours before and during six days of cell differentiation. Cells were harvested on days 1 and 6 after the induction of differentiation. Firstly, we used Con A, PHA-L and AAL lectins to analyse the glycosylation pattern of C2C12 (Fig. 1A). Con A and PHA-L recognize high mannose and complex type N-glycans, respectively, while AAL binds to fucose linked (α -1,6) to N-acetylglucosamine or to fucose linked (α -1,3) to N-acetyllactosamine. As shown in Fig. 1A, we found a significant increase in Con A, PHA-L and AAL reactivity at day 6 compared to

day 1, indicating a rise in high mannose, complex N-glycans and fucosylated proteins, respectively. Notably, the lectin binding profile of TUN-treated cells was similar to CTR at day 1 but markedly differed at day 6, showing a general reduction of N-glycosylation. The expression level of ER-stress-related genes *Chop* and *Hspa5* and the *s/uXBP* ratio increased after TUN treatment both at day 1 and 6 compared to CTR, as expected (Fig. 1B). Subsequently, we analyse the effect of TUN treatment on C2C12 differentiation by immunofluorescence analysis of the Myosin heavy chain (MF20) (Fig 1C). CTR cells appeared as long multinucleated cells at day 6 (fusion index of 53.8 ± 8.0%) while myotube formation was markedly inhibited in TUN-treated cells (fusion index at day 6 = 18.2 ± 10.7%). We next examined the mRNA levels of myogenic markers *Ccnd1*, *MyoD*, *Myogenin* and *Mrf4* during differentiation (Fig. 1D). In CTR cells, *Ccnd1* was expressed on day 1 and was downregulated on day 6, as expected. *MyoD* and *Myogenin* showed the opposite trend. In TUN-treated cells, *Ccnd1* was not downregulated on day 6 but appeared to increase. In addition, TUN-treated cells expressed significantly lower levels of *MyoD* and *Myogenin* mRNAs compared to CTR on day 1. *MyoD*, *Myogenin* and *Mrf4* mRNA expression was still lower in TUN-treated than in CTR cells on day 6. Finally, we found that TUN treatment increased the PCNA protein expression on day 1 and markedly reduced the myosin heavy chain (MF20) protein expression compared to CTR on day 6 (Fig. 1E). We found that TUN treatment inhibited the differentiation (Fig S2A), increased *Ccnd1* mRNA expression on day 1 and decreased *MyoD*, *Myogenin* and *Mrf4* mRNA levels on day 4 (Fig S2B) of rat L6E9 myoblasts, similar to C2C12 myoblasts, which suggested the universality of the crucial role played by glycosylation on myoblast differentiation.

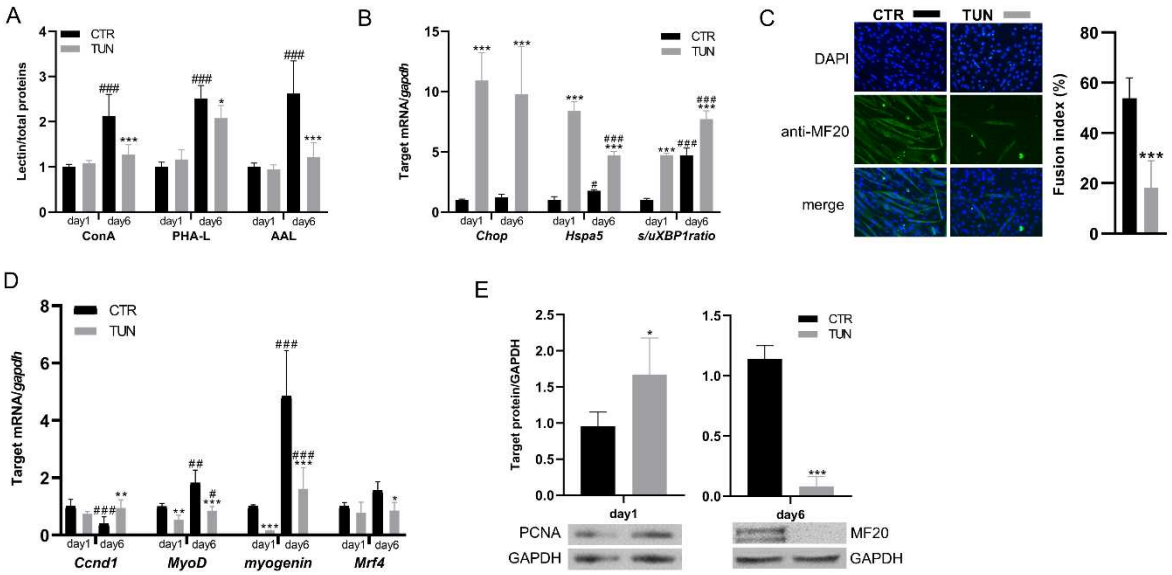

Figure 1. Effect of TUN treatment on C2C12 cell differentiation. (A) Quantification of lectin binding in C2C12 treated with TUN (0.01 µg/ml); C2C12 cells were collected on days 1 and 6 (n=4). ConA, Concanavalin A; PHA-L, *Phaseolus vulgaris* leucoagglutinin; AAL, *Aleuria aurantia* Lectin. Representative lectin blots were presented in supplementary Fig. S1A. (B) Expression of ER-stress-related genes *Chop*, *Hspa5* and *s/uXBP1* ratio in C2C12 cells treated with TUN (0.01 µg/ml); C2C12 cells were collected on days 1 and 6 (n=4). (C) Effects of TUN treatment (0.01 µg/ml) on myotubes formation at day 6 (n=8). (D) Quantification of *Ccnd1*, *MyoD*, *myogenin* and *Mrf4* mRNA expression by qRT-PCR (n=4). (E) Effects of TUN treatment (0.01 µg/ml) on PCNA (on day 1) and MF20 (on day 6) protein expression assessed by western blotting. All bar charts are presented as mean values ± s.d. Significant differences were determined using unpaired T-test or two-way ANOVA followed by Bonferroni's multiple comparison post hoc tests. *Significantly different compared to CTR; #Significantly different compared to day 1; * and # $p \leq 0.05$; ** and ## $p \leq 0.01$ *** and ### $p \leq 0.001$.

PMM2 knockdown and C2C12 myoblast differentiation

Subsequently, we knocked down *PMM2* in C2C12 by stable transfection of *PMM2* CRISPR/Cas9 double-nickase plasmid to analyse the effects of PMM2 deficiency on myoblast differentiation. RNA from PMM2-targeted cells (CRISPR-PMM2) and control plasmid-transfected cells (CRISPR-CTR) was collected to confirm the effective targeting of the *PMM2* gene. We obtained three myoblast clones with a marked reduction in *PMM2* mRNA

expression compared with the corresponding CRISPR-CTR clones (10.7 ± 2.8 fold reduction at day 1; $p < 0.0001$). Accordingly, CRISPR-PMM2 myoblasts had a significantly reduced PMM enzyme activity (CRISPR-CTR at day 1 = 1.64 ± 0.4 mU/mg of proteins; CRISPR-PMM2 at day 1= 0.34 ± 0.25 mU/mg of proteins; $p < 0.01$) and the downregulation of *PMM2* mRNA expression also persisted in cells harvested at day 6 after differentiation (16.9 ± 4.0 fold reduction; $p < 0.0001$). The lectin binding profile of CRISPR-PMM2 cells showed a reduction of PHA-L and AAL binding at day 1, while ConA binding slightly increased at day 1 compared to CRISPR-CTR (Fig. 2A). At day 6 all lectin reactivities decreased in CRISPR-PMM2 cells compared to CRISPR-CTR (Fig. 2A). The analyses of the expression level of ER-stress related genes in CRISPR-PMM2 cells showed a slight increase of *s/uXBP1* ratio on day 1 and a marked increase of *Chop* and *Hspa5* mRNA level and *s/uXBP1* ratio on day 6 compared to CRISPR-CTR (Fig. 2B). We next examined the differentiation potential of CRISPR-PMM2 myoblasts. As shown in Fig. 2C, CRISPR-PMM2 cells failed to form myotubes at day 6, showing a marked reduction in the myogenic index (CRISPR-CTR fusion index at day 6= 51.0 ± 8.7 %; CRISPR-PMM2 fusion index at day 6= 0.9 ± 0.6 %) (Fig. 2C). We found an increase of *Ccnd1* mRNA level in CRISPR-PMM2 at day 1 and day 6 compared to CRISPR-CTR cells (Fig. 2D) and an increase of PCNA protein expression at day 1 (Fig. 2E). Conversely, *MyoD*, *Myogenin*, and *Mrf4* mRNA levels (Fig. 2D) and MF20 protein expression (Fig. 2E) strongly decreased at day 6. The analysis of senescence-associated beta-galactosidase (SA-βgal) activity showed no difference between CRISPR-PMM2 and CRISPR-CTR cells (% senescence CRISPR-CTR = 2.5 ± 2.4; CRISPR-PMM2 = 2.2 ± 2.1; $p= 0.85$), suggesting that the lack of differentiation cannot be attributed to senescence in the selected CRISPR-PMM2 clones.

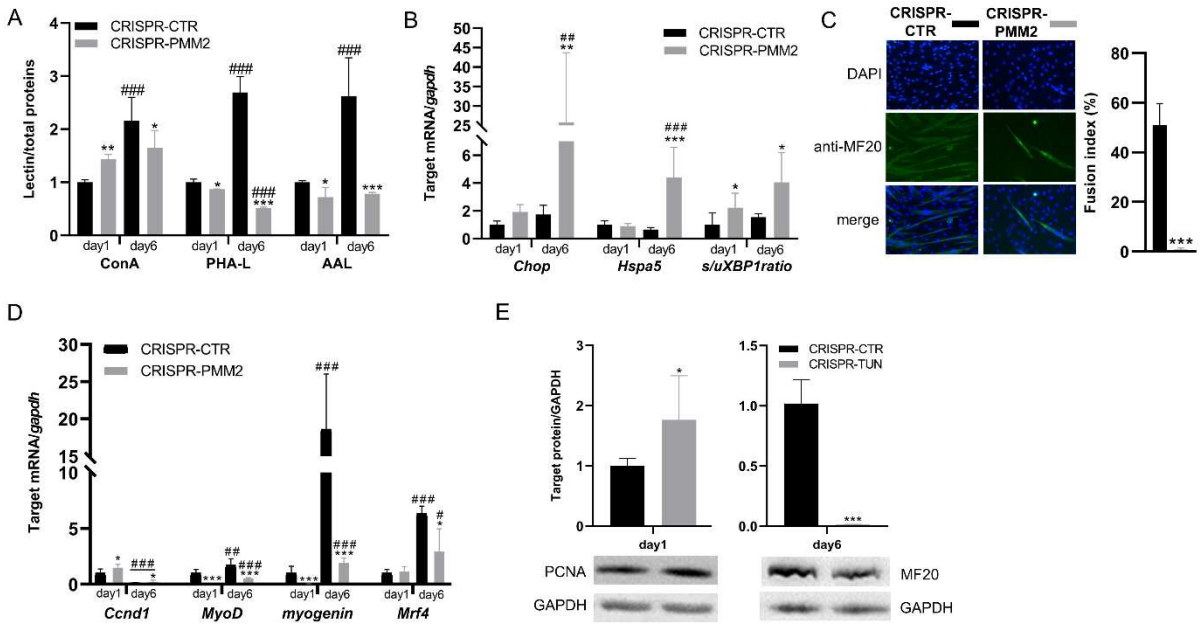

Figure 2. Effect of PMM2 downregulation on C2C12 differentiation. (A) Quantification of lectin binding after knockdown of *PMM2* gene by CRISPR/Cas9 (CRISPR-PMM2) and control plasmid-transfected cells (CRISPR-CTR). ConA, Concanavalin A; PHA-L, *Phaseolus vulgaris* leucoagglutinin; AAL, *Aleuria aurantia* Lectin. Representative lectin blots were presented in supplementary Fig. S1B. (B) Expression of ER-stress-related genes *Chop*, *Hspa5* and *s/uXBP1* ratio in CRISPR-PMM2 and CRISPR-CTR C2C12; C2C12 cells were collected on days 1 and 6 (n=4). (C) Effects of PMM2 knockdown on myotubes formation at day 6 (n=6). (D) Quantification of *Ccnd1*, *MyoD*, *myogenin* and *Mrf4* mRNA expression by qRT-PCR (n=4). (E) Effects of PMM2 knockdown on PCNA (on day 1) and MF20 (on day 6) protein expression assessed by western blotting. All bar charts are presented as mean values ± s.d. Significant differences were determined using unpaired T-test or two-way ANOVA followed by Bonferroni's multiple comparison post hoc tests. *Significantly different compared to CTR; #Significantly different compared to day 1; * and # $p \leq 0.05$; ** and ## $p \leq 0.01$ *** and ### $p \leq 0.001$.

Effects of chronic treatment with low TUN dose on TA muscle lectin binding, ER-stress-related gene expression and muscle markers of myogenesis and atrophy

To investigate the role of N-glycosylation inhibition on muscle *in vivo,* 6-week-old WT and MLC/mIgf-1 mice were chronically challenged with a low TUN dose (0.1 mg/kg for 15 days). MLC/mIgf-1 mice showed increased body and TA muscle weight compared to WT mice (Fig. 3A), as expected [21]. Conversely, body and TA muscle weight was comparable between CTR and TUN-treated mice (Fig. 3A). TUN treatment slightly decreased PHA-L and AAL lectin binding in the TA muscle of WT mice (Fig. 3B), while the ER-stress-related gene expression did not change in the TA muscle of WT and MLC/mIgf-1 mice (Fig. 3C). In TA muscle of WT and MLC/mIgf-1 mice, the mRNA expression of *Myogenin* decreased after TUN treatment, while *atrogin-1* and *MuRF-1* expression levels increased only in the WT mice (Fig. 3D).

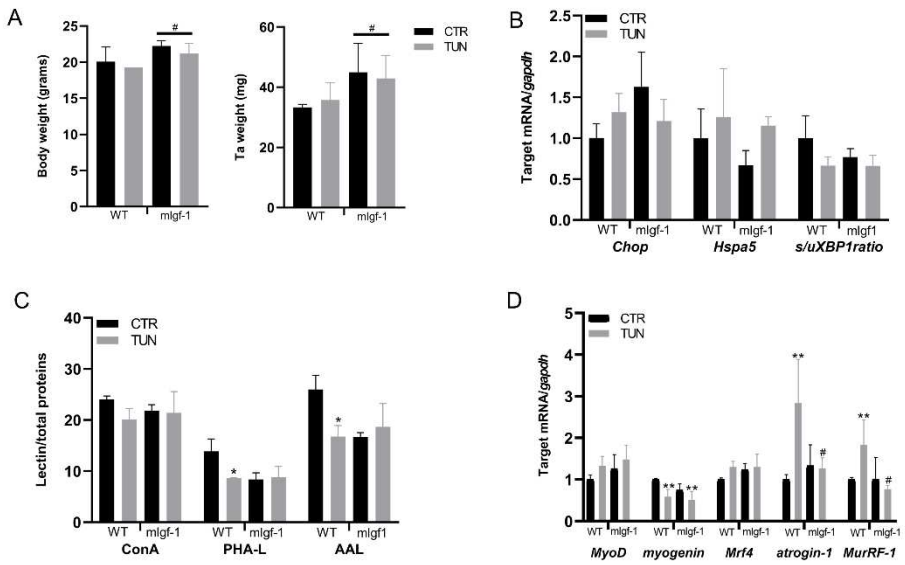

Figure 3. Effect of chronic treatment with low TUN dose (0.1 mg/kg of TUN for 15 days) on TA muscle of WT and MLC/mIgf-1 mice. (A) Body and TA muscle weight of WT (n = 3) and MLC/mIgf-1 (n = 3) mice treated with TUN for 15 days. (B) Quantification of lectin binding in the TA muscle of WT (n = 3) and MLC/mIgf-1 (n = 3) mice treated with TUN; ConA, Concanavalin A; PHA-L, *Phaseolus vulgaris* leucoagglutinin; AAL, *Aleuria aurantia* Lectin. Representative lectin blots were presented in supplementary Fig. S1C. (C) Expression of ER-stress-related genes *Chop* and *Hspa5* and *s/uXBP1* ratio in the TA muscle of WT (n = 3) and MLC/mIgf-1 (n = 3) mice treated with TUN. (C) Quantification of

MyoD, *myogenin*, *Mrf4, atrogin-1 and MuRF-1* mRNA expression by qRT-PCR in the TA muscle of WT (n = 3) and MLC/mIgf-1 (n = 3) mice treated with TUN (n = 3). All bar charts are presented as mean values ± s.d. Significant differences were determined using two-way ANOVA followed by Bonferroni's multiple comparison post hoc tests. *Significantly different compared to CTR; #Significantly different compared to mIgf1; * and # $p \leq 0.05$; ** $p \leq 0.01$.

Effects of chronic treatment with low TUN dose on Igf-1 mRNA and IGF-1 protein expression and on IGF1R pathways activation in the TA muscle of WT and MLC/mIgf1 mice

The expression of endogenous *Igf-1Ea* and *Igf-1Ec/mgf* isoforms in the TA muscle decreased after TUN treatment in WT and MLC/mIgf1 mice (Fig. 4A). We also measured the effect of TUN treatment on the expression of *mIgf-1* transgene by quantify total *Igf-1* (*Igf-1tot*) mRNA level. Although *Igf-1tot* measured both endogenous and the *mIgf-1* transgene, the former are expressed at a negligible level compared to *mIgf-1* transgene (*Igf-1Ea*: 84.2 ± 12.6 and *Igf-1Ec/mgf:* 250.2 ± 21.6 fold lower compared to *Igf-1tot*). Interestingly, we found that *mIgf-1* transgene was unaffected by the TUN treatment in the TA muscle of MLC/mIgf1 mice. Western blotting analyses showed that the TA muscle of untreated MLC/mIgf1 mice mainly expressed IGF-1Ea prohormones with three immunoreactive bands of ~22, ~17 and ~12 kDa (Fig. 4B). The ~22 and ~17 kDa bands disappeared after the deglycosylation with PNGase F, resulting in an accumulation of the ~12 kDa band (supplementary Fig. S3). Thus, the ~22 and ~17 kDa bands likely represent two N-glycosylated forms of the IGF-1Ea prohormone, while the lower band of ~12 kDa represent the unglycosylated IGF-1Ea prohormone. No IGF-1 immunoreactive signals were detected in the TA muscle of WT mice, probably because the amount of IGF-1 was below the detection limit of western blot. Band densitometry analysis showed that TUN treatment decreased the 22 kDa band in the TA muscle of MLC/mIgf-1 mice (Fig.4C). Finally, TA muscle of MLC/mIgf1 mice showed increased IGF1R phosphorylation compared to WT mice, which was markedly inhibited by TUN treatment (Fig. 4D, E). Accordingly, the MAPK ERK1/2 phosphorylation in the TA muscle of WT and MLC/mIgf1 mice decreased after TUN treatment. Similar results were obtained in the EDL muscle of WT and MLC/mIgf1 mice (Supplementary Fig S4).

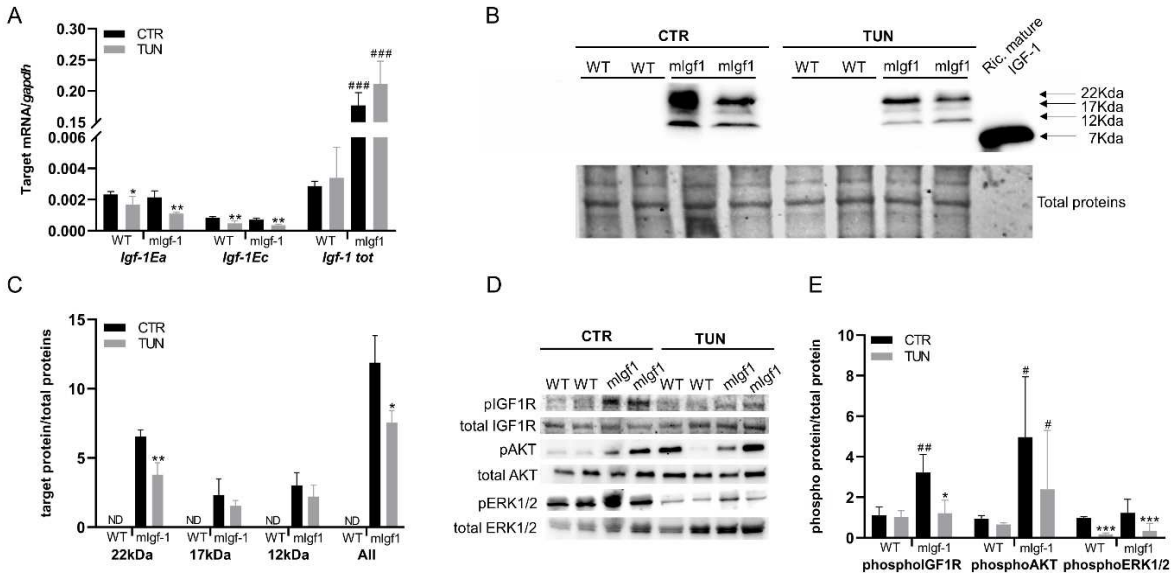

Figure 4. IGF-1 production and IGF1R signalling pathway activation in TA muscle of WT and MLC/mIgf-1 mice treatment with low TUN dose (0.1 mg/kg of TUN for 15 days). (A) Expression of endogenous *Igf-1* mRNA isoforms (i.e. *Igf-1Ea* and *Igf-1Ec* mRNAs) and total *Igf-1* (i.e. endogenous and mIgf-1 transgene mRNAs) in the TA muscle of WT (n = 3) and MLC/mIgf-1 (n = 3) mice treated with TUN. (B) Representative immunoblotting and (C) band densitometry analysis of TA muscle of WT and MLC/mIgf1 mice using an antibody directed against mature mouse IGF-1 sequence. Three bands at a molecular weight of ~22, ~17 and ~12 kDa were detected in TA muscle of MLC/mIgf1 mice. Recombinant mouse IGF-1 mature protein was loaded as a positive control for mature IGF-1 (~7 kDa). (D) Representative immunoblotting and (E) band densitometry analysis of TA muscle of WT and MLC/mIgf1 mice using antibodies directed against phosphorylated (pIGF1R) and total IGF-1R, phosphorylated (pAKT) and total AKT, and phosphorylated (pERK1/2) and total ERK1/2. All bar charts are presented as mean values ± s.d. Significant differences were determined using unpaired T-test or two-way ANOVA followed by Bonferroni's multiple comparison post hoc tests. *Significantly different compared to CTR; #Significantly different compared to mIgf1; * and # $p \leq 0.05$; ** and ## $p \leq 0.01$ *** and ### $p \leq 0.001$.

Discussion

In this study, we used two strategies, one based on TUN treatment and one based on PMM2 downregulation, to study the effects of N-glycosylation inhibition on C2C12 myoblast differentiation. Moreover, chronic treatment with a low dose of TUN, mimicking mild CDG-like conditions, was also performed in WT and MLC/mIgf-1 mice to investigate the effects of N-glycosylation inhibition on muscle *in vivo*. TUN is an inhibitor of N-acetylglucosamine transferases and blocks the N-glycosylation pathway at the first step resulting in the synthesis of glycoproteins deficient in N-linked glycans [22]. As a result of being a glycosylation inhibitor, TUN is also known as an ER stress activator due to the accumulation of hypoglycosylated and misfolded proteins [23]. In C2C12 untreated cells, we observed increased binding of ConA, PHA-L and ALL lectins during myoblast differentiation. This finding is in accordance with other studies, suggesting that specific changes in muscle cell glycosylation occur following differentiation [11,12]. Given the specificities of these lectins, glycoproteins derived from myotubes bear higher (ConA) and complex (PHA-L) mannose N-glycans and fucosylated (ALL) residues compared to undifferentiated myoblasts. Interestingly, C2C12 differentiation under TUN treatment exhibited a lectin-binding pattern more similar to the undifferentiated myoblasts. Moreover, we found an increase of ER-stress-related gene expression (*Chop* and *Hspa5* mRNAs and *s/uXbp1* ratio*)* following TUN treatment both in C2C12 myoblast and myotubes, as expected. Interestingly, TUN-induced hypoglycosylation decreased myogenic markers and prevented myotubes formation in C2C12. Previous studies have shown that doses from 1.0 to 10 µg/ml of TUN are toxic in C2C12 cells and induce strong ER stress pathways activation, inhibit mitosis, and increase apoptosis [24]. However, the effects of high TUN dose on myoblast differentiation are still unclear [14,24]. Here, we found that low TUN doses (i.e. concentration ≤ 0.01 µg/ml) did not have toxic effects on C2C12 myoblasts and rather increased the myoblast proliferation marker PCNA. Hence, the inhibition of C2C12 differentiation induced by non-toxic doses of TUN is likely to be caused by the TUN-induced hypoglycosylation instead of unexpected secondary effects (i.e. mitosis arrest and apoptosis). To further analyse the effect of hypoglycosylation on myoblast differentiation we also created C2C12 with stable downregulation of PMM2, an enzyme that converts mannose-6-phosphate to mannose-1-phosphate, the immediate precursor of GDP-mannose which is a key substrate in

glycoprotein formation. PMM2 is the most frequently mutated enzyme in the N-glycosylation pathway and patients have hypomorphic alleles and residual PMM2 activity because complete loss of PMM2 function is lethal [25]. We found that the PMM2 downregulation decreased PHA-L and AAL binding both in myoblasts and myotubes while the ER-stress-related gene expression increased, as expected. Interestingly, the differentiation program and myotubes formation were markedly inhibited in CRISPR-PMM2 cells, similar to the results obtained in TUN-treated cells. PMM2-CDG is associated with a broad range of clinical symptoms including generalized hypotonia, distal muscle atrophy and wasting also related to peripheral neuropathy. However, a natural history study on PMM2-CDG described moderate to severe signs of myopathy on the Nijmegen CDG severity scale in 6% and 2% of patients (N=68) in the current clinical assessment [26]. Importantly, cardiomyopathy is also part of systemic organ involvement and is a life-threatening condition in infants with PMM2-CDG [27,28]. Muscular histological findings in PMM2-CDG patients are scanty, with documentation of slight myopathic alterations with fiber size variations and myofibrillar disarrays [29] and mildly elevated creatine kinase levels [30]. Moreover, a recent study shows that muscle-specific PMM2 knockdown causes qualitative movement defects in a *Drosophila* PMM2-CDG model [31]. Although we are aware that the pathophysiology of hypotonia in PMM2-CDG is probably complex, the hypoglycosylation-induced defective differentiation of myoblasts into myotubes could be a contributing factor. Subsequently, we used WT and MLC/mIgf-1 mice to study the effect of sub-phenotypic doses of TUN *in vivo*. Xia et al. recently demonstrated that chronic treatment with TUN reduced body weight growth, body height, and tibia length in C57BL/6 mice, which is associated with decreased IGF-1 production and signalling [15]. Here, we focused on the effect of TUN treatment on muscle functional markers, also taking advantage of the MLC/mIgf-1 transgenic FVB mice, overexpressing the *Igf-1Ea* isoform under the control of the myosin light chain promoter. We found that TUN treatment decreased PHA-L and AAL lectin reactivity in the TA muscle of WT mice, while lectin binding did not change in the TA muscle of MLC/mIgf-1 mice. ER-stress-related gene expression did not change in the TA muscle of WT and MLC/mIgf-1 mice. Collectively, these results suggested a mild impact on glycosylation and ER-stress markers after chronic low-dose TUN challenge, potentially mimicking a mild CDG-like condition. Despite the low sub-phenotypic dose of TUN, the expression of myogenic marker *myogenin* was downregulated in the TA muscles of WT and MLC/mIgf-1 mice after TUN treatment.

Moreover, the mRNA expression of muscle atrophy markers *atrogin-1* and *MuRF-1* increased in WT mice. Interestingly, we found a slight reduction of endogenous *Igf-1* mRNA isoforms after TUN treatment both in WT and MLC/mIgf-1 mice while *mIgf-1* transgene overexpression in MLC/mIgf-1 mice did not change. Thanks to the overexpression of *Igf-1Ea* in the MLC/mIgf-1 mice we were also able to analyse the impact of TUN on muscle IGF-1Ea proteins by western blotting. Notably, we found that muscle IGF-1 was mainly expressed as proIGF-1Ea not mature IGF-1, as previously shown [32,33]. More interestingly, the expression level of the ~22 kDa band, which likely represents an N-glycosylated form of proIGF-1Ea [32 and Fig. S3], decreased after TUN treatment. Finally, IGF1R activation was reduced after TUN treatment in muscle of MLC/mIgf-1 mice while both WT and MLC/mIgf-1 mice showed reduced ERK1/2 phosphorylation compared to untreated mice. The reduction of IGF-1 prohormone production and IGF1R signalling pathway activation was also observed in EDL muscle of WT and MLC/mIgf-1 mice treated with TUN. These results are in line with previous findings showing that impaired N-glycosylation directly affects IGF-1 protein production [33,34] and dampens the IGF1 signalling IGF1R glycosylation preventing receptor activation [34–36]. Given the important role played by the IGF1R signalling pathway on myoblast proliferation and muscle cell growth [37], our results suggested that reduced IGF1/IGF1R muscle signalling may be a key mechanism explaining impaired muscle development and function found in diseases associated with aberrant N-glycosylation, such as CDG. Despite the importance of N-glycosylation in various cellular processes, the molecular mechanisms by which aberrant N-glycosylation impacts muscle functioning are only starting to be unravelled. Chronic TUN-challenge mouse models and test other different N-glycosylation inhibitors, can help to elucidate the molecular mechanisms through which diseases associated with aberrant N-glycosylation, differentially affect tissue and organ function.

Author Contributions

GA and EB conceived and designed the study. LDP, GV and MB performed cell culture, cellular senescence quantification, mRNA extraction and qRT-PCR analyses. GA and GV performed sCRISPR/Cas9 experiments. RS, LF and LB performed western blot and lectin blot analyses and PMM2 enzymatic activity. GA, LDP, GV and EB analysed the data and drafted

the manuscript. AM, RB, RG, AM, VS and EB provided overall direction to the project and revised the manuscript. All the authors contributed to the manuscript revision, read and approved the submitted version.

Acknowledgments

This study is funded by the PRIN22 framework (Project n. 202255RLB4) and from the University of Urbino Carlo Bo “Promozione della salute e della sicurezza alimentare” (D.R. 446/2020) and AFM (23608), Fondazione Roma, and PRIN 2022 (2022LZARA3). We gratefully thank the AMMeC (Associazione Malattie Metaboliche e Congenite, Italia).

Conflicts of Interest

None of the authors have any conflicts of interest or financial ties to disclose.

References

1 Bentzinger CF, Wang YX & Rudnicki MA (2012) Building Muscle: Molecular Regulation of Myogenesis. *Cold Spring Harb Perspect Biol* 4, a008342–a008342.

2 Kislinger T, Gramolini AO, Pan Y, Rahman K, MacLennan DH & Emili A (2005) Proteome Dynamics during C2C12 Myoblast Differentiation. *Molecular & Cellular Proteomics* 4, 887–901.

3 Yoshida T & Delafontaine P (2020) Mechanisms of IGF-1-Mediated Regulation of Skeletal Muscle Hypertrophy and Atrophy. *Cells* 9, 1970.

4 Glass DJ (2010) PI3 Kinase Regulation of Skeletal Muscle Hypertrophy and Atrophy. In pp. 267–278.

5 Vergé C, Bouchatal A, Chirat F, Guérardel Y, Maftah A & Petit J (2020) Involvement of ST6Gal I-mediated α2,6 sialylation in myoblast proliferation and differentiation. *FEBS Open Bio* 10, 56–69.

6 Janot M, Audfray A, Loriol C, Germot A, Maftah A & Dupuy F (2009) Glycogenome expression dynamics during mouse C2C12 myoblast differentiation suggests a sequential reorganization of membrane glycoconjugates. *BMC Genomics* 10, 483.

7 Grassot V, Da Silva A, Saliba J, Maftah A, Dupuy F & Petit J-M (2014) Highlights of glycosylation and adhesion related genes involved in myogenesis. *BMC Genomics* 15, 621.

8 Martin PT (2003) Glycobiology of neuromuscular disorders. *Glycobiology* 13, 67R – 75.

9 Blazev R, Ashwood C, Abrahams JL, Chung LH, Francis D, Yang P, Watt KI, Qian H, Quaife-Ryan GA, Hudson JE, Gregorevic P, Thaysen-Andersen M & Parker BL (2021) Integrated Glycoproteomics Identifies a Role of N-Glycosylation and Galectin-1 on Myogenesis and Muscle Development. *Molecular & Cellular Proteomics* 20, 100030.

10 Gundry RL, Raginski K, Tarasova Y, Tchernyshyov I, Bausch-Fluck D, Elliott ST, Boheler KR, Van Eyk JE & Wollscheid B (2009) The Mouse C2C12 Myoblast Cell Surface N-Linked Glycoproteome. *Molecular & Cellular Proteomics* 8, 2555–2569.

11 McMorran BJ, McCarthy FE, Gibbs EM, Pang M, Marshall JL, Nairn A V, Moremen KW, Crosbie-Watson RH & Baum LG (2016) Differentiation-related glycan epitopes identify discrete domains of the muscle glycocalyx. *Glycobiology* 26, 1120–1132.

12 McMorran BJ, Miceli MC & Baum LG (2017) Lectin-binding characterizes the healthy human skeletal muscle glycophenotype and identifies disease-specific changes in dystrophic muscle. *Glycobiology* 27, 1134–1143.

13 Godfrey C, Foley AR, Clement E & Muntoni F (2011) Dystroglycanopathies: coming into focus. *Curr Opin Genet Dev* 21, 278–285.

14 Olden K, Law J, Hunter VA, Romain R & Parent JB (1981) Inhibition of fusion of embryonic muscle cells in culture by tunicamycin is prevented by leupeptin. *Journal of Cell Biology* 88, 199–204.

15 Xia W, Wang Y, Zhang Y, Ge X, Lv P, Cheng J & Wei J (2020) Endoplasmic reticulum stress induces growth retardation by inhibiting growth hormone IGF-I axis. *Growth Hormone & IGF Research* 55, 101341.

16 Nicolau S, Liewluck T, Shen X-M, Selcen D, Engel AG & Milone M (2019) A homozygous mutation in GMPPB leads to centronuclear myopathy with combined pre- and postsynaptic defects of neuromuscular transmission. *Neuromuscular Disorders* 29, 614–617.

17 Freeze HH, Jaeken J & Matthijs G (2022) CDG or not CDG. *J Inherit Metab Dis* 45, 383–385.

18 Péanne R, de Lonlay P, Foulquier F, Kornak U, Lefeber DJ, Morava E, Pérez B, Seta N, Thiel C, Van Schaftingen E, Matthijs G & Jaeken J (2018) Congenital disorders of glycosylation (CDG): Quo vadis? *Eur J Med Genet* 61, 643–663.

19 Pettinato F, Mostile G, Battini R, Martinelli D, Madeo A, Biamino E, Frattini D, Garozzo D, Gasperini S, Parini R, Sirchia F, Sortino G, Sturiale L, Matthijs G, Morrone A, Di Rocco M, Rizzo R, Jaeken J, Fiumara A & Barone R (2021) Clinical and radiological correlates of activities of daily living in cerebellar atrophy caused by PMM2 mutations (PMM2-CDG). *The Cerebellum* 20, 596–605.

20 Serrano M, de Diego V, Muchart J, Cuadras D, Felipe A, Macaya A, Velázquez R, Poo MP, Fons C, O'Callaghan MM, García-Cazorla A, Boix C, Robles B, Carratalá F, Girós M, Briones P, Gort L, Artuch R, Pérez-Cerdá C, Jaeken J, Pérez B & Pérez-Dueñas B (2015) Phosphomannomutase deficiency (PMM2-CDG): ataxia and cerebellar assessment. *Orphanet J Rare Dis* 10, 138.

21 Musarò A, McCullagh K, Paul A, Houghton L, Dobrowolny G, Molinaro M, Barton ER, L Sweeney H & Rosenthal N (2001) Localized Igf-1 transgene expression sustains hypertrophy and regeneration in senescent skeletal muscle. *Nat Genet* 27, 195–200.

22 Lehle L & Tanner W (1976) The specific site of tunicamycin inhibition in the formation of dolichol-bound *N* -acetylglucosamine derivatives. *FEBS Lett* 71, 167–170.

23 Foufelle F & Fromenty B (2016) Role of endoplasmic reticulum stress in drug-induced toxicity. *Pharmacol Res Perspect* 4.

24 Nakanishi K, Dohmae N & Morishima N (2007) Endoplasmic reticulum stress increases myofiber formation *in vitro*. *The FASEB Journal* 21, 2994–3003.

25 Thiel C, Lübke T, Matthijs G, von Figura K & Körner C (2006) Targeted Disruption of the Mouse Phosphomannomutase 2 Gene Causes Early Embryonic Lethality. *Mol Cell Biol* 26, 5615–5620.

26 Witters P, Honzik T, Bauchart E, Altassan R, Pascreau T, Bruneel A, Vuillaumier S, Seta N, Borgel D, Matthijs G, Jaeken J, Meersseman W, Cassiman D, Pascale de L & Morava E (2019) Long-term follow-up in PMM2-CDG: are we ready to start treatment trials? *Genetics in Medicine* 21, 1181–1188.

27 Footitt EJ, Karimova A, Burch M, Yayeh T, Dupré T, Vuillaumier-Barrot S, Chantret I, Moore SEH, Seta N & Grunewald S (2009) Cardiomyopathy in the congenital disorders of glycosylation (CDG): a case of late presentation and literature review. *J Inherit Metab Dis* 32, 313–319.

28 Resende C, Carvalho C, Alegria A, Oliveira D, Quelhas D, Bandeira A & Proenca E (2014) Congenital disorders of glycosylation with neonatal presentation. *Case Reports* 2014, bcr2013010037–bcr2013010037.

29 Aronica E, van Kempen AAMW, van der Heide M, Poll-The BT, van Slooten HJ, Troost D & Rozemuller-Kwakkel JM (2005) Congenital disorder of glycosylation type Ia: a clinicopathological report of a newborn infant with cerebellar pathology. *Acta Neuropathol* 109, 433–442.

30 Wu R, Li D, Tang W, Qiu K, Li Y, Liao X, Tang D, Qin L, Deng B & Luo X (2018) Atrial septal defect in a patient with congenital disorder of glycosylation type 1a: a case report. *J Med Case Rep* 12, 17.

31 Parkinson WM, Dookwah M, Dear ML, Gatto CL, Aoki K, Tiemeyer M & Broadie K (2016) Neurological roles for phosphomannomutase type 2 in a new *Drosophila* congenital disorder of glycosylation disease model. *Dis Model Mech*.

32 Durzyńska J, Philippou A, Brisson BK, Nguyen-McCarty M & Barton ER (2013) The pro-Forms of Insulin-Like Growth Factor I (IGF-I) Are Predominant in Skeletal Muscle and Alter IGF-I Receptor Activation. *Endocrinology* 154, 1215–1224.

33 Annibalini G, Contarelli S, De Santi M, Saltarelli R, Di Patria L, Guescini M, Villarini A, Brandi G, Stocchi V & Barbieri E (2018) The intrinsically disordered E-domains regulate the IGF-1 prohormones stability, subcellular localisation and secretion. *Sci Rep* 8, 8919.

34 Di Patria L, Annibalini G, Morrone A, Ferri L, Saltarelli R, Galluzzi L, Diotallevi A, Bocconcelli M, Donati MA, Barone R, Guerrini R, Jaeken J, Stocchi V & Barbieri E (2022) Defective IGF-1 prohormone N-glycosylation and reduced IGF-1 receptor signaling activation in congenital disorders of glycosylation. *Cellular and Molecular Life Sciences* 79, 150.

35 Itkonen HM & Mills IG (2013) N-Linked Glycosylation Supports Cross-Talk between Receptor Tyrosine Kinases and Androgen Receptor. *PLoS One* 8, e65016.

36 Klaver E, Zhao P, May M, Flanagan-Steet H, Freeze HH, Gilmore R, Wells L, Contessa J & Steet R (2019) Selective inhibition of N-linked glycosylation impairs receptor tyrosine kinase processing. *Dis Model Mech*.

37 Velloso CP (2008) Regulation of muscle mass by growth hormone and IGF-I. *Br J Pharmacol* 154, 557–568.

38 Musarò A & Rosenthal N (1999) Maturation of the Myogenic Program Is Induced by Postmitotic Expression of Insulin-Like Growth Factor I. *Mol Cell Biol* 19, 3115–3124.

39 Sestili P, Barbieri E, Martinelli C, Battistelli M, Guescini M, Vallorani L, Casadei L, D'Emilio A, Falcieri E, Piccoli G, Agostini D, Annibalini G, Paolillo M, Gioacchini AM & Stocchi V (2009) Creatine supplementation prevents the inhibition of myogenic differentiation in oxidatively injured C2C12 murine myoblasts. *Mol Nutr Food Res* 53, 1187–1204.

40 Chen J-H, Ozanne SE & Hales CN (2007) Methods of Cellular Senescence Induction Using Oxidative Stress. In pp. 179–189.

41 Van Schaftingen E & Jaeken J (1995) Phosphomannomutase deficiency is a cause of carbohydrate-deficient glycoprotein syndrome type I. *FEBS Lett* 377, 318–320.

Supplementary informations

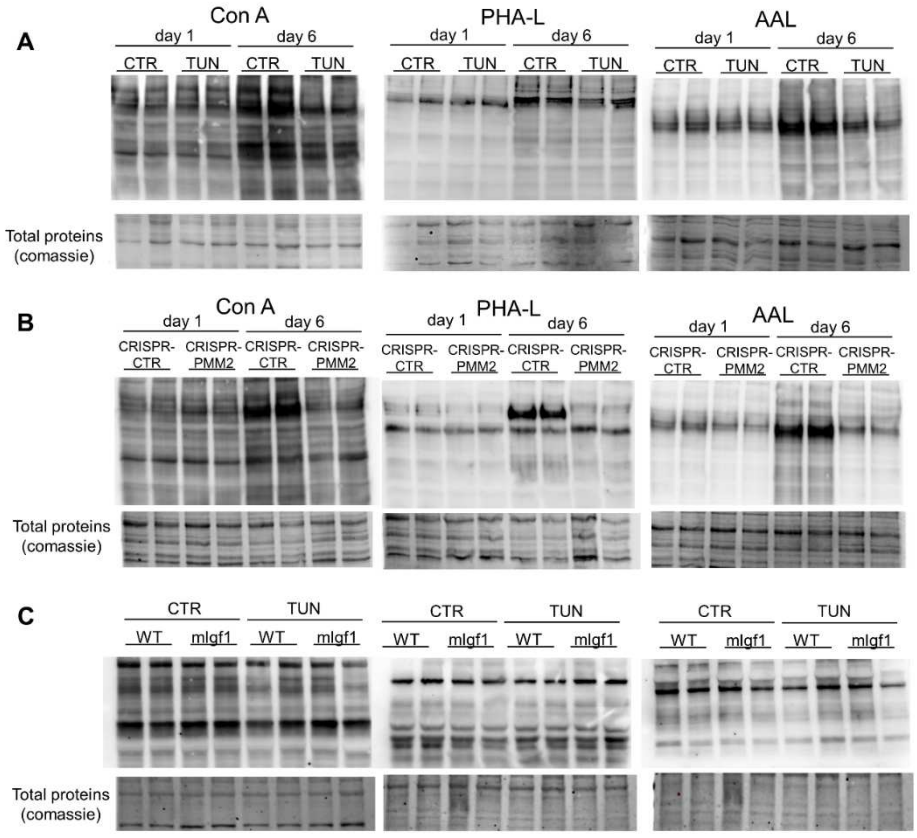

Figure S1. (A) Representative blots of Con A, PHA-L and AAL lectin binding after TUN treatment of C2C12 cells; (B) CRISPR-CTR and CRISPR-PMM2 C2C12 cells: and (C) Tibialis anterior (TA) muscle of CTR and TUN-treated WT and MLC/mIgf1 mice. Biological replicates of C2C12 cells and WT and MLC/mIgf1 mice were shown. TUN, tunicamycin; ConA, Concanavalin A; PHA-L, *Phaseolus vulgaris* leucoagglutinin; AAL, *Aleuria aurantia* Lectin.

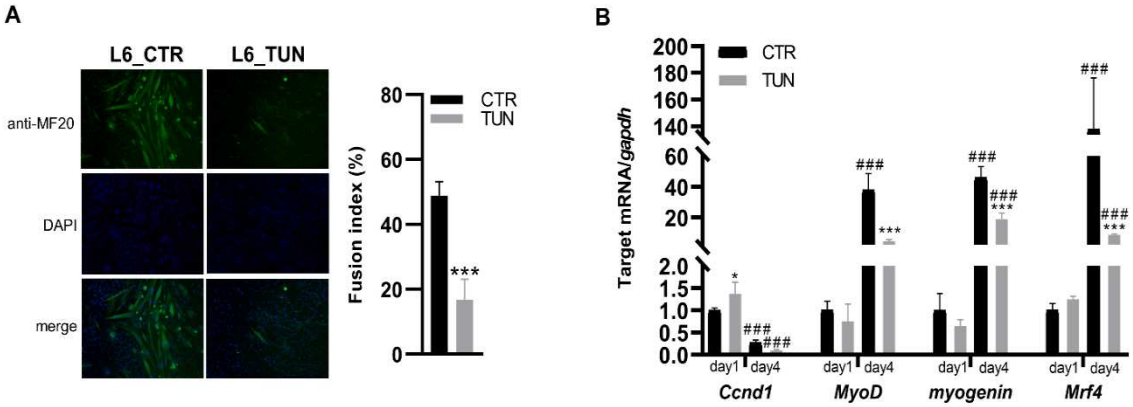

Figure S2. Effect of TUN treatment on rat L6 cell differentiation. (A) Effects of TUN treatment (0.01 µg/ml) on L6 myotubes formation at day 4 (n=6). (B) Quantification of *Ccnd1*, *MyoD*, *myogenin* and *Mrf4* mRNA expression by qRT-PCR; cells were collected on days 1 and 4 (n=4). All bar charts are presented as mean values ± s.d. Significant differences were determined using unpaired T-test or two-way ANOVA followed by Bonferroni's multiple comparison post hoc tests. *Significantly different compared to CTR; #Significantly different compared to day 1; * $p \leq 0.05$; *** and ### $p \leq 0.001$.

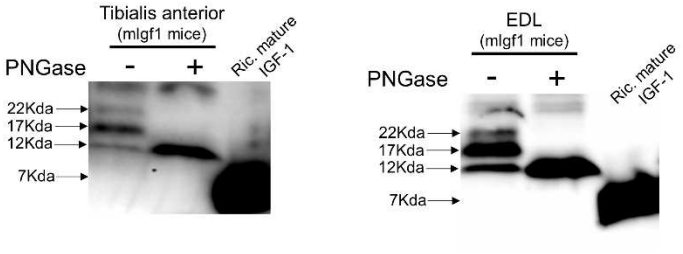

Figure S3. Deglycosylation of Tibialis anterior (TA) and EDL proteins using the *N*-Glycosidase F (PNGase F). The ~22 and ~17 kDa bands disappeared after PNGase treatment determining an accumulation of the band at ~12 kDa, which probably corresponds to unglycosylated IGF-1Ea prohormone.

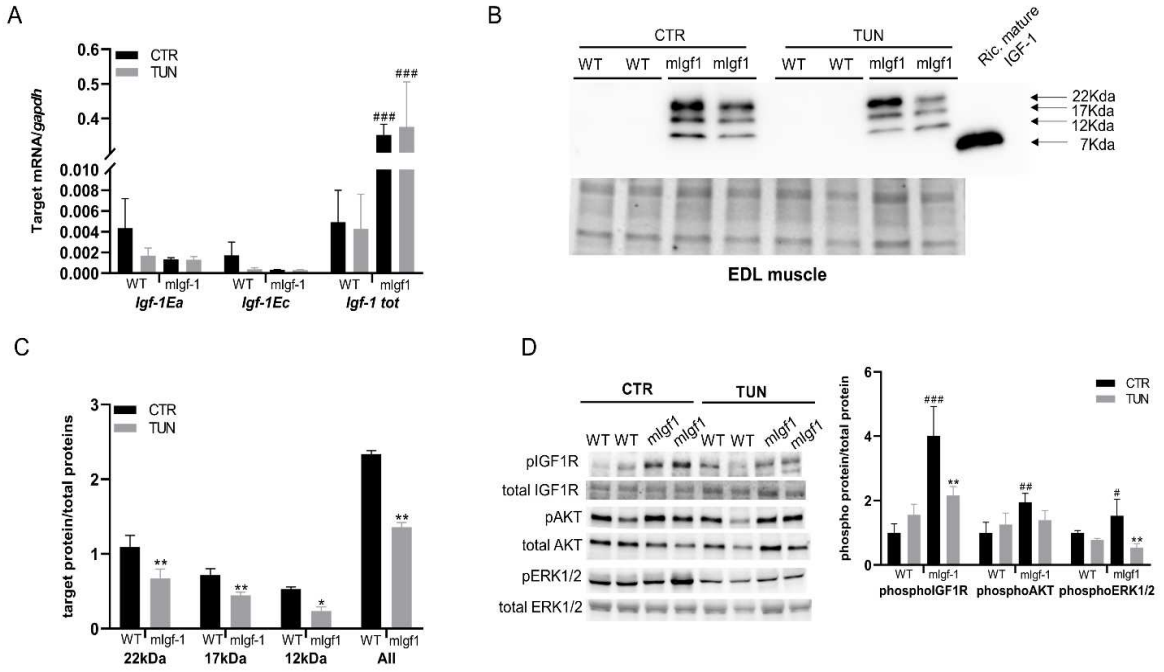

Figure S4. IGF-1 production and IGF1R signalling pathway activation in EDL muscle of WT and MLC/mIgf-1 mice treatment with low TUN dose (0.1 mg/kg of TUN for 15 days). (A) Expression of endogenous *Igf-1* mRNA isoforms (i.e. *Igf-1Ea* and *Igf-1Ec* mRNAs) and total *Igf-1* (i.e. endogenous and exogenous *Igf-1* mRNAs) in the EDL muscle of WT (n = 3) and MLC/mIgf-1 (n = 3) mice treated with TUN. (B) Representative immunoblotting and (C) band densitometry analysis of EDL muscle of WT and MLC/mIgf1 mice using an antibody directed against mature mouse IGF-1 sequence. Three bands at a molecular weight of ~22, ~17 and ~12 kDa were detected in EDL muscle of MLC/mIgf1 mice. Recombinant mouse IGF-1 mature protein was loaded as a positive control for mature IGF-1 (~7 kDa). (D) Representative immunoblotting and (E) band densitometry analysis of EDL muscle of WT and MLC/mIgf1 mice using antibodies directed against phosphorylated (pIGF1R) and total IGF-1R, phosphorylated (pAKT) and total AKT, and phosphorylated (pERK1/2) and total ERK1/2.

Gene	Primer forward (5'-3')	Primer reverse (5'-3')
Ccnd1	**CTTCCTCTCCAAAATGCCAG**	**TGGAGGGTGGGTTGGAAAT**
MyoD	**TTCTTCACCACTCCTCTGAC**	**GCCGTGAGAGTCGTCTTAT**
Myogenin	**CAACCCAGGAGATCATTG**	**CATATCCTCCACCGTGATGC**
Mrf4	**GTGGCCAAGTGTTTCGGAT**	**AAAGGCGCTGAAGACTGC**
PMM2	**TTGCCTGAGACACCTGGAAC**	**AGATCCTGCGTGTGTCTTCG**
Igf-1Ea	**GCCCAAGACTCAGAAGGAAGTAC**	**CGGTGATGTGGCATTTTCTG**
Igf-1Ec	**GCTGCAAAGGAGAAGGAAAG**	**CGGTGATGTGGCATTTTCTG**
Igf-1 tot	**GCTATGGCTCCAGCATTCG**	**TCCGGAAGCAACACTCATCC**
GAPDH	**GGCAAATTCAACGGCACAGT**	**CGCTCCTGGAAGATGGTGAT**

Note: *Ccnd1*, cyclin D1; *MyoD*, myogenic differentiation 1; *MRF4*, myogenic factor 6; *Myf5*, myogenic factor 5; *PMM2*, phosphomannomutase 2; *Igf-1*, insulin-like growth factor-1 isoform; *GAPDH*, gliceraldeyde-3-phosphate dehydrogenase.

Table S1.

Conclusions

The complexity of transcriptional, post-transcriptional and post-translational regulation of IGF-1 give rises to different protein isoforms. This thesis described the development of innovative biomolecular methods for the detection and quantification of the IGF-1 protein variants. The mechanism of IGF-1 protein variants production and their biological roles were also investigated in different pathological conditions including breast cancer and disease related to aberrant protein N-glycosylation. The main results are summarized in the following graphical abstract.

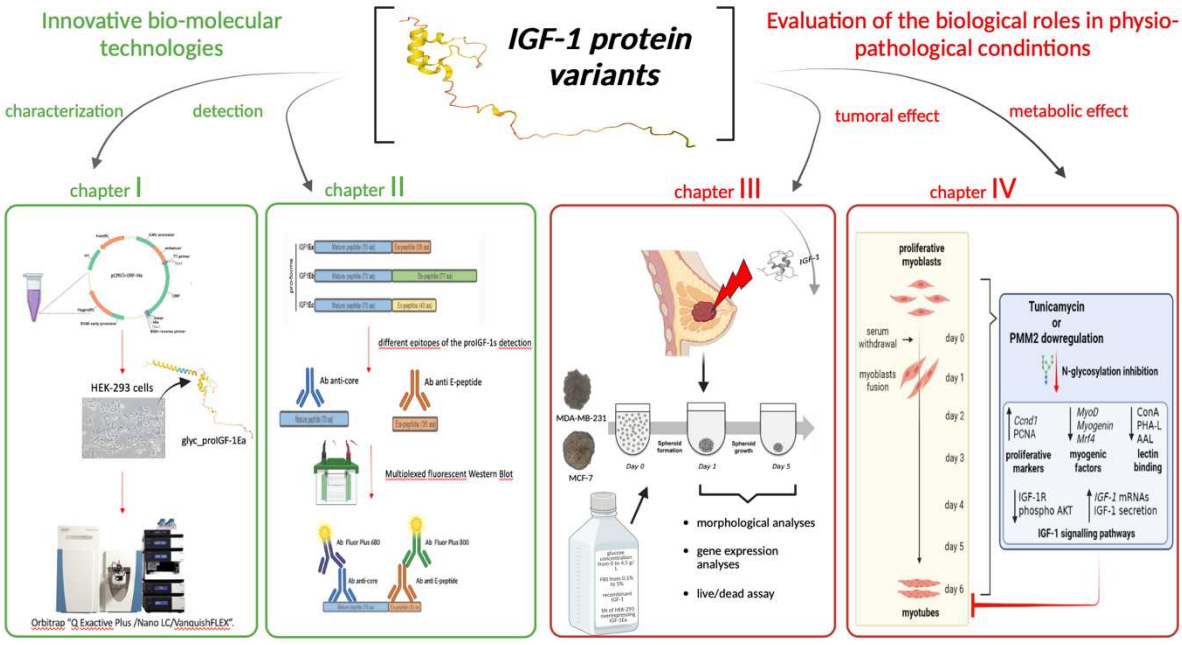

Graphical abstract. The complexity of insulin-like growth factor 1 (IGF-1): development of innovative bio-molecular methods for detection and quantification of IGF-1 protein variants and study of their biological roles in physio-pathological conditions.

In the first chapter we described the development of HEK-293 cells stably expressing the human N-glycosylated IGF-1Ea prohormone (glyc_proIGF-1Ea). The cell culture supernatants of these HEK-293 cells were used to identify and characterize the peptides corresponding to the different IGF-1 domains using high-resolution mass spectrometry (HRMS). The synthesis of new protein standards corresponding to different IGF-1 isoforms, combined with the use of HRMS technology, may provide a useful tool to characterize and quantify the different

components of the IGF-1 pool (i.e. glyc_proIGF-1Ea, proIGF-1Ea, mature IGF-1 and E-peptides) in complex biological matrices. In the second chapter, we described the development of a fluorescent-based Western Blot (WB) to simultaneously detect the proIGF-1s, mature IGF-1 and E-peptides in the same biological sample. Specifically, we used two different primary antibodies, which recognize different epitopes of proIGF-1 sequences, and two secondary antibodies conjugated to different fluorophores to develop a multiplex fluorescent WB able to discriminate between the different IGF-1 protein variants. This finding provides a proof of concept of the possibility to increase the specificity and selectivity of detection of target protein isoforms in complex samples by fluorescent WB. In the third chapter we evaluate the effect of tumor microenvironment changes on IGF-1 production and breast cancer (BC) cell lines MCF-7 and MDA-MB-231 spheroid formation, viability and mRNA expression of metabolic and epithelial-mesenchymal transition (EMT) gene expression. We found that cell culture conditions, and especially the glucose concentration in the culture media, markedly affected the IGF-1 production. Treatment of BC cell lines with normal high level of recombinant IGF-1 increased the BC spheroids formation and viability and expression of genes related to glycolytic metabolism and EMT process. Similar results were obtained with the cell culture supernatant (SN) obtained from the *IGF-1Ea*-overexpressing HEK-293 cells grown in high glucose media (≥ 2.4 mg/dL; ≥ 13.3 mM). On the contrary, SN obtained from HEK-293 cells starved for 24 h in glucose-free media were unable to promote BC spheroid formation due to reduced proIGF-1Ea N-glycosylation and consequent IGF-1 secretion. These results showed the importance of the tumor microenvironment on the biological behaviour of cancer cells and highlight the possibility to reduced IGF-1 production and BC spheroid formation by N-glycosylation inhibition. In the fourth chapter, we provided new evidence of a direct link between aberrant N-glycosylation, impaired IGF-1/IGF-1R signaling activation and myoblast differentiation in the context of the congenital disorder of glycosylation (CDG). The pharmacological inhibition of N-glycosylation by tunicamycin or the genetic knockdown of the phosphomannomutase 2 (PMM2) gene generated by CRISPR/Cas9 disrupted the coordinated temporal expression of myogenic markers in murine muscle cell lines. Moreover, chronic low-dose of tunicamycin increased atrophy markers and decreased the IGF-1R signaling pathway activation and proIGF-1 production in muscles of mice models. *In vitro* and *in vivo* models chronic challenged with low dose of tunicamycin can help to

elucidate the molecular mechanisms through which diseases associated with aberrant N-glycosylation, such as CDG, affect muscle and other tissue functions.

Conflicts of interest

The author declares no conflict of interest.

Acknowledgments

A special thanks to this elaborate at the Supervisor Prof. Elena Barbieri, who gave me the opportunity to live this unforgettable experience in the laboratory, fundamental for my professional and personal education. Also, I wanted to give thanks to her for the utmost seriousness and enthusiasm she gave me in facing this path and for all the time and effort she dedicated to me. For her I will always have a grateful memory, I dedicate an immense thank you to the Co-supervisor Prof. Giosuè Annibalini, for the help he has provided me all these three years and the great knowledge he has given me, for the helpfulness and precision he has shown me during the whole experimental period and above all for the wonderful person you are. Rarely have I met in my academic career a person so scientifically competent and dedicated to the work without him, this work would not have come to life. I would also like to thank the whole group of the Laboratory of the Biomol at the Division of Health and Physical Exercise of the Department of Biomolecular Sciences of Urbino for the help and support always shown to me. A special is beholden to the Dr. Roberta Saltarelli. Without her technical support constant supervision. I would not have come this far. She has always helped me in the experiments from the very beginning. She was always helpful both professionally and humanely. Of people like you one meets few in life. Thank you for your immense understanding, sensitivity and wonderful humanity shown to me. Thanks for contributing to this work, and more also goes to Prof. Amelia Morrone, Dr. Lorenzo Ferri and Prof. Renzo Guerrini from Meyer Children's Hospital, Florence. A special thanks also to the Dr. Rita Emili from the Department of Oncology Unit at the Ospedale Santa Maria della Misericordia, Urbino, Italy. Other thanks for supporting my research to Prof. Rita Barone from University of Catania and to Prof. Antonio Musarò from “Università La Sapienza” Roma. Moreover, I would like to thank Prof. Giorgio Arnaldi from the Division of Endocrinology Department of Clinical and Molecular Sciences Polytechnic University of Marche, Umberto I Hospital, Via Conca 71, 60126, Ancona, Italy, for his continuous support throughout each stage of the PhD thesis project. I wish to extend my gratitude firstly Dr. Barbara Pistilli, who were really precious in introducing me to the world of the “Institute Gustave Roussy Faculty of Medicine, University Paris-Saclay”. A special thank goes to my French supervisor Prof. Pierre Savagner. Rarely I have met such an enthusiastic person who was polite and always helpful to me, you were essential to my 6 months in Paris. Another thanks go to PhD Flora

Doffe, who followed me through the experiments during these 6 months. I will never cease to thank you and never forget the time we spent together. A big thanks goes also to the people who helped me in this experience in Paris: Dr. Fathia Mami-Chouaïb, Prof. Thiery Jerome Moreover, all the other guys and girls in the Unit 1186 of the “Institute Gustave Roussy” Lucille, Abdoul, Omar, Karol, Melanie, Areski, Stephanie, Isabelle. I wish to warmly thank especially Prof. Mauro Magnani, and Elena La Guardia e Thomas Di Mambro from DIATHEVA for providing support to the project and welcoming me into the company. Finally, I would like to thank the ‘Industrial Innovation Doctoral Programme’ was supported by Marche Region in collaboration with DIATHEVA S.r.L. Thanks, again to the Dr. Roberta Saltarelli for a critical reading of this work.